UC Berkeley
UC Berkeley Electronic Theses and Dissertations

Title

Identification and characterization of genetic and molecular components of Arabidopsis thaliana PBS3-mediated salicylic acid induction during defense against microbial pathogens

Permalink

https://escholarship.org/uc/item/293216bj

Author

Mackelprang, Rebecca

Publication Date

2017

Peer reviewed|Thesis/dissertation

eScholarship.org Powered by the California Digital Library
University of California

Identification and characterization of genetic and molecular components of *Arabidopsis thaliana* PBS3-mediated salicylic acid induction during defense against microbial pathogens

By

Rebecca Mackelprang

A dissertation submitted in partial satisfaction of the

requirements for the degree of

Doctor of Philosophy

in

Plant Biology

in the

Graduate Division

of the

University of California, Berkeley

Committee in charge:

Professor Mary Wildermuth, Chair
Professor Steve Lindow
Professor Sarah Stanley

Fall 2017

Abstract

Identification and characterization of genetic and molecular components of *Arabidopsis thaliana* PBS3-mediated salicylic acid induction during defense against microbial pathogens

By

Rebecca Mackelprang

Doctor of Philosophy in Plant Biology

University of California, Berkeley

Professor Mary Wildermuth, Chair

The plant hormone salicylic acid (SA; 2-hydroxybenzoic acid) is essential for plant defense in response to biotrophic and hemibiotrophic microbial pathogens. The concentration of SA increases during infection, determining the extent of defense gene induction and cellular responses to the pathogen. In *Arabidopsis thaliana*, plants with non-functional *avrPphB Susceptible 3* (*PBS3*) fail to accumulate significant induced SA and consequently lack induction of associated defense genes such as *pathogenesis related 1* (*PR1*). These plants have increased susceptibility to pathogens such as the bacterial pathogen *Pseudomonas syringae*. PBS3 is a member of the GH3 family of enzymes, which conjugate small acyl substrates to amino acids. PBS3 conjugates 4-substituted hydroxybenzoic acids preferentially to glutamic acid, but this activity does not clarify its function in defense. Metabolic analyses showed that *pbs3* mutants accumulate the product of another GH3 family enzyme, SA conjugated to aspartic acid (SA-Asp).

The kinetics of the known SA-Asp synthetase, GH3.5, were investigated to better understand the formation of SA-Asp *in vitro*. GH3.5 is also active on the growth hormone indole-3-acetic acid (IAA) and has a higher affinity for IAA than SA under moderate to high concentrations of Asp. However, when the concentration of Asp decreased, the affinity of GH3.5 for SA increased. The concentration of Asp decreases in response to pathogens, likely as part of nitrogen reallocation during the transition from growth to defense. This suggests that acyl substrate preference amongst these promiscuous enzymes can be affected by the amino acid substrate, and that GH3.5 affinity for SA is greatest during pathogen challenge.

The production of SA-Asp could serve to pull SA away from the pool used for defense in *pbs3* mutants. Therefore, a *pbs3gh3.5* double mutant line was created to see if the elimination of SA-Asp restored defense responses in the *pbs3* background. SA-Asp was not significantly reduced in this line, so a multiplexed knockout line of likely SA-Asp synthetases was created to reduce genetic redundancy. This *pbs3gh3.1gh3.3gh3.4gh3.5gh3.6* line, named *gh6x,* did eliminate induced SA-Asp in *pbs3*. However, *gh6x* failed to restore SA accumulation and pathogen resistance.

A genetic suppressor screen was used to identify new components in PBS3-mediated defense. Over 5,000 M2 lines were screened and ultimately two lines out of six with restored SA accumulation were chosen for further characterization. To this point, candidate causal mutations *PAD4*^{S135F} and *RAP2.6*^{A93V} have been identified for these two lines. PAD4 is a well-known regulator of SA-induced defense responses but may also be involved in cross talk with the SA antagonist jasmonic acid (JA). RAP2.6 is a transcription factor associated with JA and ethylene responses. The identification of these genes as candidates suggests that PBS3 may have SA-independent roles as well. RNA-sequencing identified de-repression of many JA genes in induced *pbs3* as compared to induced Col-0. Furthermore, exogenous application of SA failed to restore wild type susceptibility to *Pseudomonas syringae* in *pbs3* mutants. Taken together, these data suggest that PBS3 is important not just for the accumulation of SA, but as a higher order regulator of the complex cross talk between the mutually antagonistic SA and necrotroph-induced jasmonic acid signaling pathways.

I dedicate this dissertation to the intelligent and curious women who never had access to the education I have cherished.

TABLE OF CONTENTS

FIGURES AND TABLES

ACKNOWLEDGEMENTS

I would first like to acknowledge my advisor and mentor, Mary Wildermuth. Mary's patience, optimism, and excitement for science are contagious and inspired me to continually challenge myself through this graduate school experience. She allowed me the time to learn and develop as a scientist and supported my professional development during these years. On a personal level, I never doubted that she cared about me as a person and wanted to see me succeed.

The other members of the Wildermuth Laboratory were critical for shaping my graduate school experience. Michael Steinwand was a friend, mentor and colleague who patiently provided endless support. I will sorely miss the hours of talking about each other's projects, results, and experimental plans. Post-docs Divya Chandran and Sara Hotton helped train me early on. Jyoti Taneja, Johan Jaenisch and Amanda McRae have been excellent lab-mates to bounce ideas off of and have fostered a collaborative environment. The undergraduate students I have worked with, particularly Román Ramos and Haneih Barkhodari, were patient as I learned to mentor and provided critical support in moving this project forward.

The department of Plant & Microbial Biology has been a wonderful home for me. Faculty and staff, especially members of my committees, have provided guidance, access to equipment and resources, and mentorship. Rocio Sanchez has continually been a helpful and guiding presence for all of graduate school's critical moments. Dr. Peggy Lemaux created the space for me to explore science communication and community engagement. Peggy has also been an honest and understanding source of advice, and I truly appreciate her.

I give heartfelt thanks to my fellow graduate students, especially those in my own cohort. Since we started this journey together in 2012, I have looked to each of you for advice, encouragement, and friendship. Kate Scheibel, Carine Marshall, Riva Bruenn, and Monika Fischer, you have greatly enriched this experience. You have supported me during the hard times, celebrated the good, and together we have moved through the daily challenges and uncertainty of graduate school.

Finally, I'd like to acknowledge my family. Growing up as the youngest child, all I ever wanted was to be like my older siblings. As an adult, I have found my own way but did not stray far from the path they blazed. Joining the ranks of my two sisters, Rachel and Emily, and brother Romel as the final Ph.D. in the family is certainly one of my proudest accomplishments. And to our parents, Romel and Susan, who taught us that we could do and be anything, know that the success of your children is possible because of the unconditional love and support you have given each of us every day of our lives. To my dearly loved niece and nephews, you brought so much joy into my life. To my parents- and siblings-in-law, you have loved and supported me like your own daughter and sister. Thank you. To my dear husband, Ryan Bettilyon, you stood beside me as I took each step of this journey. You are my best friend, my confidant, and bring my greatest joy. Thank you. I can't wait to live what comes next.

CHAPTER I: Introduction

Plants are responsible for feeding a growing human population and face challenges from pathogens, climate conditions and soil health. The Green Revolution increased farm production and efficiency, saving millions from starvation, but also bringing new agricultural challenges. As crop varieties are bred or modified for high yield and ease of harvest, genetic diversity decreases and monocultures become more common. These conditions are conducive to the rapid spread of pathogens through a field and region, massively compromising local food supplies. Coupled with the ease of international travel and exporting of agricultural products, plant pathogens can rapidly spread around the globe and destroy a given crop. For example, a new strain of *Fusarium oxysporum f.sp. cubense* (Panama disease) was identified in Southeast Asia in the early 1990s to which the common Cavendish banana is highly susceptible (Ploetz, 2005). Since then, Panama disease has spread rapidly worldwide and threatens the existence of the beloved Cavendish (Ploetz, 2015).

Research on the mechanisms of plant/pathogen interactions is essential to maintain the benefits of our international food system and decrease some of the devastating effects of rapid pathogen spread. Use of the model plant *Arabidopsis thaliana* has facilitated great progress in understanding these interactions over the past few decades. Herein, *Arabidopsis* is used to elucidate the controls over active forms of salicylic acid, the key plcant hormone mediating defense in response to biotrophic and hemibiotrophic pathogens.

Salicylic acid underlies plant responses to (hemi-) biotrophic pathogens

The accumulation of salicylic acid (SA; 2-hydroxybenzoic acid) controls the cellular response to (hemi-)biotrophic bacterial and fungal pathogens. In mutant plant lines that do not produce SA, plant susceptibility is greatly increased. SA is synthesized from chorismate in a multistep process. First, chorismate is converted to isochorismate in plastids via isochorismate synthase 1 (ICS1; EDS16; SID2; At1g74710) (Strawn et al., 2007; Wildermuth et al., 2001). Subsequently, isochorismate is converted to salicylic acid via an unknown enzyme with isochorismate pyruvate lyase (IPL) activity or via a different unknown mechanism. Once synthesized, SA is exported from the plastid via enhanced disease susceptibility 5 (EDS5; At4g39030) (Nawrath et al., 2002; Serrano et al., 2013). It can then be converted to alternate forms such as methyl salicylate, which may serve as a mobile signal (Attaran et al., 2009; Park et al., 2007), SA-Asp, which seems to be an inactive catabolite (Chapter III), 2,3- or 2,5-DHBA (Zhang et al., 2013, 2017), readily hydrolysable SA glucosides (Dean and Delaney, 2008; Lim et al., 2002; Song, 2006), or other forms (see Dempsey et al., 2011). Because SA glucosides are efficiently converted back to free SA, the amount of "total SA" in a cell is given as the amount of free SA plus SA glucosides.

The concentration of SA determines the extent of plant defense induction. These defenses have three tiers, which exist on a continuous spectrum but have distinct characteristics. Initially, pathogens are detected by plant pattern recognition receptors (PRRs) in the plant cell membrane. PRRs recognize microbial signatures, termed microbial associated molecular patterns (MAMPs), such as flagellin and initiate intracellular responses (Zipfel, 2014). These responses include bursts of cytosolic Ca^{2+}, production of reactive oxygen species, production of anti-microbial compounds, and changes in gene transcription (Li et al., 2016). The signaling that accompanies MAMP recognition initiates production of low levels of SA which may serve to prime the cell for further defense induction if necessary (Fig. 1.1a; Dempsey et al., 2011; Vlot et al., 2009).

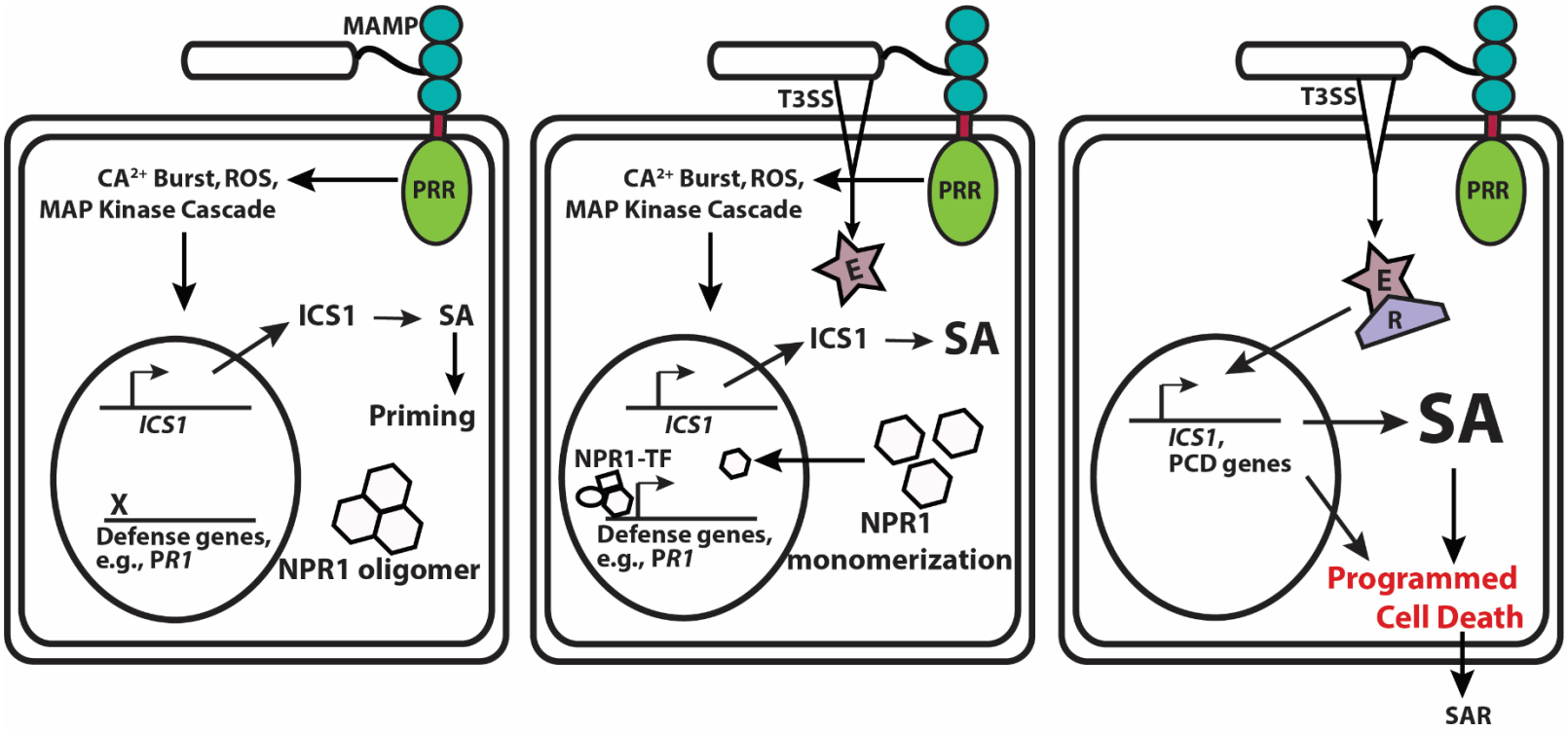

Figure 1.1: The concentration of salicylic acid increases through the course of pathogen infection (shown here for a bacterial pathogen).

(A) When a microbial associated molecular pattern (MAMP) is detected by a plant pattern recognition receptor (PRR), there are several rapid responses including a burst of cytosolic calcium and reactive oxygen species (ROS. A MAP kinase cascade is initiated that results in transcription of genes responsible for priming the cell and systemic cells/tissues for infection.

(B) Further defense activation in response to a pathogenic microbe results in moderate, robust defense induction. Pathogens secrete effectors (shown here via a bacterial type three secretion system) into the plant cell to inhibit plant defenses and promot pathogen growth. This is associated with enhanced accumulation of total SA. NPR1 monomerizes and migrates to the nucleus, where it actively binds with other transcription factors to initiate robust defense gene expression.

(C) Effector recognition by host resistance (R) proteins can trigger a hypersensitive response which results in very high levels of SA accumulation, NPR1 turnover (not shown), programmed cell death (PCD), and systemic acquired resistance in distal cells.

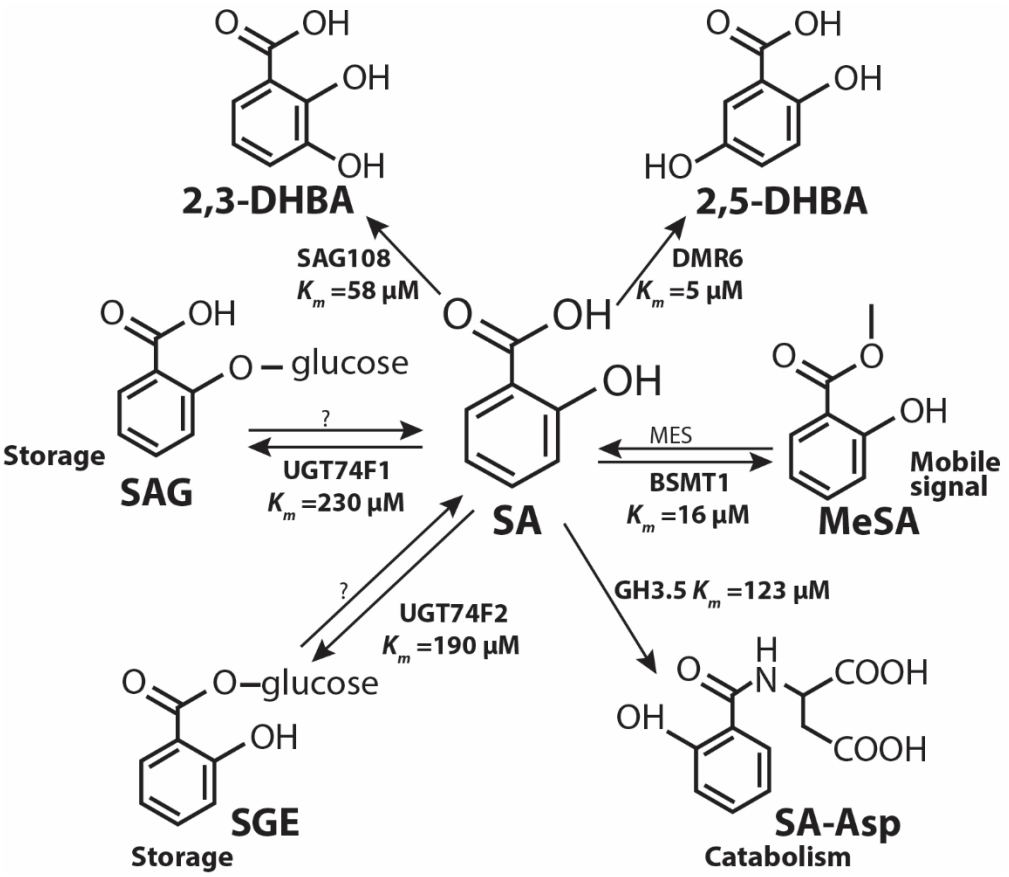

Figure 1.2: Mechanisms of control over active salicylic acid concentration
Cytosolic SA can be altered in various ways to maintain cellular homeostasis. SA can be methylated, possibly to serve as a mobile signal. It can be irreversibly conjugated to Asp by GH3.5, which has differing affinities for SA depending on the concentration of Asp. SA can be converted to 2,3- or 2,5-DHBA by SAG108/S3H and DMR6/S5H, respectively. SA can be reversibly glucosylated to form SA 2-O-β-D-glucoside (SAG) or SA glucose ester (SGE). B-glucosidase treatment releases both SAG and SGE glucose conjugates, and together SAG, SGE, and free SA comprise "total SA," which is a stronger indicator of defense induction than free SA alone.

If the microbe is pathogenic to the particular plant host, levels of SA will increase to moderate levels resulting in a pathogen-induced defense response (Fig. 1.1B). Pathogens may secrete effector proteins into the plant cell to suppress plant defense induction. At this stage, defense induction includes cytosolic redox associated with reduction of disulfide bonds holding oligomeric nonexpressor of pathogenesis related 1 (NPR1; At1g64280) proteins together (Mou et al., 2003). The breaking of these disulfide bonds likely reveals the bipartite nuclear localization signal (NLS) on NPR1 and allows for its translocation to the nucleus (Kinkema et al., 2000; Mou et al., 2003). In the nucleus, SA binding to NPR1 changes its conformation, exposing its transactivation domain. This NPR1 conformation, coupled with TGA transcription factors, enables transcription of defense associated genes, including *WRKY* transcription factors and *pathogenesis related* (*PR*) genes (Rochon et al., 2006; Wu et al., 2012). *Pathogenesis related 1* (*PR1*; At2g14610) is induced in this manner and because of its strong correlation with SA, can be used as a readout of moderate SA accumulation associated with defense activation.

The third tier of plant defense response is initiated by host recognition of pathogen effectors secreted directly into plant cells (Fig. 1.1C). As a result of this detection, signaling ensues that results in increased NPR1 turnover by NPR3 (Fu et al., 2012), increased SA accumulation, and the Hypersensitive Response (HR). HR often includes programmed cell death (PCD), which may release lytic enzymes and/or eliminate the living tissue needed by the biotroph to survive (e.g., Dempsey et al., 2011; Vlot et al., 2009). This localized response is associated with induced systemic acquired resistance (SAR) and moderate levels of SA in adjacent cells.

Control of active hormone concentration

As is clear from the vastly different cellular outcomes determined by the intracellular concentration of SA, cells must exert careful control over the concentration of SA. Balancing the concentration of phytohormones requires not just regulation of biosynthesis, but also regulation of active hormone forms. For such fine tuning, hormones can be reversibly conjugated into storage or transport forms, or they can be degraded. Common methods of hormone permanent or temporary inactivation include glycosylation, methylation, and amino acid conjugation (Dempsey et al., 2011; Rosquete et al., 2012; Woldemariam et al., 2012) among others that are less well characterized. In *Arabidopsis*, cytokinins, indole-3-acetic acid (IAA; an auxin), and SA can by glycosylated to maintain hormone homeostasis (Bowles et al., 2005; Hou et al., 2004; Kleczkowski et al., 1995; Lim et al., 2002). Methylation increases hormone volatility and mobility, and MeJA and MeSA may both be mobile hormone forms (Attaran et al., 2009; Park et al., 2007; Seo et al., 2001). Hormone oxidation (e.g. SA converstion to 2,3-DHBA) can initiate catabolism (Zhang et al., 2013). Finally, conjugation to amino acids can activate a hormone (i.e. JA-Ile), store a hormone (e.g. IAA-Ala), or irreversibly alter the hormone, initiating its degradation (e.g. IAA-Asp) (Ludwig-Müller, 2011; Ostin et al., 1998; Rampey et al., 2004; Staswick and Tiryaki, 2004; Woodward and Bartel, 2005). The coordination of hormone biosynthesis coupled with these mechanisms of hormone diversion from active forms are essential to coordinate appropriate cellular responses to internal and external stimuli.

By finding an enzyme's K_m for SA, we can better understand the hormone concentration at which that enzyme is most active. SA is methylated by Arabidopsis BSMT1, which has a K_m for SA of 16 μM (Chen et al., 2003), consistent with activity at the low concentrations in SAR activation and priming in Figure 1.1A (Fu and Dong, 2013). SAG108 catabolizes SA to 2,3-DHBA, delaying SA-induced senescence (Zhang et al., 2013). UGT74F1 and UGT74F2 glucosylate SA and have K_ms of around 200 μM (Lim et al., 2002; Song, 2006). Glucosylated

SA is readily hydrolyzed to free SA, and during pathogen infection, most cellular SA is present in glucosylated forms. Therefore, the quantity of SA is usually given in terms of free SA and total SA, where total SA is the free SA + SA glucosides. This stage of defense is associated with defense gene induction as in Fig. 1.1b. SA is conjugated to the amino acid Asp by GH3.5 (WES1; At4g27260) with a K_m that changes in response to the concentration of Asp (Chapter II; Mackelprang et al., 2017; Staswick et al., 2002; Westfall et al., 2016). GH3.5 is also active on auxins, and so it seems that GH3.5 activity on SA varies based on the concentrations of multiple substrates (Chapter II; Mackelprang et al., 2017). Exogenous application of SA-Asp did not induce robust SA accumulation or pathogen defense, suggesting that SA-Asp is an inactive form and is not hydrolyzed back to SA (see Chapter II; Chapter III; Chen et al., 2013; Mackelprang et al., 2017; Westfall et al., 2016).

SA cross talk with jasmonic acid (JA):

SA is important for induction of responses to biotrophic and hemi-biotrophic pathogens, and jasmonic acid (JA) is critical to the regulation of the response to necrotrophic pathogens and herbivores (Glazebrook, 2005). JA perception is well characterized; in the absence of active JA, jasmonate ZIM-domain (JAZ) proteins transcriptionally repress expression of jasmonate related genes through binding to transcriptional activators such as MYC2 (Chini et al., 2007; Thines et al., 2007; Yan et al., 2007). This repression is lifted when JA binds to the F-box COI1, which is part of a SKP1-Cullin-F-box E3 ubiquitin-ligase complex (Xie et al., 1998; Xu et al., 2002). JA binding to COI1 facilitates the ubiquitination and degradation of JAZ proteins, allowing for MYC2-dependent gene expression (Chini et al., 2007; Thines et al., 2007; Yan et al., 2007).

Because SA and JA induce broad cellular reprogramming in response to different pathogenic challenges, the regulation of the cross talk between the two pathways is very important (Pieterse et al., 2014; Thaler et al., 2012, 2002). SA and JA are antagonistic, and the mechanisms of cross talk between the two pathways is an active area of research. The transcription factor *ANAC032* is induced by biotrophic and necrotrophic pathogens and by SA and methyl jasmonate (MeJA) (Allu et al., 2016). ANAC032 promotes the expression of the SA-mediated defense regulators *PAD4* and *EDS1*, while repressing the expression of JA-associated *PDF1.2*, *THI2.1*, *VSP1*, and *VSP2* (Allu et al., 2016).

Coronatine is a JA-mimicking *Pseudomonas syringae* metabolite that stimulates JA signaling in plants (Brooks et al., 2005; Thines et al., 2007). It thereby changes the balance of SA:JA intracellularly, causing greater activation of the JA pathway at the expense of the SA pathway. This contributes to the success of *P. syringae*. Coronatine activates three other ANAC family transcription factors, *ANAC019*, *ANAC055*, and *ANAC072* via direct action of *MYC2* (Zheng et al., 2012). ANAC019 and potentially ANAC055 and ANAC072 bind to the promoters of the SA associated *ICS1*, *UGT74F2*, and *BSMT1* genes as well as the JA associated *MYC2* and *PDF1.2*. In the *anac019anac055anac072* triple mutant, the expression of *ICS1* increased and pathogen growth decreased, suggesting that these coronatine-induced ANAC transcription factors repress SA and promote JA (Zheng et al., 2012).

PBS3 mediation of salicylic acid metabolism:

PBS3 (*Avr<u>P</u>ph<u>B</u> <u>S</u>usceptible <u>3</u>*; *GH3.12*; At5g13320) is a member of the GH3 family of adenylating enzymes. It is critical for accumulation of induced total SA and downstream defense responses (Jagadeeswaran et al., 2007; Lee et al., 2008, 2007; Nobuta et al., 2007). PBS3 was enzymatically characterized to identify potential biological substrates. It was found to have activity on 4-substituted benzoic acids such as 4-hydroxybenzoic acid (4-HBA) and para-

aminobenzoate (pABA), conjugating them preferentially to Glu (Okrent et al., 2009). Such enzymatic activity does not present a clear mechanism by which SA concentration would be controlled. In fact, SA inhibited PBS3 activity as identified through biochemical assays and its crystal structure (Okrent et al., 2009; Westfall et al., 2012). Of the 19 GH3 enzymes in Arabidopsis, only GH3.5 has been shown to have activity on SA, converting it to SA-Asp. GH3.5 is also active on IAA, conjugating it to make the IAA catabolite IAA-Asp (Mackelprang et al., 2017; Staswick et al., 2002; Westfall et al., 2016). Metabolic analyses from the Wildermuth lab identified three compounds with dramatically different levels in Col-0 (wild type) vs *pbs3*. SA-Asp was the most dramatically impacted, increasing 30 fold in *pbs3* (Okrent, 2010, see Chapter III). Given this evidence, it is reasonable to hypothesize that *pbs3* mutants are compromised in SA accumulation due to shunting of SA metabolism towards inactive forms (e.g. SA-Asp).

With this hypothesis, the kinetics of the SA-Asp synthetase GH3.5 were investigated (see Chapter II). GH3 enzymes have a two-step reaction mechanism and were reported to use a bi uni uni bi ping pong mechanism (Chen et al., 2010). In the first step, an acyl substrate is adenylated, releasing pyrophosphate. In step two, an amino acid enters the binding pocket and displaces AMP to make a final acyl-amino product (Fig. 1.3). Because this reaction releases product at two distinct phases, it allows for monitoring of the reaction progression as opposed to only measuring end product. Surprisingly, we find that the amino acid concentration can affect the affinity of the enzyme for acyl substrate, creating questions about the proposed ping pong reaction mechanism. IAA is the preferred substrate when the concentration of Asp is high. However, decreasing concentrations of Asp lead to a lower K_m of GH3.5 for SA while the K_m for IAA remains the same. The concentration of Asp decreases in response to pathogens (Návarová et al., 2012), reflecting nitrogen mobilization as resources are shifted towards defense. We hypothesize that GH3.5 and potentially other GH3 proteins fine tune the cross talk between SA and IAA, incorporating feedback of SA concentration, IAA concentration, and Asp concentration (Chapter II).

In Chapter III, I describe research that genetically tests the impact of (potential) SA-conjugating GH3s and related metabolites on *pbs3* mutants. Compromising the ability of the plant to make SA-Asp does not restore SA accumulation. I also test the effects of small metabolic substrates and products of PBS3 or GH3.5 on susceptibility to virulent pathogens. Neither the PBS3 substrate 4-HBA nor SA-Asp altered pathogen growth in *pbs3* or WT plants. Interestingly, exogenous application of SA did not fully restore WT resistance in *pbs3*, suggesting an SA-independent function of PBS3 in addition to its strong effect on SA. Unable to identify a direct mechanism of PBS3 function, I use a forward genetic suppressor screen in Chapter IV to identify additional genes that may be involved in PBS3-mediated defense responses, finding several mutants with restored SA accumulation (*suppressors of pbs3 susceptibility*; *sops*). High-throughput sequencing identified candidate causal mutations for *sops* mutants that are involved in both promotion of SA and cross talk with JA. Transcriptional profiling of induced changes in *pbs3* and WT showed significant upregulation of JA-associated genes in *pbs3*. In fact, greater than 80% of differentially expressed genes in induced *pbs3* vs WT were upregulated in *pbs3*, indicating that not only does PBS3 promote SA, but it plays a major inhibitory role. Together, these data suggest that PBS3 may be a higher-level regulator of the cross talk between SA and JA, inhibiting JA to allow for robust accumulation of SA and associated gene expression.

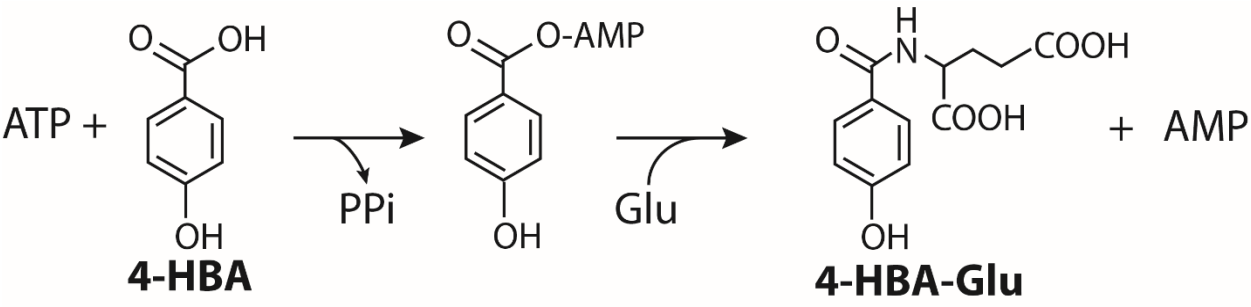

Figure 1.3: GH3 conjugation of acyl acid substrates to amino acids, shown for PBS3 conjugation of 4-hydroxybenzoic acid to Glu

GH3 family enzymes conjugate small acyl acids to amino acids via a two step reaction. In the first step, ATP and the acyl substrate (e.g. 4-hydroxybenzoic acid; 4-HBA) bind to the enzyme. The substrate is adenylated, and pyrophosphate (PPi) is released. In the second step, the amino acid substrate (e.g. Glu) binds to the enzyme. Subsequently, the conjugated product is released followed by AMP. 4-HBA-Glu is a product of PBS3 enzymatic activity.

REFERENCES

Allu, A.D., Brotman, Y., Xue, G.-P., Balazadeh, S., 2016. Transcription factor ANAC032 modulates JA/SA signalling in response to Pseudomonas syringae infection. EMBO Rep. 17, 1578–1589. doi:10.15252/embr.201642197

Attaran, E., Zeier, T.E., Griebel, T., Zeier, J., 2009. Methyl salicylate production and jasmonate signaling are not essential for systemic acquired resistance in Arabidopsis. Plant Cell 21, 954–71. doi:10.1105/tpc.108.063164

Bowles, D., Isayenkova, J., Lim, E.-K., Poppenberger, B., 2005. Glycosyltransferases: managers of small molecules. Curr. Opin. Plant Biol. 8, 254–263. doi:10.1016/J.PBI.2005.03.007

Brooks, D.M., Bender, C.L., Kunkel, B.N., 2005. The Pseudomonas syringae phytotoxin coronatine promotes virulence by overcoming salicylic acid-dependent defences in Arabidopsis thaliana. Mol. Plant Pathol. 6, 629–639. doi:10.1111/j.1364-3703.2005.00311.x

Chen, F., D'Auria, J.C., Tholl, D., Ross, J.R., Gershenzon, J., Noel, J.P., Pichersky, E., 2003. An Arabidopsis thaliana gene for methylsalicylate biosynthesis, identified by a biochemical genomics approach, has a role in defense. Plant J. 36, 577–588. doi:10.1046/j.1365-313X.2003.01902.x

Chen, Q., Westfall, C.S., Hicks, L.M., Wang, S., Jez, J.M., 2010. Kinetic basis for the conjugation of auxin by a GH3 family indole-acetic acid-amido synthetase. J. Biol. Chem. 285, 29780–6. doi:10.1074/jbc.M110.146431

Chen, Y., Shen, H., Wang, M., Li, Q., He, Z., 2013. Salicyloyl-aspartate synthesized by the acetyl-amido synthetase GH3 . 5 is a potential activator of plant immunity in Arabidopsis. Acta Biochim Biophys Sin 45, 827–836. doi:10.1093/abbs/gmt078.Advance

Chini, A., Fonseca, S., Fernández, G., Adie, B., Chico, J.M., Lorenzo, O., García-Casado, G., López-Vidriero, I., Lozano, F.M., Ponce, M.R., Micol, J.L., Solano, R., 2007. The JAZ family of repressors is the missing link in jasmonate signalling. Nature 448, 666–671. doi:10.1038/nature06006

Dean, J. V., Delaney, S.P., 2008. Metabolism of salicylic acid in wild-type, ugt74f1 and ugt74f2 glucosyltransferase mutants of Arabidopsis thaliana. Physiol. Plant. 132, 417–425. doi:10.1111/j.1399-3054.2007.01041.x

Dempsey, D.A., Vlot, a C., Wildermuth, M.C., Klessig, D.F., 2011. Salicylic Acid biosynthesis and metabolism. Arabidopsis Book 9, e0156. doi:10.1199/tab.0156

Fu, Z.Q., Dong, X., 2013. Systemic acquired resistance: turning local infection into global defense. Annu. Rev. Plant Biol. 64, 839–63. doi:10.1146/annurev-arplant-042811-105606

Fu, Z.Q., Yan, S., Saleh, A., Wang, W., Ruble, J., Oka, N., Mohan, R., Spoel, S.H., Tada, Y., Zheng, N., Dong, X., 2012. NPR3 and NPR4 are receptors for the immune signal salicylic acid in plants. Nature 486, 228–32. doi:10.1038/nature11162

Glazebrook, J., 2005. Contrasting Mechanisms of Defense Against Biotrophic and Necrotrophic

Pathogens. Annu. Rev. Phytopathol. 43, 205–227. doi:10.1146/annurev.phyto.43.040204.135923

Hou, B., Lim, E.-K., Higgins, G.S., Bowles, D.J., 2004. N-glucosylation of cytokinins by glycosyltransferases of Arabidopsis thaliana. J. Biol. Chem. 279, 47822–32. doi:10.1074/jbc.M409569200

Jagadeeswaran, G., Raina, S., Acharya, B.R., Maqbool, S.B., Mosher, S.L., Appel, H.M., Schultz, J.C., Klessig, D.F., Raina, R., 2007. Arabidopsis GH3-LIKE DEFENSE GENE 1 is required for accumulation of salicylic acid, activation of defense responses and resistance to Pseudomonas syringae. Plant J. 51, 234–46. doi:10.1111/j.1365-313X.2007.03130.x

Kinkema, M., Fan, W., Dong, X., 2000. Nuclear localization of NPR1 is required for activation of PR gene expression. Plant Cell 12, 2339–2350. doi:10.1105/TPC.12.12.2339

Kleczkowski, K., Schell, J., Bandur, R., 1995. Phytohormone Conjugates: Nature and Function. CRC. Crit. Rev. Plant Sci. 14, 283–298. doi:10.1080/07352689509382361

Lee, M.W., Jelenska, J., Greenberg, J.T., 2008. Arabidopsis proteins important for modulating defense responses to Pseudomonas syringae that secrete HopW1-1. Plant J. 54, 452–65. doi:10.1111/j.1365-313X.2008.03439.x

Lee, M.W., Lu, H., Jung, H.W., Greenberg, J.T., 2007. A key role for the Arabidopsis WIN3 protein in disease resistance triggered by Pseudomonas syringae that secrete AvrRpt2. Mol. Plant. Microbe. Interact. 20, 1192–200. doi:10.1094/MPMI-20-10-1192

Li, B., Meng, X., Shan, L., He, P., 2016. Transcriptional Regulation of Pattern-Triggered Immunity in Plants. Cell Host Microbe 19, 641–650. doi:10.1016/J.CHOM.2016.04.011

Lim, E.-K., Doucet, C.J., Li, Y., Elias, L., Worrall, D., Spencer, S.P., Ross, J., Bowles, D.J., 2002. The Activity of Arabidopsis Glycosyltransferases toward Salicylic Acid, 4-Hydroxybenzoic Acid, other Benzoates. J. Biol. Chem. 277, 586–592.

Ludwig-Müller, J., 2011. Auxin conjugates: their role for plant development and in the evolution of land plants. J. Exp. Bot. 62, 1757–73. doi:10.1093/jxb/erq412

Mackelprang, R., Okrent, R.A., Wildermuth, M.C., 2017. Preference of Arabidopsis thaliana GH3.5 acyl amido synthetase for growth versus defense hormone acyl substrates is dictated by concentration of amino acid substrate aspartate. Phytochemistry 143, 19–28. doi:10.1016/j.phytochem.2017.07.001

Mou, Z., Fan, W., Dong, X., 2003. Inducers of plant systemic acquired resistance regulate NPR1 function through redox changes. Cell 113, 935–44.

Návarová, H., Bernsdorff, F., Döring, A.-C., Zeier, J., 2012. Pipecolic acid, an endogenous mediator of defense amplification and priming, is a critical regulator of inducible plant immunity. Plant Cell 24, 5123–41. doi:10.1105/tpc.112.103564

Nawrath, C., Heck, S., Parinthawong, N., Métraux, J.-P., 2002. EDS5, an essential component of salicylic acid-dependent signaling for disease resistance in Arabidopsis, is a member of the MATE transporter family. Plant Cell 14, 275–86.

Nobuta, K., Okrent, R. a, Stoutemyer, M., Rodibaugh, N., Kempema, L., Wildermuth, M.C., Innes, R.W., 2007. The GH3 acyl adenylase family member PBS3 regulates salicylic acid-dependent defense responses in Arabidopsis. Plant Physiol. 144, 1144–56. doi:10.1104/pp.107.097691

Okrent, R.A., 2010. Biochemical and Functional Characterization of the GH3 Amino Acid-Conjugase PBS3 of Arabidopsis thaliana. Dissertation.

Okrent, R. a, Brooks, M.D., Wildermuth, M.C., 2009. Arabidopsis GH3.12 (PBS3) conjugates amino acids to 4-substituted benzoates and is inhibited by salicylate. J. Biol. Chem. 284, 9742–54. doi:10.1074/jbc.M806662200

Ostin, a, Kowalyczk, M., Bhalerao, R.P., Sandberg, G., 1998. Metabolism of indole-3-acetic acid in Arabidopsis. Plant Physiol. 118, 285–96.

Park, S.-W., Kaimoyo, E., Kumar, D., Mosher, S., Klessig, D.F., 2007. Methyl salicylate is a critical mobile signal for plant systemic acquired resistance. Science 318, 113–6. doi:10.1126/science.1147113

Pieterse, C.M.J., Zamioudis, C., Berendsen, R.L., Weller, D.M., Van Wees, S.C.M., Bakker, P.A.H.M., 2014. Induced Systemic Resistance by Beneficial Microbes. Annu. Rev. Phytopathol. 52, 347–375. doi:10.1146/annurev-phyto-082712-102340

Ploetz, R.C., 2015. Fusarium Wilt of Banana. Phytopathology 105, 1512–1521. doi:10.1094/PHYTO-04-15-0101-RVW

Ploetz, R.C., 2005. Panama Disease: An Old Nemesis Rears its Ugly Head Part 2: The Cavendish Era and Beyond. APSnet Featur. Artic. doi:10.1094/APSnetFeature-2005-1005

Rampey, R.A., Leclere, S., Kowalczyk, M., Ljung, K., Bartel, B., Biology, C., Texas, R.A.R., 2004. A Family of Auxin-Conjugate Hydrolases That Contributes to Free Indole-3-Acetic Acid Levels during Arabidopsis Germination 1. Plant Physiol. 135, 978–988. doi:10.1104/pp.104.039677.978

Rochon, A., Boyle, P., Wignes, T., Fobert, P.R., Després, C., 2006. The coactivator function of Arabidopsis NPR1 requires the core of its BTB/POZ domain and the oxidation of C-terminal cysteines. Plant Cell 18, 3670–85. doi:10.1105/tpc.106.046953

Rosquete, M.R., Barbez, E., Kleine-Vehn, J., 2012. Cellular Auxin Homeostasis: Gatekeeping Is Housekeeping. Mol. Plant 5, 772–786. doi:10.1093/MP/SSR109

Seo, H.S., Song, J.T., Cheong, J.J., Lee, Y.H., Lee, Y.W., Hwang, I., Lee, J.S., Choi, Y.D., 2001. Jasmonic acid carboxyl methyltransferase: a key enzyme for jasmonate-regulated plant responses. Proc. Natl. Acad. Sci. U. S. A. 98, 4788–93. doi:10.1073/pnas.081557298

Serrano, M., Wang, B., Aryal, B., Garcion, C., Abou-Mansour, E., Heck, S., Geisler, M., Mauch, F., Nawrath, C., Métraux, J.-P., 2013. Export of salicylic acid from the chloroplast requires the multidrug and toxin extrusion-like transporter EDS5. Plant Physiol. 162, 1815–21. doi:10.1104/pp.113.218156

Song, J.T., 2006. Induction of a Salicylic Acid Glucosyltransferase, AtSGT1, Is an Early Disease Response in Arabidopsis thaliana. Mol. Cells 22, 233–238.

Staswick, P.E., Tiryaki, I., 2004. The Oxylipin Signal Jasmonic Acid Is Activated by an Enzyme That Conjugates It to Isoleucine in Arabidopsis. Plant Cell 16, 2117–2127. doi:10.1105/tpc.104.023549.1

Staswick, P.E., Tiryaki, I., Rowe, M.L., 2002. Jasmonate Response Locus JAR1 and Several Related Arabidopsis Genes Encode Enzymes of the Firefly Luciferase Superfamily That Show Activity on Jasmonic , Salicylic , and Indole-3-Acetic Acids in an Assay for Adenylation. Plant Cell 14, 1405–1415. doi:10.1105/tpc.000885.defect

Strawn, M. a, Marr, S.K., Inoue, K., Inada, N., Zubieta, C., Wildermuth, M.C., 2007. Arabidopsis isochorismate synthase functional in pathogen-induced salicylate biosynthesis exhibits properties consistent with a role in diverse stress responses. J. Biol. Chem. 282, 5919–33. doi:10.1074/jbc.M605193200

Thaler, J.S., Fidantsef, A.L., Bostock, R.M., 2002. Antagonism between jasmonate- and salicylate-mediated induced plant resistance: effects of concentration and timing of elicitation on defense-related proteins, herbivore, and pathogen performance in tomato. J. Chem. Ecol. 28, 1131–59.

Thaler, J.S., Humphrey, P.T., Whiteman, N.K., 2012. Evolution of jasmonate and salicylate signal crosstalk. Trends Plant Sci. 17, 260–270. doi:10.1016/j.tplants.2012.02.010

Thines, B., Katsir, L., Melotto, M., Niu, Y., Mandaokar, A., Liu, G., Nomura, K., He, S.Y., Howe, G.A., Browse, J., 2007. JAZ repressor proteins are targets of the SCFCOI1 complex during jasmonate signalling. Nature 448, 661–665. doi:10.1038/nature05960

Vlot, a C., Dempsey, D.A., Klessig, D.F., 2009. Salicylic Acid, a multifaceted hormone to combat disease. Annu. Rev. Phytopathol. 47, 177–206. doi:10.1146/annurev.phyto.050908.135202

Westfall, C.S., Sherp, A.M., Zubieta, C., Alvarez, S., Schraft, E., Marcellin, R., Ramirez, L., Jez, J.M., 2016. Arabidopsis thaliana GH3.5 acyl acid amido synthetase mediates metabolic crosstalk in auxin and salicylic acid homeostasis. Proc. Natl. Acad. Sci. U. S. A. 113, 13917–13922. doi:10.1073/pnas.1612635113

Westfall, C.S., Zubieta, C., Herrmann, J., Kapp, U., Nanao, M.H., Jez, J.M., 2012. Structural basis for prereceptor modulation of plant hormones by GH3 proteins. Science 336, 1708–11. doi:10.1126/science.1221863

Wildermuth, M.C., Dewdney, J., Wu, G., Ausubel, F.M., 2001. Isochorismate synthase is required to synthesize salicylic acid for plant defence. Nature 414, 562–5. doi:10.1038/35107108

Woldemariam, M.G., Onkokesung, N., Baldwin, I.T., Galis, I., 2012. Jasmonoyl-L-isoleucine hydrolase 1 (JIH1) regulates jasmonoyl-L-isoleucine levels and attenuates plant defenses against herbivores. Plant J. 72, 758–67. doi:10.1111/j.1365-313X.2012.05117.x

Woodward, A.W., Bartel, B., 2005. Auxin: regulation, action, and interaction. Ann. Bot. 95, 707–35. doi:10.1093/aob/mci083

Wu, Y., Zhang, D., Chu, J.Y., Boyle, P., Wang, Y., Brindle, I.D., De Luca, V., Després, C.,

2012. The Arabidopsis NPR1 protein is a receptor for the plant defense hormone salicylic acid. Cell Rep. 1, 639–47. doi:10.1016/j.celrep.2012.05.008

Xie, D.X., Feys, B.F., James, S., Nieto-Rostro, M., Turner, J.G., 1998. COI1: an Arabidopsis gene required for jasmonate-regulated defense and fertility. Science 280, 1091–4.

Xu, L., Liu, F., Lechner, E., Genschik, P., Crosby, W.L., Ma, H., Peng, W., Huang, D., Xie, D., 2002. The SCF(COI1) ubiquitin-ligase complexes are required for jasmonate response in Arabidopsis. Plant Cell 14, 1919–35. doi:10.1105/TPC.003368

Yan, Y., Stolz, S., Chételat, A., Reymond, P., Pagni, M., Dubugnon, L., Farmer, E.E., 2007. A downstream mediator in the growth repression limb of the jasmonate pathway. Plant Cell 19, 2470–83. doi:10.1105/tpc.107.050708

Zhang, K., Halitschke, R., Yin, C., Liu, C.-J., Gan, S.-S., 2013. Salicylic acid 3-hydroxylase regulates Arabidopsis leaf longevity by mediating salicylic acid catabolism. Proc. Natl. Acad. Sci. U. S. A. 110, 14807–12. doi:10.1073/pnas.1302702110

Zhang, Y., Zhao, L., Zhao, J., Li, Y., Wang, J., Guo, R., Gan, S., Liu, C.-J., Zhang, K., 2017. S5H/DMR6 Encodes a Salicylic Acid 5-Hydroxylase That Fine-Tunes Salicylic Acid Homeostasis. Plant Physiol. 175, 1082–1093. doi:10.1104/pp.17.00695

Zheng, X.-Y., Spivey, N.W., Zeng, W., Liu, P.-P., Fu, Z.Q., Klessig, D.F., He, S.Y., Dong, X., 2012. Coronatine promotes Pseudomonas syringae virulence in plants by activating a signaling cascade that inhibits salicylic acid accumulation. Cell Host Microbe 11, 587–96. doi:10.1016/j.chom.2012.04.014

Zipfel, C., 2014. Plant pattern-recognition receptors. Trends Immunol. 35, 345–351. doi:10.1016/J.IT.2014.05.004

CHAPTER II: Preference of *Arabidopsis thaliana* GH3.5 acyl amido synthetase for growth versus defense hormone acyl substrates is dictated by concentration of amino acid substrate aspartate

PREFACE

The material presented below was previously published in:

Mackelprang, R., Okrent, R.A., Wildermuth, M.C. (2017). Preference of *Arabidopsis thaliana* GH3.5 acyl amido synthetase for growth versus defense hormone acyl substrates is dictated by concentration of amino acid substrate aspartate. Phytochemistry 143, 19-28. https://doi.org/10.1016/j.phytochem.2017.07.001

R. Okrent created original GH3.5 construct which I utilized in the experiments presented below.

ABSTRACT

The GH3 family of adenylating enzymes conjugate acyl substrates such as the growth hormone indole-3-acetic acid (IAA) to amino acids via a two-step reaction of acyl substrate adenylation followed by amino acid conjugation. Previously, *Arabidopsis thaliana* GH3.5 was shown to adenylate IAA and other auxins as well as the defense hormone salicylic acid (SA, 2-hydroxybenzoate), but kinetic parameters were only recently reported. Our contemporaneous, independent examination of the kinetics of GH3.5 on a variety of auxin and benzoate substrates supports and extends these findings. For example, we found GH3.5 activity on substituted benzoates is not defined by the substitution position as it is for GH3.12/PBS3. Most importantly, we show that GH3.5 strongly prefers Asp as the amino acid conjugate and that the concentration of Asp dictates the functional activity of GH3.5 on IAA vs. SA. Not only is Asp used in amino acid biosynthesis, but it also plays an important role in nitrogen mobilization and in the production of downstream metabolites, including pipecolic acid which propagates defense systemically. During active growth, [IAA] and [Asp] are high and the catalytic efficiency (k_{cat}/K_m) of GH3.5 for IAA is 360-fold higher than with SA. *GH3.5* is expressed under these conditions and conversion of IAA to inactive IAA-Asp would provide fine spatial and temporal control over local auxin developmental responses. By contrast, [SA] is dramatically elevated in response to (hemi)-biotrophic pathogens which also induce *GH3.5* expression. Under these conditions, [Asp] is low and GH3.5 has equal affinity (K_m) for SA and IAA with similar catalytic efficiencies. However, the concentration of IAA tends to be very low, well below the K_m for IAA. Therefore, GH3.5 catalyzed formation of SA-Asp would occur, fine-tuning localized defensive responses through conversion of active free SA to SA-Asp. Taken together, we show how GH3.5, with dual activity on IAA and SA, can integrate cellular metabolic status via Asp to provide fine control of growth vs. defense outcomes and hormone homeostasis.

INTRODUCTION

Plant hormones regulate development and response to their environment (Jaillais and Chory, 2010; Robert-Seilaniantz et al., 2011a). Indole-3-acetic acid (IAA – an auxin) and salicylic acid (SA) are plant hormones that predominantly promote development and defense,

respectively (Dempsey et al., 2011; Spoel and Dong, 2012; Vanneste and Friml, 2009; Woodward and Bartel, 2005). Auxin regulates plant developmental processes such as organogenesis through its accumulation in organ primordia where it binds to its receptor, resulting in the degradation of transcriptional repressors of auxin-associated genes and the transcription of a myriad of auxin-associated genes (Kepinski and Leyser, 2005; Vanneste and Friml, 2009). SA synthesis is induced in response to (hemi)biotrophic pathogens such as the powdery mildew fungus *Golovinomyces orontii* (Dewdney et al., 2000; Wildermuth et al., 2001), the bacterium *Pseudomonas syringae* (Rasmussen et al., 1991), and tobacco mosaic virus (Malamy et al., 1990). When sufficient SA accumulates, the master plant immune regulator NPR1 is stable, active, and properly localized, resulting in the transcription of a suite of genes that mediate a robust local defense (Fu et al., 2012; Wu et al., 2012). Even higher levels of SA accumulate when a pathogen induces a hypersensitive response (HR) with programmed cell death (PCD) (Dempsey et al., 2011).

To control amplified downstream effects of hormones, hormone cellular concentrations are tightly regulated both spatially and temporally. For example, high local levels of SA accumulate and cause cell death in tobacco in response to tobacco mosaic virus or a fungal elicitor. Neighboring cells accumulate moderate levels of SA and mount a local defense response, and more distal cells accumulate minimal SA and mount no defense (Dorey et al., 1997; Huang et al., 2006). For auxin, spatial control of concentration and associated downstream impacts is mediated to a large extent by auxin transport and catabolism (Adamowski and Friml, 2015; Mellor et al., 2016). Furthermore, developmental and environmental context and inputs are integrated to coordinate and fine-tune cellular responses. For example, the atypical E2F transcription factor *DEL1*, which is only expressed in dividing tissue, promotes cell division by inhibiting endoreduplication, SA accumulation and defense (Chandran et al., 2014; Vlieghe et al., 2005).

Given their opposing roles in promoting growth versus defense, IAA and SA have long been known to act antagonistically (Denancé et al., 2013; Robert-Seilaniantz et al., 2011a). Exogenous auxin can suppress SA-dependent defense (J.-E. Park et al., 2007; Robert-Seilaniantz et al., 2011a, 2011b), while exogenous SA treatment decreases *Arabidopsis* biomass in an auxin-dependent manner (Canet et al., 2010). However, a sophisticated understanding of the variety of mechanisms by which IAA and SA modify each other's accumulation, activity, and function with cellular resolution remains limited (Denancé et al., 2013; Robert-Seilaniantz et al., 2011a)

One means by which hormone activity is directly regulated is via conjugation to amino acids. For example, IAA conjugation to Asp initiates auxin catabolism (Ostin et al., 1998), while conjugation to Ala stores IAA as an inactive form that is rapidly reactivated through hydrolysis by a dedicated enzyme (Rampey et al., 2004). The only SA-amino acid conjugate found in plants thus far is salicyloyl-aspartate (SA-Asp) (Bourne et al., 1991; Chen et al., 2013; Steffan et al., 1988). Similar to IAA-Asp, SA-Asp is not hydrolyzed back to SA (Chen et al., 2013, Okrent & Wildermuth, unpublished). Furthermore, SA-Asp was unable to induce robust defense gene expression or resistance (Chen et al., 2013; Okrent & Wildermuth, unpublished), suggesting SA-Asp, like IAA-Asp, is also an inactive form of the hormone dedicated to catabolism. However, an additional possibility is that it functions as a mobile form of SA involved in low level priming of defense (Chen et al., 2013).

Hormone-amino acid conjugation in plants is catalyzed by enzymes belonging to the GH3 (Gretchen Hagen 3) family which are members of the greater firefly luciferase family of adenylating enzymes (Staswick et al., 2005, 2002). GH3 enzymes are divided into three groups

based on syntenic analysis and preferred substrates (Okrent and Wildermuth, 2011; Staswick et al., 2002). GH3s that conjugate JA are classified as Group I. GH3s that conjugate IAA are classified as Group II (Okrent and Wildermuth, 2011; Staswick et al., 2005). Group III is less well characterized. In *Arabidopsis*, active acyl substrates are known only for one Group III member, GH3.12 /PBS3, which prefers 4-substituted benzoates such as 4-hydroxybenzoic acid (4-HBA) and *para*-aminobenzoic acid (pABA) (Okrent et al., 2009; Okrent and Wildermuth, 2011).

Surprisingly, in addition to auxins, the Group II member GH3.5 (At4g27260) is also active on SA and is the only GH3 enzyme known with this activity (Chen et al., 2013; Staswick et al., 2005, 2002; Westfall et al., 2016). Endpoint assays indicated the possibility of GH3.5 conjugation of auxins to a variety of amino acids (Staswick et al., 2005; Wang et al., 2012), though *in planta* measurements point to Asp as the dominant amino acid conjugate (J.-E. Park et al., 2007; Zhang et al., 2007). As IAA-Asp and SA-Asp appear to be inactive or hypoactive non-hydrolyzable forms of these hormones, GH3.5 conjugation could play an important role in IAA and SA homeostasis and hormone cross-talk.

To better understand the function of GH3.5 in auxin and SA metabolism and response, we undertook a biochemical kinetic study of GH3.5 to accurately determine its acyl substrate preference for IAA, SA, and related substrates as well as its amino acid substrate preference (e.g. Asp). Because IAA, SA, and Asp concentrations vary at the cellular level with developmental and environmental context, understanding GH3.5 activity and preference in the context of physiologically-relevant concentrations of these substrates allows us to specifically predict GH3.5 function in a context-dependent manner. These predictions are consistent with observed *GH3.5* gene expression and provide a mechanistic understanding for the dual function of GH3.5 in hormone homeostasis in growth and defense.

MATERIALS AND METHODS

AtGH3.5 expression and purification

AtGH3.5 cDNA was amplified and inserted into a pET-28a vector (Novagen), then expressed in *Escherichia coli* Rosetta2 (DE3) cells, as in (Okrent et al., 2009). Purification of His-GH3.5 was done with nickel-nitriolotriacetic acid His-Bind resin (Novagen) according to manufacturer's directions and run on an SDS-PAGE gel. No other proteins were present. Initially, the His tag was cleaved with Thrombin (Novagen), but kinetic assays testing GH3.5 vs His-GH3.5 showed no difference in enzyme activity, so His-GH3.5 was used for experiments. Protein concentration was quantified using a Bradford assay with a 96-well plate using Coomassie Blue G-250 (EM Biosciences). Bovine serum albumin was used as a standard. Protein was dialyzed into 100 mM Tris, pH 7.7, 10% glycerol, and 1 mM DTT and stored at -80°C. Assays were repeated with enzyme from different batches to confirm results.

Determination of kinetic parameters: Adenylation

His-GH3.5 activity was measured spectrophotometrically at 340 nm using pyrophosphate reagent (Sigma). The production of pyrophosphate after adenylation is coupled to fructose-6-phophate kinase, adolase, triose-phosphate isomerase, and glycerophosphate dehydrogenase ending with the oxidation of NADH to NAD^+, visible by absorbance at 340 nm and measured with a Spectromax Plus microplate spectrophotometer (Molecular Devices) at 340 nm using SOFTMax PRO 3.0 (Molecular Devices) software. 1 mM DTT, 5 mM MgCl2, 2.5 mM ATP and 10-20 µg of His-GH3.5 were added. Pyrophosphate reagent (Sigma) vials were reconstituted in 4 mL double distilled H_2O and 65 µl was used in each 200 µl reaction.

Determination of kinetic parameters: Full reaction

His-GH3.5 activity was measured using a coupled, high-throughput spectrophotometric assay. Briefly, the reaction coupled the release of AMP to the conversion of NADH to NAD^+ using myokinase, pyruvate kinase, and lactate dehydrogenase, as described in (Chen et al., 2010). Loss of NADH was measured with a Spectromax Plus microplate spectrophotometer (Molecular Devices) at 340 nm using SOFTMax PRO 3.0 (Molecular Devices) software. Assays were conducted in 200 µl volumes in 96 well plates in 20 mM Tris (pH 8.0), 5 mM $MgCl_2$, 20 mM ATP, 20mM phosphoenolpyruvate, 2 mM NADH and 1 mM DTT with 20 µg GH3.5 and 4 units each of myokinase, pyruvate kinase, and lactate dehydrogenase.

Kinetic data analysis

Substrates were added immediately prior to loading into Spectromax Plus microplate spectrophotometer (Molecular Devices) for absorbance measurements at 340 nm every 15-20 seconds for 20-60 minutes. All experiments were repeated 2 to 5 times with similar results. The velocity of a no GH3.5 control was subtracted and for comparison between assays, velocities were normalized to zero. The extinction coefficient for NADH, 6.22 $\mu M^{-1} * cm^{-1}$ was used for conversion of velocities from Δabsorbance/min to µmol/min. Estimates of kinetic parameters were initially determined using the Hanes-Woolf equation fit to initial velocity values, then refined with Kaleidagraph (Synergy Software).

RESULTS

Kinetic parameters of GH3.5 adenylation on auxin-like substrates

Hormone acyl substrate specificity for GH3.5 was initially explored using an endpoint PP_i Exchange Assay, which found GH3.5 to be active on a variety of auxins and SA (Staswick et al., 2005, 2002). To better understand the preference of GH3.5 for auxins, SA, and related compounds, we employed a high throughput kinetic assay of adenylation (Okrent et al., 2009), shown in Figure 2.1. Similar to Staswick et al. 2005, we found GH3.5 was active on IAA, indole-3-pyruvic acid (IPA), indole-3-butyric acid (IBA), indole-3-carboxylic acid (ICA), 2-phenylacetic acid (PAA) and the synthetic auxin 1-napthaleneacetic acid (NAA) (Fig. 2.2). GH3.5 exhibited the greatest affinity for IAA (K_m=45 µM) and least for IBA (K_m=733 µM). The V_{max} of all auxin-like substrates tested were very similar, 53-104 nmol * min^{-1} * μg^{-1} (Fig. 2.2B). The catalytic efficiency (k_{cat}/K_m) of GH3.5 was highest with IAA at 5.12 min^{-1} * mM^{-1}. Westfall et al., (2016) also found GH3.5 to be active on IAA, PAA, and NAA and to exhibit similar catalytic efficiencies. The affinities of AtGH3.5 and OsGH3.8 for IAA, IBA, PAA and NAA are similar, (Chen et al., 2010) as are the affinities of AtGH3.5, VvGH3-1, and VvGH3-6 for IAA (Böttcher et al., 2012). OsGH3.8, VvGH3-1 and VvGH3-6 are also Group II GH3 enzymes; however, these enzymes are not reported to be active on SA or other benzoates.

As IAA is the dominant auxin, our further studies with GH3.5 focus on IAA as the auxin substrate. However, the ability of GH3.5 to act on a variety of naturally occurring auxin-like substrates is important, as they appear to play distinct roles in both plant development and in plant-microbe interactions (Hagemeier et al., 2001; Schlicht et al., 2013; Sugawara et al., 2015; Tao et al., 2008). In addition, conjugation and inactivation of synthetic auxins such as NAA by GH3.5 or related GH3s could evolve to limit the effect of synthetic auxins as herbicides (which inhibit the function of endogenous auxins). On the other hand, neutralization of synthetic auxin herbicides by engineered or bred plants with herbicide-specific GH3 activity could specifically promote growth of desired plants.

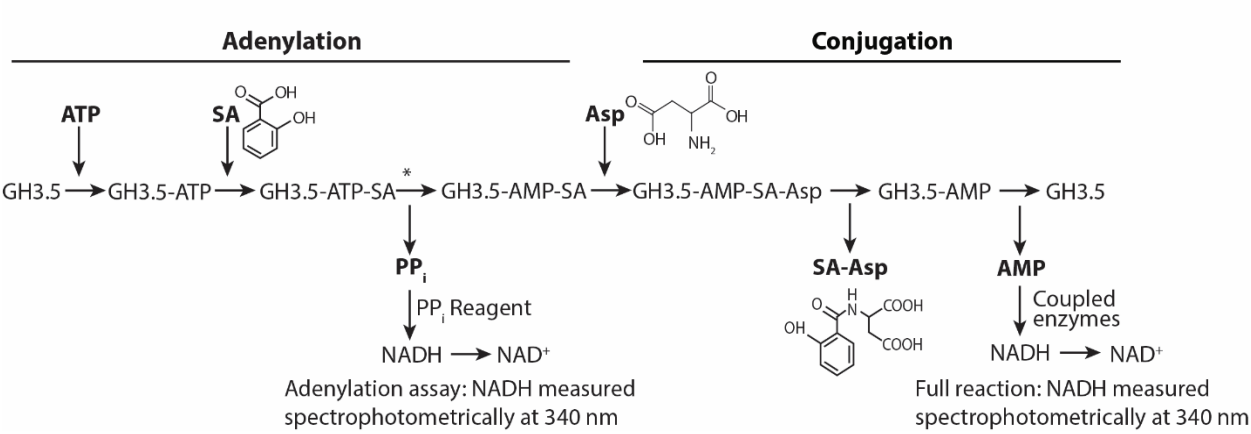

Figure 2.1: Progression of GH3.5 reaction
GH3.5 enzymatic activity, shown here with SA as the acyl substrate and Asp as the amino acid substrate, appears to proceed via a bi uni uni bi ping pong reaction mechanism: two substrates (ATP and SA) bind to the enzyme, one product (PP_i) leaves, another substrate (Asp) binds, and finally two products (SA-Asp and AMP) leave (Chen et al., 2010). The enzyme's C-terminus undergoes a 180° conformation change (*) prior to PP_i release (Westfall et al., 2016). The release of product at two distinct steps allows for measurement of the enzyme activity at two reaction points. Assays were done by either coupling the release of PP_i or AMP to loss of NADH (see methods). Modified from Chen et al., 2010.

A

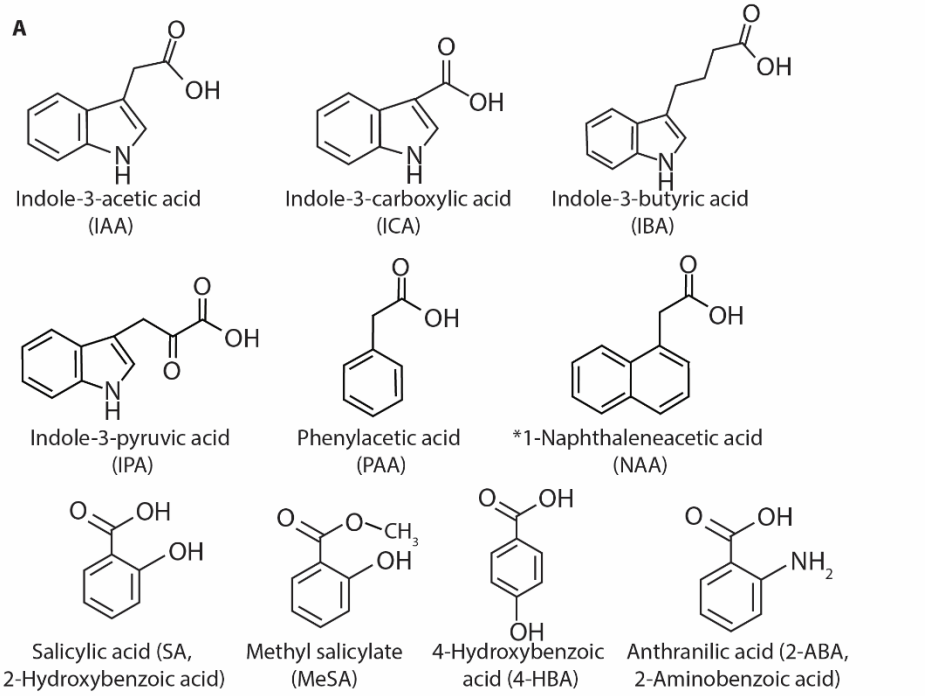

*synthetic auxin

B

	K_m (μM)	V_{max} (nmol * min^{-1} * μg^{-1})	k_{cat} (min^{-1})	k_{cat}/K_m (min^{-1} * mM^{-1})	katal (mol * s^{-1})
IAA	45 ± 11	66 ± 3	0.23	5.12	0.033
IBA	733 ± 172	88 ± 5	0.31	0.42	0.01
IPA	321 ± 94	98 ± 9	0.34	1.06	0.009
ICA	501 ± 86	96 ± 3	0.33	0.66	0.009
PAA	220 ± 59	53 ± 5	0.19	0.84	0.016
NAA*	211 ± 50	104 ± 8	0.36	1.29	0.011
SA	1171 ± 473	24 ± 4	0.08	0.07	0.035
4-HBA	404 ± 80	32 ± 2	0.11	0.27	0.027
MeSA	--	--	--	--	--
2-ABA	--	--	--	--	--

Figure 2.2: Kinetic parameters of GH3.5 adenylation of auxins and benzoates
(A) Structures of auxins (IAA, ICA, IBA, IPA, PAA, NAA) and benzoates (SA, MeSA, 4-HBA, and 2-ABA) assayed for activity with GH3.5. **(B)** Table showing auxin analogues (top) and benzoates (bottom) that were tested as acyl substrates of GH3.5 in adenylation reactions. Experiments were repeated 3 times, each in triplicate with similar results.

Kinetic parameters of GH3.5 adenylation on benzoate substrates

We found GH3.5 to have a much higher K_m (1171 µM) for SA compared with IAA, with 73-fold lower catalytic efficiency (Fig. 2.2B). Similarly, Westfall et al. (2016) reported a significantly lower catalytic efficiency with SA compared to IAA. In contrast to GH3.12/PBS3 which is active on multiple 4-subsituted benzoates (4-HBA and 4-ABA/pABA) (Okrent et al., 2009), we found GH3.5 was only active on SA (2-HBA), and not on 2-ABA/anthranilate (Fig. 2.2). Additionally, GH3.5 was also active on 4-HBA (Fig. 2.2), showing that GH3.5 substrate preference is not determined by substitution position. GH3.5 exhibited extremely low activity (just above control) with methyl salicylate (MeSA), a transported form of SA (S.-W. Park et al., 2007). However, due to its limited activity, we could not reliably calculate kinetic parameters with MeSA.

To gain further insight into GH3.5 acyl substrate preferences, we looked at the binding site using UCSF Chimera (Pettersen et al., 2004) to overlay the crystal structures for GH3.5 with AMP and IAA bound (Westfall et al., 2016) and PBS3 with AMP and SA (an inhibitor of PBS3) bound (Westfall et al., 2012). The PBS3 crystal structure shows the carboxylic acid group of SA is unable to bind to AMP as it is oriented in the opposite direction, bound to Tyr120 and Arg123. In GH3.5, Leu137 replaces Arg123 and our modeling shows Leu137 would be unable to hold SA in the nonproductive orientation. In addition, GH3.5 Met337 may spatially exclude SA from binding to GH3.5 in the inhibitory orientation, as it extends further into the binding pocket than the PBS3 analogue Thr324. Additional GH3 crystal structures coupled with kinetic characterization of wild type and site-directed mutants should further resolve residues that dictate inhibitory and productive acyl substrate binding in the active site.

GH3.5 utilizes Asp as its amino acid substrate

Thin layer chromatography end point assays suggested GH3.5 can conjugate Asp, Glu, and several other amino acids to IAA (Staswick et al., 2005). Using a high throughput kinetic assay for the full reaction (see methods), which is based on real time values of the final product AMP (Fig. 2.1), we determined that GH3.5 utilizes Asp as its preferred amino acid substrate (Fig. 2.3). Results with IAA or SA as the acyl substrate showed minimal activity with Glu. GH3.5 was also reported to conjugate ICA to Cys to form an intermediate in the synthesis of the phytoalexin camalexin (Wang et al., 2012). However, we saw no evidence for this activity using our full kinetic assay. Wang et al. (2012) incubated their reaction for 3 hours followed by endpoint product detection by UPLC/ESI-QTOF-MS. While debate continues on camalexin biosynthetic pathways (Geu-Flores et al., 2011; Klein et al., 2013; Møldrup et al., 2013; Su et al., 2013, 2011), our kinetic data indicate GH3.5 is not likely involved.

Using our high throughput kinetic full reaction assay, we next determined the K_m of GH3.5 for Asp with 1 mM IAA or SA. The K_ms of GH3.5 for Asp with IAA or SA are not significantly different, 414 µM and 371 µM, respectively (Table 2.1). For both SA and IAA, the concentration of Asp had to rise to greater than 1 mM for saturation to occur. Furthermore, physiologically-relevant concentrations of Asp (> 3mM) resulted in significant inhibition (~60% of V_{max}) of the full reaction with either IAA or SA, with further inhibition observed at higher [Asp]. OsGH3-8 also exhibited inhibition of the full reaction with IAA with Asp above 5 mM (Chen et al., 2009). Therefore, it is important that assessments of GH3 activity do not routinely employ high levels of amino acid substrates (i.e. >= 3 mM) as this could misrepresent acyl and amino acid substrate preference.

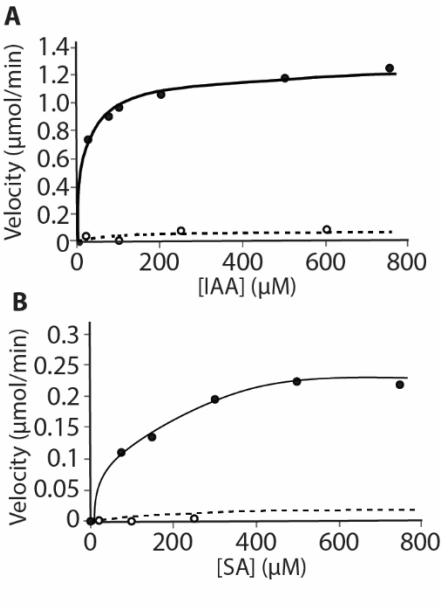

Figure 2.3: Asp is preferred to Glu as the amino acid substrate of GH3.5 with IAA and SA
Initial velocity measurements of GH3.5 activity show that Asp (•) is preferred to Glu (○) in conjugation reactions with **(A)** IAA and **(B)** SA. Experiments were repeated 3 times, each in triplicate with similar results.

	K_m (µM)	V_{max} (nmol * min^{-1} * μg^{-1})	K_{cat} (min^{-1})	k_{cat}/K_m (min^{-1} * mM^{-1})	katal (mol * s^{-1})
IAA	**414 ± 42**	**60.0 ± 2.3**	**0.83**	**2.01**	**0.014**
SA	**371 ± 72**	**15.4 ± 1.1**	**0.21**	**0.58**	**0.055**

Table 2.1: Kinetic parameters for Asp with IAA and SA in the full reaction
Independent experiments, run in triplicate, gave similar results.

GH3.5 Preference for IAA versus SA depends on Asp concentration

The cellular concentration of IAA, SA, and Asp varies with development and pathogen infection. Asp is required for protein synthesis, synthesis of the essential amino acids Lys, Thr, Met, and Ile, induced plant defense systemic signals such as pipecolic acid, and local nitrogen transport in source tissue (Galili, 2011; Less et al., 2010; Li et al., 2014; Návarová et al., 2012; Stuttmann et al., 2011; Vidal et al., 2014). Physiologically relevant values of Asp in plant leaves range from 0.12 mM to 3 mM based on analytical quantification and K_m values for plant enzymes that use Asp as a substrate (e.g. Curien et al., 2007; Lin and Wu, 2004; Miesak and Coruzzi, 2002; Návarová et al., 2012; Torre et al., 2006; Watanabe et al., 2013). Therefore, to provide insight on GH3.5 activity and function in a physiological context, we assessed GH3.5 kinetic parameters for the full reactions of IAA and SA at three relevant concentrations of Asp: 0.2, 1, and 2.5 mM Asp (Table 2.2A, Fig. 2.4A,B).

The full reactions with IAA resulted in similar K_ms for IAA of ~20 µM independent of [Asp]. V_{max} increases with [Asp], consistent with our reported K_m for Asp of 414 µM (**Table 1**) and failure to fully saturate at 1 mM Asp. However, with SA, we obtained an unexpected result. The K_m for SA increased dramatically with increasing [Asp], particularly at 2.5 mM Asp and V_{max} did not increase when [Asp] was increased from 1 to 2.5 mM. Functionally, this results in a 50-fold higher affinity for SA at low concentrations of Asp (i.e. 0.2 vs. 2.5 mM Asp). Catalytic efficiency of GH3.5 with SA is also more favorable, with 10-fold higher k_{cat}/K_m at 0.2 and 1 mM Asp than with 2.5 mM Asp. Comparison of GH3.5 preference for IAA vs. SA (Table 2B) shows a dramatic variation with [Asp], with 5-fold higher catalytic efficiency with IAA vs. SA at 0.2 mM Asp and 357-fold higher catalytic efficiency with IAA vs. SA at 2.5 mM Asp.

The double reciprocal plot with IAA and varied Asp shows parallel lines (Fig. 2.4C), consistent with results obtained for OsGH3-8 and a bi uni uni bi ping pong GH3 reaction mechanism (Chen et al., 2010). For SA, while the 0.2 mM Asp and 1 mM Asp double reciprocal plots have the same slope, the slope at 2.5 mM Asp is much steeper (Fig. 2.4D) suggestive of competitive inhibition under these conditions.

The crystal structure of GH3.5 (Westfall et al., 2016) is similar to other published GH3 crystal structures (Peat et al., 2012; Westfall et al., 2012). Based on these structures, it appears that the smaller C-terminal domain pivots 180° to move from open (ATP bound) to closed (AMP bound) conformations after the acyl substrate is adenylated (See Fig. 2.1). PP_i is likely released immediately after the conformation change because PP_i is a competitive inhibitor of Asp and a noncompetitive inhibitor of IAA and ATP (Chen et al., 2010). With the proposed GH3 bi uni uni bi ping pong reaction mechanism, Asp should not affect acyl substrate binding as the acyl substrate and amino acid substrate should bind to different forms of the enzyme (Chen et al., 2010) (Fig. 2.1). However, Asp and PP_i could act as competitive inhibitors of each other as they are predicted to bind the same form of the enzyme (Chen et al., 2010). We found no significant impact of Asp on SA adenylation measured as PP_i release (not shown), suggesting the SA-dependent impact of Asp at high concentrations may function after PP_i release. Clearly, the reaction profile is altered and deviates from standard Michaelis-Menten kinetics for the GH3.5 reaction with SA at 2.5 mM Asp (Fig. 2.4B). The crystal structure of GH3.5 does not include Asp, leaving us to speculate about the role of Asp in substrate-specific catalytic efficiency.

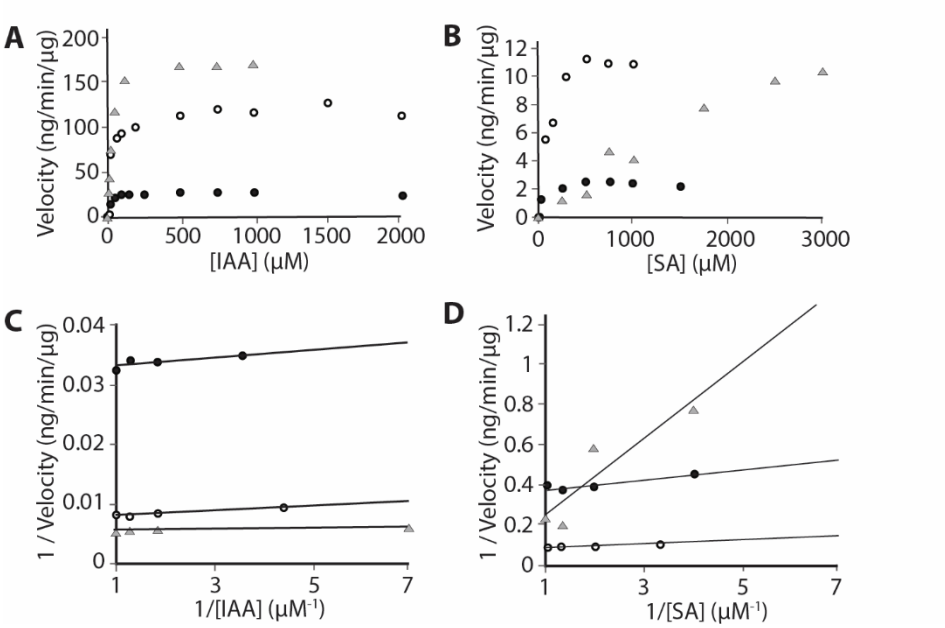

Figure 2.4: Initial velocity and reciprocal plots for IAA and SA full conjugation reactions by GH3.5

Concentration vs velocity plot for **(A)** IAA and **(B)** SA. While V_{max} is similar in **(B)** for 1 and 2.5 mM, the K_m is much greater with 2.5 mM Asp. Double reciprocal plots for **(C)** IAA and **(D)** SA showing 1/velocity vs 1/concentration acyl substrate, ranging from 0.125 – 1 mM, at fixed ATP (2.5 mM) concentration. Aspartate was varied between 0.2 mM (•), 1 mM (○) and 2.5 mM (▲). Parallel lines indicate a lack of competition between Asp and acyl substrate. High concentrations of Asp may lead to Asp competition with SA, but not IAA.

A

		Full Reaction				
		K_m (μM)	V_{max} (nmol * min^{-1} * μg^{-1})	K_{cat} (min^{-1})	k_{cat}/K_m (min^{-1} * mM^{-1})	katal (mol * s^{-1})
IAA	[Asp] = 0.2 mM	12 ± 3	29.5 ± 1.0	0.10	8.3	0.029
	[Asp] = 1 mM	22 ± 4	120 ± 2.8	0.42	19.2	0.007
	[Asp] = 2.5 mM	25 ± 1	179.4 ± 2.0	1.25	50.0	0.005
SA	[Asp] = 0.2 mM	23 ± 7	2.5 ± 0.1	0.04	1.6	0.336
	[Asp] = 1 mM	123 ± 23	13.6 ± 0.7	0.19	1.5	0.063
	[Asp] = 2.5 mM	1246 ± 344	12.5 ± 1.0	0.17	0.14	0.068

B

[Asp] (mM)	Catalytic Efficiency IAA/SA
0.2	5
1	13
2.5	357

Table 2.2: Kinetic Parameters of GH3.5 for IAA and SA in the full reaction with varied [Asp]

(A) Comparisons of kinetic parameters of IAA and SA with GH3.5 in the full reaction with varying concentrations of amino acid substrate. Reactions were repeated at least three times, in triplicate. Results showed similar trends, and a representative result is shown. Additionally, similar results were found with independent enzyme preps. **(B)** The catalytic efficiency (k_{cat}/K_m) for the full reaction of GH3.5 with IAA compared with SA increases with [Asp].

DISCUSSION

Herein, we demonstrate the novel finding that the amino acid concentration can affect the kinetics of a GH3 family enzyme. Mechanistically, this is quite notable. In the previously proposed GH3 bi uni uni bi ping pong reaction mechanism, Asp should not affect binding of the acyl substrate (Chen et al., 2010) (Fig. 2.1). Indeed, in our work it did not affect IAA. It did, however, affect SA in the full reaction, indicating that, after PP_i is released, Asp can affect the SA-AMP-GH3.5 intermediate, perhaps through alteration of the C-terminus pivot. While several GH3s have been surveyed in recent years, extensive profiling with varied amino acid concentrations has been lacking. We suggest that analysis of one amino acid concentration may miss other important information as to enzyme substrate preference

Expression data of Group II *GH3*s overlap with the expression of *GH3.5*, suggesting genetic redundancy and/or fine tuning via paralogous genes. Indeed, the lack of strong *gh3.5* mutant phenotype suggests an important role for genetic redundancy *in vivo* in the GH3 family, and potentially in other multi-step enzymatic reactions.

By integrating information on GH3.5 enzyme kinetics, described herein, with knowledge of IAA, SA, and Asp concentrations *in planta* and *GH3.5* expression patterns, we developed a model that illustrates the dual function of GH3.5 *in planta* to regulate auxin homeostasis during growth or salicylic acid homeostasis during defense (Figure 2.5).

Plant nitrogen flux through Asp may contribute to GH3.5 specificity

Asp is a central metabolic amino acid. It is the entry point for the Asp family metabolic pathway and, along with glutamate, glutamine, and asparagine, controls nitrogen flux through the plant (Gaufichon et al., 2013, 2010; Lea et al., 2007). Nitrogen mobilization is important not only during development, but also in plant-pathogen interactions as it affects pathogen access to nutrients and plant defense resource allocation (Brauc et al., 2011; Chandran et al., 2010; Gupta et al., 2013; Snoeijers et al., 2000; Wang et al., 2011; Winter et al., 2007). GH3.5 catalytic efficiency for IAA vs. SA is dependent on Asp, allowing nitrogen and source/sink status to act as a lever to control GH3.5 function in growth hormone vs. defense hormone homeostasis.

Kinetic and expression data of GH3.5 at auxin maxima supports concentration moderating role of GH3.5

GH3.5 kinetics show a K_m of ~20 □M for IAA independent of Asp concentration (**Table 2**). This IAA concentration is high and is associated with local IAA cellular maxima, for example with organ initiation and polar growth (Aloni et al., 2003; Bohn-Courseau, 2010; Marchant et al., 2002; Sabatini et al., 1999; Tanaka et al., 2006). Similarly, *GH3.5* is specifically expressed in these cells (Brady et al., 2007; Winter et al., 2007; Zhang et al., 2008). Approximate cellular concentrations for auxin are based on studies using the *DR5* promoter driving *GUS* gene expression (*DR5::GUS*), which has a functional range of 100 nM to 100 □M IAA (Sabatini et al., 1999; Ulmasov et al., 1997), the DII-VENUS sensor (1 nM to 1 □M IAA functional range; Brunoud et al., 2012) and GC-MS analysis of extracted plant tissue (e.g., Tam et al., 2000; Uggla et al., 1996). For example, *DR5::GUS* accumulates at the lateral root primordium (Mei et al., 2012) where *GH3.5* is expressed (Brady et al., 2007; Winter et al., 2007; Zhang et al., 2008). Taken together, these data strongly support a functional role for GH3.5 as a means of spatially and temporally limiting active auxin during organ initiation/polar growth through its irreversible conversion to the inactive IAA-Asp, which is designated for catabolism (Ostin et al., 1998; Woodward and Bartel, 2005).

The principal degradation pathways for auxin in *Arabidopsis* include the irreversible conversion of IAA to IAA-Asp or IAA-Glu via GH3 enzymes (Ostin et al., 1998; Staswick et al., 2005) and the oxidation of IAA via DIOXYGENASE FOR AUXIN OXIDATION 1 and 2 (AtDAO1/2) (Porco et al., 2016; Woodward and Bartel, 2005; Zhang et al., 2016). Consistent with our kinetic data for GH3.5 and model (Fig. 2.5), modeling of auxin homeostasis indicates that GH3-mediated degradation of auxin (e.g. to IAA-Asp) is critical to auxin homeostasis when [auxin] is high, whereas degradation via oxidation operates at low auxin levels (Mellor et al., 2016). The high rate of auxin conjugation to form IAA-Asp has long been noted in response to exogenously supplied auxin (e.g., Andreae and Good, 1955). And, a detailed examination of auxin metabolism rates as reported in Kramer and Ackelsberg, 2015 supports our kinetic studies and functional model (Fig. 2.5), suggesting that GH3.5 conjugation of IAA to IAA-Asp spatially controls local IAA maxima. As SA levels in developing tissue are very low (discussed further below), GH3.5 would not be active on SA. Moreover, given high [Asp] in developing tissue, the catalytic efficiency of GH3.5 is 357-fold higher with IAA vs. SA (Table 2).

Kinetic and expression data of GH3.5 at locally high levels of SA supports concentration moderating role of GH3.5

By contrast, our kinetic analyses indicate a role for GH3.5 in SA homeostasis under conditions when SA is elevated and auxin and Asp concentrations are low, such as during infection of mature leaves by (hemi)-biotrophic pathogens. Unless specifically produced/manipulated by the pathogen, [IAA] is very low in mature fully expanded leaves (Marchant et al., 2002; Staswick et al., 2005). By contrast, SA levels in leaves rise dramatically with infection by (hemi)-biotrophs (Dempsey et al., 2011).

Approximate cellular concentrations for SA have been deduced from analytical measurements of SA extracted from plant tissue (e.g., Meuwly and Metraux, 1993; Müller et al., 2002), expression *of PR-1::GUS* as a proxy for robust SA accumulation associated with local defense (Dempsey et al., 2011), and knowledge of the K_ms for enzymes that utilize SA as their *in planta* substrate. In tobacco, spatially resolved SA analysis in response to Tobacco Mosaic Virus or a fungal HR elicitor showed zones of concentration-dependent SA accumulation and associated defense response (Dorey et al., 1997; Huang et al., 2006). SA concentrations increased from below detection (0.1 µM) to 380 µM in localized spots preceding HR cell death (Huang et al., 2006). Cells in areas neighboring the HR site exhibited free SA of ~75-200 µM, consistent with robust local defense, while distal cells exhibited minimal SA (e.g. 10 µM) associated with defense priming or no appreciable SA. Furthermore, knowledge of the K_ms for SA of enzymes involved in SA priming (SA methyltranferase, K_m= 16 µM; Chen et al., 2003) or conjugating SA to reversible SA-glucosides as part of robust local defense (SA glucosyltransferases: K_m's ~200 µM; Lim et al., 2002; Song, 2006) support the approximate [SA] ranges and associated functional activities shown in Figure 2.5. Therefore, in response to (hemi)biotrophic pathogens, cellular SA concentrations are in the range of 4-400 µM depending on the specific pathogen-host interaction, the time frame, and specific cell.

***In planta* context for SA, Asp, and GH3.5 flux**

Our kinetic data for GH3.5 suggests that it could operate to mediate SA homeostasis in SA functional ranges involved in defense priming or local robust defense (Fig. 2.5). SA-Asp is not hydrolyzed back to active SA nor is it able to induce robust *PR-1* expression associated with local defense (Chen et al., 2013; Okrent and Wildermuth, unpublished). Therefore, conversion of

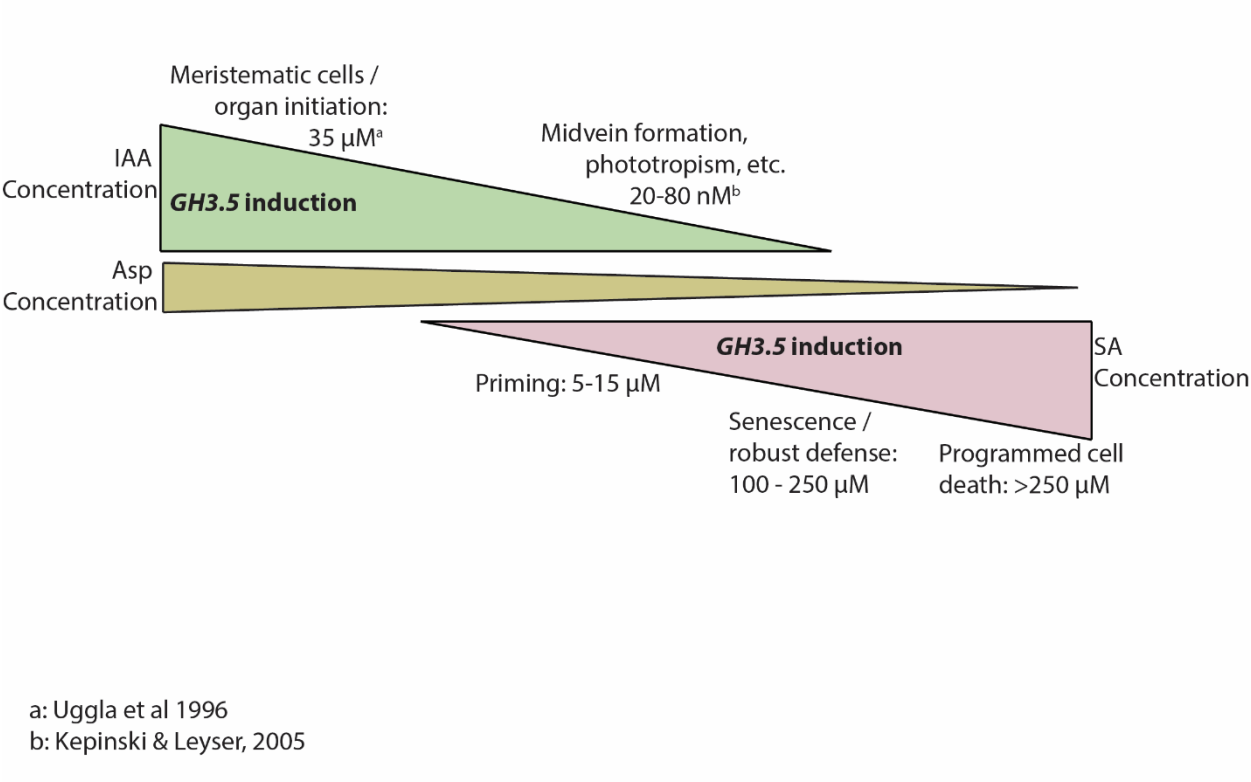

Figure 2.5: Model for GH3.5 function as a mediator of growth vs defense
Localized high levels of auxin are associated with meristematic cells, organ initiation, and polar growth, and *GH3.5* is specifically expressed in these cells. For leaves, younger developing leaves exhibit moderate levels of IAA and high Asp. As leaves mature and senescence and/or are infected by a pathogen, the concentrations of IAA and Asp decrease. By contrast, SA increases with senescence and is induced dramatically by (hemi)-biotrophic pathogens. *GH3.5* is also induced by these pathogens concordant with SA accumulation. The kinetics of GH3.5 dependence on Asp show a dramatic preference for IAA when Asp is high, consistent with GH3.5 function to regulate IAA homeostasis via conversion of IAA to inactive IAA-Asp during growth/development when both IAA and Asp are high. Decreasing Asp through age and/or stress creates more favorable conditions for GH3.5 conjugation of SA to SA-Asp, thereby controlling SA homeostasis and defense. See text for additional details.

SA to SA-Asp could irreversibly inactivate SA in specific cells, confining robust defense. It could even act to limit the extent of HR and PCD by converting accumulating free SA to SA-Asp, thereby preventing SA levels from rising to a threshold associated with PCD. Alternatively, as SA-Asp was able to induce very low level *PR-1* expression at levels associated with defense priming (Chen et al., 2013; Okrent and Wildermuth, unpublished) and there is a possibility that it is mobile (Chen et al., 2013), it could potentially act to promote defense priming within a leaf or systemically. Further research is needed to unravel the complexity of both SA homeostasis in general, and the role of GH3.5 in spatially and/or temporally influencing SA accumulation and defense.

CONCLUDING REMARKS

In summary, we show how GH3.5, with dual activity on IAA and SA, can integrate cellular metabolic status via Asp to provide fine control of growth vs. defense outcomes and hormone homeostasis (Fig. 2.5). While it would be desirable to have data of SA vs IAA for GH3.5 under variable Asp concentrations, our assay is unable to distinguish between IAA-Asp and SA-Asp formation. During active growth, [IAA] and [Asp] are high and the catalytic efficiency (k_{cat}/K_m) of GH3.5 for IAA is 360-fold higher than with SA. *GH3.5* is expressed under these conditions and conversion of IAA to inactive IAA-Asp would provide fine spatial and temporal control over local auxin developmental responses such as lateral root initiation. By contrast, [SA] is dramatically elevated in response to (hemi)-biotrophic pathogens. Under these conditions, [Asp] is low and GH3.5 has equal affinity (K_m) for SA and IAA with similar catalytic efficiencies. The concentration of IAA tends to be very low under these conditions, well below the K_m for IAA. *GH3.5* is induced by these pathogens and the elevated [SA] would favor GH3.5 catalyzed formation of SA-Asp, fine-tuning localized defensive responses.

ACKNOWLEDGEMENTS

We thank Michael Steinwand for assistance with protein modeling and critical review of the manuscript. This work was supported by a National Science Foundation (NSF) Graduate Research Fellowship to R.M., the UC Berkeley William Carrol Smith Graduate Research Fellowship in Plant Pathology to R.A.O., and NSF IOS-1449110 to M.C.W.

ADDENDUM

The work published above investigated the kinetics of GH3.5 with the hypothesis that *Arabidopsis PBS3* inhibits GH3.5 activity *in planta* and as a result increases the supply of SA, allowing for robust defense induction. As such, I also tested the ability of a product of PBS3 enzymatic activity, 4-HBA-Glu, to inhibit GH3.5 activity on IAA. IAA was used as opposed to SA because it had a higher Vmax and was easier to visualize. As SA inhibits PBS3 enzymatic activity with an inhibition constant of 15 µM (Okrent et al., 2009), I tested the ability of 10 and 35 µM of 4-HBA-Glu to inhibit IAA-Asp formation in the full kinetic reaction of GH3.5. 4-HBA-Glu did not inhibit GH3.5 activity (Fig. 2.6).

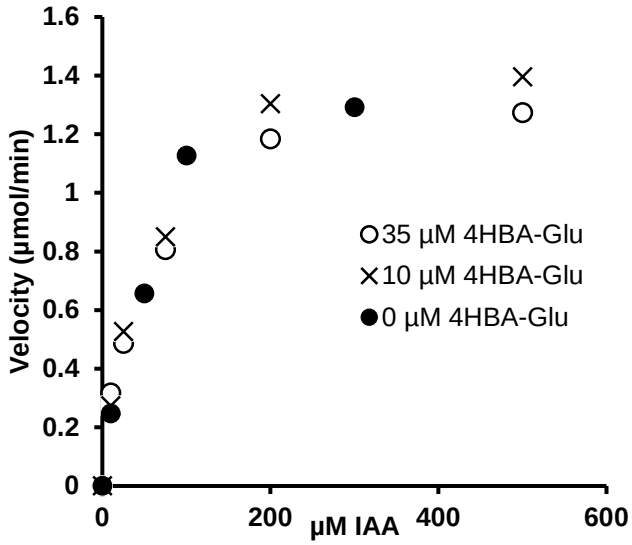

Figure 2.6: **4-HBA-Glu does not inhibit GH3.5 conjugation of IAA to Asp**

The PBS3 product, 4-HBA-Glu, was added to GH3.5 full reaction kinetic assays with IAA and Asp. 4-HBA-Glu does not inhibit GH3.5 activity at the concentrations tested.

REFERENCES

Adamowski, M., Friml, J., 2015. PIN-Dependent Auxin Transport: Action, Regulation, and Evolution. Plant Cell Online 27, 20–32. doi:10.1105/tpc.114.134874

Aloni, R., Schwalm, K., Langhans, M., Ullrich, C.I., 2003. Gradual shifts in sites of free-auxin production during leaf-primordium development and their role in vascular differentiation and leaf morphogenesis in Arabidopsis. Planta 216, 841–853. doi:10.1007/S00425-002-0937-8

Andreae, W.A., Good, N.E., 1955. The Formation of Indoleacetylaspartic Acid in Pea Seedlings. Plant Physiol. 30, 380–382.

Bohn-Courseau, I., 2010. Auxin: A major regulator of organogenesis. C. R. Biol. 333, 290–296. doi:10.1016/j.crvi.2010.01.004

Böttcher, C., Dennis, E.G., Booker, G.W., Polyak, S.W., Boss, P.K., Davies, C., 2012. A novel tool for studying auxin-metabolism: the inhibition of grapevine indole-3-acetic acid-amido synthetases by a reaction intermediate analogue. PLoS One 7, e37632. doi:10.1371/journal.pone.0037632

Bourne, D.J., Barrow, K.D., Milborrow, B. V., 1991. Salicyloylaspartate as an endogenous component in the leaves of Phaseolus vulgaris. Phytochemistry 30, 4041–4044.

Brady, S.M., Orlando, D.A., Lee, J.-Y., Wang, J.Y., Koch, J., Dinneny, J.R., Mace, D., Ohler, U., Benfey, P.N., 2007. A High-Resolution Root Spatiotemporal Map Reveals Dominant Expression Patterns. Science (80-.). 318, 801–806. doi:10.1126/science.1146265

Brauc, S., De Vooght, E., Claeys, M., Höfte, M., Angenon, G., 2011. Influence of over-expression of cytosolic aspartate aminotransferase on amino acid metabolism and defence responses against Botrytis cinerea infection in Arabidopsis thaliana. J. Plant Physiol. 168, 1813–9. doi:10.1016/j.jplph.2011.05.012

Brunoud, G., Wells, D.M., Oliva, M., Larrieu, A., Mirabet, V., Burrow, A.H., Beeckman, T., Kepinski, S., Traas, J., Bennett, M.J., Vernoux, T., 2012. A novel sensor to map auxin response and distribution at high spatio-temporal resolution. Nature 482, 103–106. doi:10.1038/nature10791

Canet, J. V., Dobón, A., Ibáñez, F., Perales, L., Tornero, P., 2010. Resistance and biomass in Arabidopsis: a new model for Salicylic Acid perception. Plant Biotechnol. J. 8, 126–141. doi:10.1111/j.1467-7652.2009.00468.x

Chandran, D., Inada, N., Hather, G., Kleindt, C.K., Wildermuth, M.C., 2010. Laser microdissection of Arabidopsis cells at the powdery mildew infection site reveals site-specific processes and regulators. Proc. Natl. Acad. Sci. U. S. A. 107, 460–5. doi:10.1073/pnas.0912492107

Chandran, D., Rickert, J., Huang, Y., Steinwand, M. a, Marr, S.K., Wildermuth, M.C., 2014. Atypical E2F transcriptional repressor DEL1 acts at the intersection of plant growth and immunity by controlling the hormone salicylic acid. Cell Host Microbe 15, 506–13.

doi:10.1016/j.chom.2014.03.007

Chen, F., D'Auria, J.C., Tholl, D., Ross, J.R., Gershenzon, J., Noel, J.P., Pichersky, E., 2003. An Arabidopsis thaliana gene for methylsalicylate biosynthesis, identified by a biochemical genomics approach, has a role in defense. Plant J. 36, 577–588. doi:10.1046/j.1365-313X.2003.01902.x

Chen, Q., Westfall, C.S., Hicks, L.M., Wang, S., Jez, J.M., 2010. Kinetic basis for the conjugation of auxin by a GH3 family indole-acetic acid-amido synthetase. J. Biol. Chem. 285, 29780–6. doi:10.1074/jbc.M110.146431

Chen, Q., Zhang, B., Hicks, L.M., Wang, S., Jez, J.M., 2009. A liquid chromatography-tandem mass spectrometry-based assay for indole-3-acetic acid-amido synthetase. Anal. Biochem. 390, 149–54. doi:10.1016/j.ab.2009.04.027

Chen, Y., Shen, H., Wang, M., Li, Q., He, Z., 2013. Salicyloyl-aspartate synthesized by the acetyl-amido synthetase GH3 . 5 is a potential activator of plant immunity in Arabidopsis. Acta Biochim Biophys Sin 45, 827–836. doi:10.1093/abbs/gmt078.Advance

Curien, G., Laurencin, M., Robert-Genthon, M., Dumas, R., 2007. Allosteric monofunctional aspartate kinases from *Arabidopsis*. FEBS J. 274, 164–176. doi:10.1111/j.1742-4658.2006.05573.x

Dempsey, D.A., Vlot, a C., Wildermuth, M.C., Klessig, D.F., 2011. Salicylic Acid biosynthesis and metabolism. Arabidopsis Book 9, e0156. doi:10.1199/tab.0156

Denancé, N., Sánchez-Vallet, A., Goffner, D., Molina, A., 2013. Disease resistance or growth: the role of plant hormones in balancing immune responses and fitness costs. Front. Plant Sci. 4, 155. doi:10.3389/fpls.2013.00155

Dewdney, J., Reuber, T.L., Wildermuth, M.C., Devoto, A., Cui, J., Stutius, L.M., Drummond, E.P., Ausubel, F.M., 2000. Three unique mutants of Arabidopsis identify eds loci required for limiting growth of a biotrophic fungal pathogen. Plant J. 24, 205–218. doi:10.1046/j.1365-313x.2000.00870.x

Dorey, S., Baillieul, F., Pierrel, M.-A., Saindrenan, P., Fritig, B., Kauffmann, S., 1997. Spatial and Temporal Induction of Cell Death, Defense Genes, and Accumulation of Salicylic Acid in Tobacco Leaves Reacting Hypersensitively to a Fungal Glycoprotein Elicitor. Mol. Plant-Microbe Interact. 10, 646–655. doi:10.1094/MPMI.1997.10.5.646

Fu, Z.Q., Yan, S., Saleh, A., Wang, W., Ruble, J., Oka, N., Mohan, R., Spoel, S.H., Tada, Y., Zheng, N., Dong, X., 2012. NPR3 and NPR4 are receptors for the immune signal salicylic acid in plants. Nature 486, 228–32. doi:10.1038/nature11162

Galili, G., 2011. The aspartate-family pathway of plants: linking production of essential amino acids with energy and stress regulation. Plant Signal. Behav. 6, 192–5.

Gaufichon, L., Masclaux-Daubresse, C., Tcherkez, G., Reisdorf-Cren, M., Sakakibara, Y., Hase, T., Clément, G., Avice, J.-C., Grandjean, O., Marmagne, A., Boutet-Mercey, S., Azzopardi, M., Soulay, F., Suzuki, A., 2013. Arabidopsis thaliana ASN2 encoding asparagine synthetase is involved in the control of nitrogen assimilation and export during vegetative

growth. Plant. Cell Environ. 36, 328–342. doi:10.1111/j.1365-3040.2012.02576.x

Gaufichon, L., Reisdorf-Cren, M., Rothstein, S.J., Chardon, F., Suzuki, A., 2010. Biological functions of asparagine synthetase in plants. Plant Sci. 179, 141–153. doi:10.1016/j.plantsci.2010.04.010

Geu-Flores, F., Møldrup, M.E., Böttcher, C., Olsen, C.E., Scheel, D., Halkier, B.A., 2011. Cytosolic γ-glutamyl peptidases process glutathione conjugates in the biosynthesis of glucosinolates and camalexin in Arabidopsis. Plant Cell 23, 2456–69. doi:10.1105/tpc.111.083998

Gupta, K.J., Brotman, Y., Segu, S., Zeier, T., Zeier, J., Persijn, S.T., Cristescu, S.M., Harren, F.J.M., Bauwe, H., Fernie, A.R., Kaiser, W.M., Mur, L.A.J., 2013. The form of nitrogen nutrition affects resistance against Pseudomonas syringae pv. phaseolicola in tobacco. J. Exp. Bot. 64, 553–68. doi:10.1093/jxb/ers348

Hagemeier, J., Schneider, B., Oldham, N.J., Hahlbrock, K., 2001. Accumulation of soluble and wall-bound indolic metabolites in Arabidopsis thaliana leaves infected with virulent or avirulent Pseudomonas syringae pathovar tomato strains. Proc. Natl. Acad. Sci. 98, 753–758. doi:10.1073/pnas.98.2.753

Huang, W.E., Huang, L., Preston, G.M., Naylor, M., Carr, J.P., Li, Y., Singer, A.C., Whiteley, A.S., Wang, H., 2006. Quantitative *in situ* assay of salicylic acid in tobacco leaves using a genetically modified biosensor strain of *Acinetobacter* sp. ADP1. Plant J. 46, 1073–1083. doi:10.1111/j.1365-313X.2006.02758.x

Jaillais, Y., Chory, J., 2010. Unraveling the paradoxes of plant hormone signaling integration. Nat. Struct. Mol. Biol. 17, 642–5. doi:10.1038/nsmb0610-642

Kepinski, S., Leyser, O., 2005. The Arabidopsis F-box protein TIR1 is an auxin receptor. Nature 435, 446–451.

Klein, A.P., Anarat-Cappillino, G., Sattely, E.S., 2013. Minimum set of cytochromes P450 for reconstituting the biosynthesis of camalexin, a major Arabidopsis antibiotic. Angew. Chem. Int. Ed. Engl. 52, 13625–8. doi:10.1002/anie.201307454

Kramer, E.M., Ackelsberg, E.M., 2015. Auxin metabolism rates and implications for plant development. Front. Plant Sci. 6, 150. doi:10.3389/fpls.2015.00150

Lea, P.J., Sodek, L., Parry, M.A.J., Shewry, P.R., Halford, N.G., 2007. Asparagine in plants. Ann. Appl. Biol. 150, 1–26. doi:10.1111/j.1744-7348.2006.00104.x

Less, H., Angelovici, R., Tzin, V., Galili, G., 2010. Principal transcriptional regulation and genome-wide system interactions of the Asp-family and aromatic amino acid networks of amino acid metabolism in plants. Amino Acids 39, 1023–8. doi:10.1007/s00726-010-0566-7

Li, Y., Krouk, G., Coruzzi, G.M., Ruffel, S., 2014. Finding a nitrogen niche: a systems integration of local and systemic nitrogen signalling in plants. J. Exp. Bot. 65, 5601–5610. doi:10.1093/jxb/eru263

Lim, E.-K., Doucet, C.J., Li, Y., Elias, L., Worrall, D., Spencer, S.P., Ross, J., Bowles, D.J.,

2002. The Activity of ArabidopsisGlycosyltransferases toward Salicylic Acid, 4-Hydroxybenzoic Acid, and Other Benzoates. J. Biol. Chem. 277, 586–592. doi:10.1074/jbc.M109287200

Lin, J.-F., Wu, S.-H., 2004. Molecular events in senescing *Arabidopsis* leaves. Plant J. 39, 612–628. doi:10.1111/j.1365-313X.2004.02160.x

Malamy, J., Car, J.P., Klessig, D.F., Raskin, I., 1990. Salicylic Acid: A Likely Endogenous Signal in the Resistance Response of Tobacco to Viral Infection. Science (80-.). 250, 1002–1004.

Marchant, A., Bhalerao, R., Casimiro, I., Eklöf, J., Casero, P.J., Bennett, M., Sandberg, G., 2002. AUX1 promotes lateral root formation by facilitating indole-3-acetic acid distribution between sink and source tissues in the Arabidopsis seedling. Plant Cell 14, 589–97. doi:10.1105/TPC.010354

Mei, Y., Jia, W.-J., Chu, Y.-J., Xue, H.-W., 2012. Arabidopsis phosphatidylinositol monophosphate 5-kinase 2 is involved in root gravitropism through regulation of polar auxin transport by affecting the cycling of PIN proteins. Cell Res. 22, 581–97. doi:10.1038/cr.2011.150

Mellor, N., Band, L.R., Pěnčík, A., Novák, O., Rashed, A., Holman, T., Wilson, M.H., Voß, U., Bishopp, A., King, J.R., Ljung, K., Bennett, M.J., Owen, M.R., 2016. Dynamic regulation of auxin oxidase and conjugating enzymes *AtDAO1* and *GH3* modulates auxin homeostasis. Proc. Natl. Acad. Sci. 113, 11022–11027. doi:10.1073/pnas.1604458113

Meuwly, P., Metraux, J.P., 1993. Ortho-Anisic Acid as Internal Standard for the Simultaneous Quantitation of Salicylic Acid and Its Putative Biosynthetic Precursors in Cucumber Leaves. Anal. Biochem. 214, 500–505. doi:10.1006/abio.1993.1529

Miesak, B.H., Coruzzi, G.M., 2002. Molecular and physiological analysis of Arabidopsis mutants defective in cytosolic or chloroplastic aspartate aminotransferase. Plant Physiol. 129, 650–60. doi:10.1104/pp.005090

Møldrup, M.E., Geu-Flores, F., Halkier, B.A., 2013. Assigning gene function in biosynthetic pathways: camalexin and beyond. Plant Cell 25, 360–7. doi:10.1105/tpc.112.104745

Müller, A., Düchting, P., Weiler, E., 2002. A multiplex GC-MS/MS technique for the sensitive and quantitative single-run analysis of acidic phytohormones and related compounds, and its application to Arabidopsis thaliana. Planta 216, 44–56. doi:10.1007/s00425-002-0866-6

Návarová, H., Bernsdorff, F., Döring, A.-C., Zeier, J., 2012. Pipecolic acid, an endogenous mediator of defense amplification and priming, is a critical regulator of inducible plant immunity. Plant Cell 24, 5123–41. doi:10.1105/tpc.112.103564

Okrent, R. a, Brooks, M.D., Wildermuth, M.C., 2009. Arabidopsis GH3.12 (PBS3) conjugates amino acids to 4-substituted benzoates and is inhibited by salicylate. J. Biol. Chem. 284, 9742–54. doi:10.1074/jbc.M806662200

Okrent, R. a, Wildermuth, M.C., 2011. Evolutionary history of the GH3 family of acyl adenylases in rosids. Plant Mol. Biol. 76, 489–505. doi:10.1007/s11103-011-9776-y

Ostin, a, Kowalyczk, M., Bhalerao, R.P., Sandberg, G., 1998. Metabolism of indole-3-acetic acid in Arabidopsis. Plant Physiol. 118, 285–96.

Park, J.-E., Park, J.-Y., Kim, Y.-S., Staswick, P.E., Jeon, J., Yun, J., Kim, S.-Y., Kim, J., Lee, Y.-H., Park, C.-M., 2007. GH3-mediated auxin homeostasis links growth regulation with stress adaptation response in Arabidopsis. J. Biol. Chem. 282, 10036–46. doi:10.1074/jbc.M610524200

Park, S.-W., Kaimoyo, E., Kumar, D., Mosher, S., Klessig, D.F., 2007. Methyl salicylate is a critical mobile signal for plant systemic acquired resistance. Science 318, 113–6. doi:10.1126/science.1147113

Peat, T.S., Böttcher, C., Newman, J., Lucent, D., Cowieson, N., Davies, C., 2012. Crystal structure of an indole-3-acetic acid amido synthetase from grapevine involved in auxin homeostasis. Plant Cell 24, 4525–38. doi:10.1105/tpc.112.102921

Pettersen, E.F., Goddard, T.D., Huang, C.C., Couch, G.S., Greenblatt, D.M., Meng, E.C., Ferrin, T.E., 2004. UCSF Chimera--a visualization system for exploratory research and analysis. J. Comput. Chem. 25, 1605–12. doi:10.1002/jcc.20084

Porco, S., Pěnčík, A., Rashed, A., Voß, U., Casanova-Sáez, R., Bishopp, A., Golebiowska, A., Bhosale, R., Swarup, R., Swarup, K., Peňáková, P., Novák, O., Staswick, P., Hedden, P., Phillips, A.L., Vissenberg, K., Bennett, M.J., Ljung, K., 2016. Dioxygenase-encoding AtDAO1 gene controls IAA oxidation and homeostasis in Arabidopsis. Proc. Natl. Acad. Sci. U. S. A. 113, 11016–21. doi:10.1073/pnas.1604375113

Rampey, R.A., Leclere, S., Kowalczyk, M., Ljung, K., Bartel, B., Biology, C., Texas, R.A.R., 2004. A Family of Auxin-Conjugate Hydrolases That Contributes to Free Indole-3-Acetic Acid Levels during Arabidopsis Germination 1. Plant Physiol. 135, 978–988. doi:10.1104/pp.104.039677.978

Rasmussen, J.B., Hammerschmidt, R., Zook, M.N., 1991. Systemic Induction of Salicylic Acid Accumulation in Cucumber after Inoculation with Pseudomonas syringae pv syringae. Plant Physiol. 97, 1342–7.

Robert-Seilaniantz, A., Grant, M., Jones, J.D.G., 2011a. Hormone crosstalk in plant disease and defense: more than just jasmonate-salicylate antagonism. Annu. Rev. Phytopathol. 49, 317–43. doi:10.1146/annurev-phyto-073009-114447

Robert-Seilaniantz, A., MacLean, D., Jikumaru, Y., Hill, L., Yamaguchi, S., Kamiya, Y., Jones, J.D.G., 2011b. The microRNA miR393 re-directs secondary metabolite biosynthesis away from camalexin and towards glucosinolates. Plant J. 67, 218–231. doi:10.1111/j.1365-313X.2011.04591.x

Sabatini, S., Beis, D., Wolkenfelt, H., Murfett, J., Guilfoyle, T., Malamy, J., Benfey, P., Leyser, O., Bechtold, N., Weisbeek, P., Scheres, B., 1999. An Auxin-Dependent Distal Organizer of Pattern and Polarity in the Arabidopsis Root. Cell 99, 463–472. doi:10.1016/S0092-8674(00)81535-4

Schlicht, M., Ludwig-Müller, J., Burbach, C., Volkmann, D., Baluska, F., 2013. Indole-3-butyric acid induces lateral root formation via peroxisome-derived indole-3-acetic acid and nitric

oxide. New Phytol. 200, 473–82. doi:10.1111/nph.12377

Snoeijers, S.S., Pérez-García, A., Joosten, M.H.A.J., Wit, P.J.G.M. De, 2000. The Effect of Nitrogen on Disease Development and Gene Expression in Bacterial and Fungal Plant Pathogens. Eur. J. Plant Pathol. 106, 493–506. doi:10.1023/A:1008720704105

Song, J.T., 2006. Induction of a Salicylic Acid Glucosyltransferase, AtSGT1, Is an Early Disease Response in Arabidopsis thaliana. Mol. Cells 22, 233–238.

Spoel, S.H., Dong, X., 2012. How do plants achieve immunity? Defence without specialized immune cells. Nat. Rev. Immunol. 12, 89–100. doi:10.1038/nri3141

Staswick, P.E., Serban, B., Rowe, M., Tiryaki, I., 2005. Characterization of an Arabidopsis Enzyme Family That Conjugates Amino Acids to Indole-3-Acetic Acid. Plant Cell 17, 616–627. doi:10.1105/tpc.104.026690.1

Staswick, P.E., Tiryaki, I., Rowe, M.L., 2002. Jasmonate Response Locus JAR1 and Several Related Arabidopsis Genes Encode Enzymes of the Firefly Luciferase Superfamily That Show Activity on Jasmonic , Salicylic , and Indole-3-Acetic Acids in an Assay for Adenylation. Plant Cell 14, 1405–1415. doi:10.1105/tpc.000885.defect

Steffan, H., Ziegler, A., Rapp, A., 1988. N-salicyloyl-aspartic acid: A new phenolic compound in grapevines. Vitis 27, 79–86.

Stuttmann, J., Hubberten, H.-M., Rietz, S., Kaur, J., Muskett, P., Guerois, R., Bednarek, P., Hoefgen, R., Parker, J.E., 2011. Perturbation of Arabidopsis amino acid metabolism causes incompatibility with the adapted biotrophic pathogen Hyaloperonospora arabidopsidis. Plant Cell 23, 2788–803. doi:10.1105/tpc.111.087684

Su, T., Li, Y., Yang, H., Ren, D., 2013. Reply: complexity in camalexin biosynthesis. Plant Cell 25, 367–70. doi:10.1105/tpc.113.109975

Su, T., Xu, J., Li, Y., Lei, L., Zhao, L., Yang, H., Feng, J., Liu, G., Ren, D., 2011. Glutathione-indole-3-acetonitrile is required for camalexin biosynthesis in Arabidopsis thaliana. Plant Cell 23, 364–80. doi:10.1105/tpc.110.079145

Sugawara, S., Mashiguchi, K., Tanaka, K., Hishiyama, S., Sakai, T., Hanada, K., Kinoshita-Tsujimura, K., Yu, H., Dai, X., Takebayashi, Y., Takeda-Kamiya, N., Kakimoto, T., Kawaide, H., Natsume, M., Estelle, M., Zhao, Y., Hayashi, K.-I., Kamiya, Y., Kasahara, H., 2015. Distinct Characteristics of Indole-3-Acetic Acid and Phenylacetic Acid, Two Common Auxins in Plants. Plant Cell Physiol. 56, 1641–54. doi:10.1093/pcp/pcv088

Tam, Y.Y., Epstein, E., Normanly, J., 2000. Characterization of auxin conjugates in Arabidopsis. Low steady-state levels of indole-3-acetyl-aspartate, indole-3-acetyl-glutamate, and indole-3-acetyl-glucose. Plant Physiol. 123, 589–96.

Tanaka, H., Dhonukshe, P., Brewer, P.B., Friml, J., 2006. Spatiotemporal asymmetric auxin distribution: a means to coordinate plant development. Cell. Mol. Life Sci. 63, 2738–2754. doi:10.1007/s00018-006-6116-5

Tao, Y., Ferrer, J.-L., Ljung, K., Pojer, F., Hong, F., Long, J.A., Li, L., Moreno, J.E., Bowman, M.E., Ivans, L.J., Cheng, Y., Lim, J., Zhao, Y., Ballaré, C.L., Sandberg, G., Noel, J.P.,

Chory, J., 2008. Rapid synthesis of auxin via a new tryptophan-dependent pathway is required for shade avoidance in plants. Cell 133, 164–76. doi:10.1016/j.cell.2008.01.049

Torre, F., Santis, L. De, Suárez, M.F., Crespillo, R., Cánovas, F.M., 2006. Identification and functional analysis of a prokaryotic-type aspartate aminotransferase: implications for plant amino acid metabolism. Plant J. 46, 414–425. doi:10.1111/j.1365-313X.2006.02713.x

Uggla, C., Moritz, T., Sandberg, G., Sundberg, B., 1996. Auxin as a positional signal in pattern formation in plants. Proc. Natl. Acad. Sci. U. S. A. 93, 9282–9286. doi:10.1073/pnas.93.17.9282

Ulmasov, T., Murfett, J., Hagen, G., Guilfoyle, T.J., 1997. Aux/IAA proteins repress expression of reporter genes containing natural and highly active synthetic auxin response elements. Plant Cell 9, 1963–71. doi:10.1105/tpc.9.11.1963

Vanneste, S., Friml, J., 2009. Auxin: a trigger for change in plant development. Cell 136, 1005–16. doi:10.1016/j.cell.2009.03.001

Vidal, E.A., Moyano, T.C., Canales, J., Gutierrez, R.A., 2014. Nitrogen control of developmental phase transitions in Arabidopsis thaliana. J. Exp. Bot. 65, 5611–5618. doi:10.1093/jxb/eru326

Vlieghe, K., Boudolf, V., Beemster, G.T.S., Maes, S., Magyar, Z., Atanassova, A., de Almeida Engler, J., De Groodt, R., Inzé, D., De Veylder, L., 2005. The DP-E2F-like Gene DEL1 Controls the Endocycle in Arabidopsis thaliana. Curr. Biol. 15, 59–63. doi:10.1016/j.cub.2004.12.038

Wang, M., Liu, X., Chen, Y., Xu, X., Yu, B., Zhang, S., 2012. Involvement in Camalexin Biosynthesis through Conjugation of Indole-3-Carboxylic Acid and Cysteine and Upregulation of Camalexin Biosynthesis Genes 54, 471–485. doi:10.1111/j.1744-7909.2012.01131.x

Wang, W., Barnaby, J.Y., Tada, Y., Li, H., Tör, M., Caldelari, D., Lee, D., Fu, X.-D., Dong, X., 2011. Timing of plant immune responses by a central circadian regulator. Nature 470, 110–114. doi:10.1038/nature09766

Watanabe, M., Balazadeh, S., Tohge, T., Erban, A., Giavalisco, P., Kopka, J., Mueller-Roeber, B., Fernie, A.R., Hoefgen, R., 2013. Comprehensive Dissection of Spatiotemporal Metabolic Shifts in Primary, Secondary, and Lipid Metabolism during Developmental Senescence in Arabidopsis. PLANT Physiol. 162, 1290–1310. doi:10.1104/pp.113.217380

Westfall, C.S., Sherp, A.M., Zubieta, C., Alvarez, S., Schraft, E., Marcellin, R., Ramirez, L., Jez, J.M., 2016. Arabidopsis thaliana GH3.5 acyl acid amido synthetase mediates metabolic crosstalk in auxin and salicylic acid homeostasis. Proc. Natl. Acad. Sci. U. S. A. 113, 13917–13922. doi:10.1073/pnas.1612635113

Westfall, C.S., Zubieta, C., Herrmann, J., Kapp, U., Nanao, M.H., Jez, J.M., 2012. Structural basis for prereceptor modulation of plant hormones by GH3 proteins. Science 336, 1708–11. doi:10.1126/science.1221863

Wildermuth, M.C., Dewdney, J., Wu, G., Ausubel, F.M., 2001. Isochorismate synthase is

required to synthesize salicylic acid for plant defence. Nature 414, 562–5. doi:10.1038/35107108

Winter, D., Vinegar, B., Nahal, H., Ammar, R., Wilson, G. V, Provart, N.J., 2007. An "Electronic Fluorescent Pictograph" browser for exploring and analyzing large-scale biological data sets. PLoS One 2, e718. doi:10.1371/journal.pone.0000718

Woodward, A.W., Bartel, B., 2005. Auxin: regulation, action, and interaction. Ann. Bot. 95, 707–35. doi:10.1093/aob/mci083

Wu, Y., Zhang, D., Chu, J.Y., Boyle, P., Wang, Y., Brindle, I.D., De Luca, V., Després, C., 2012. The Arabidopsis NPR1 protein is a receptor for the plant defense hormone salicylic acid. Cell Rep. 1, 639–47. doi:10.1016/j.celrep.2012.05.008

Zhang, J., Lin, J.E., Harris, C., Campos Mastrotti Pereira, F., Wu, F., Blakeslee, J.J., Peer, W.A., 2016. DAO1 catalyzes temporal and tissue-specific oxidative inactivation of auxin in Arabidopsis thaliana. Proc. Natl. Acad. Sci. U. S. A. 113, 11010–5. doi:10.1073/pnas.1604769113

Zhang, Z., Li, Q., Li, Z., Staswick, P.E., Wang, M., Zhu, Y., He, Z., 2007. Dual regulation role of GH3.5 in salicylic acid and auxin signaling during Arabidopsis-Pseudomonas syringae interaction. Plant Physiol. 145, 450–64. doi:10.1104/pp.107.106021

Zhang, Z., Wang, M., Li, Z., Li, Q., He, Z., 2008. Arabidopsis GH3.5 regulates salicylic acid-dependent and both NPR1-dependent and independent defense responses. Plant Signal. Behav. 3, 537–42.

CHAPTER III: Altered SA metabolism in *Arabidopsis thaliana* mutants of the GH3 acyl adenylase *PBS3* is independent of ICS1 and insufficient to explain *pbs3* pathogen susceptibility

PREFACE

This work has been submitted for publication to the *The Plant Journal* and is included herein with permission from the authors.

For this work, I identified the candidate SA-Asp synthetases (Table 3.S1) and created the *pbs3gh3.5* double mutant and the *gh6x* sextuple mutant line using *pbs3* and the *gh3.1gh3.3gh3.4gh3.5gh3.6* pentuple mutant. I performed experiments and quantified the accumulation of SA, SA-Asp, and *PR1* expression in these lines (Figure 3.6). I tested the impact of metabolites on pathogen growth in Col-0 and *pbs3* (Fig. 3.7). With M.W., I performed analysis on previously published data (see Figure 3.S7), wrote the manuscript, and created the model (Fig. 3.8).

AUTHORS

Okrent[1]*, Rachel A., Mackelprang[1]*, Rebecca, Marr[1], Sharon K., Burgess[1], Diane, Wong[1], Alyssa, Cohn[1], Megan, Huang[1], Yingxiang, Staswick[2], Paul, [3]Simmons, Eric, and Wildermuth[1], Mary C.

*co-first authors:

[1]Department of Plant and Microbial Biology, University of California, Berkeley

[2]Department of Agronomy and Horticulture, University of Nebraska, Lincoln

[3] Department of Chemistry, University of California, Berkeley

Corresponding Author email: mwildermuth@berkeley.edu

ABSTRACT

The *Arabidopsis thaliana* GH3 acyl adenylase PBS3 promotes active salicylic acid (SA) defense hormone accumulation and response. *Pbs3* mutants exhibit dramatically reduced total SA glucoside (SAG) accumulation, expression of the SA-dependent *pathogenesis-related* (PR) *PR-1* gene, and resistance to *Pseudomonas syringae*. However, reports of the impact of PBS3 disruption on free SA accumulation have been inconsistent. To investigate the role of PBS3 in SA metabolism and response, we used UV-C treatment to reproducibly assess early and late phases of SA synthesis and response. An initial peak in expression of the SA biosynthetic gene *isochorismate synthase 1* (*ICS1*) at 1-2 hours post treatment (hpt) is followed by a second peak at 18 hpt, accompanied by SAG formation and robust *PR-1* expression. ICS1 protein expression parallels *ICS1* transcript for both WT and *pbs3* mutants, even though both free SA and SAG accumulation are compromised in *pbs3*. Metabolite analyses focused on chorismate-derived compounds found SAG and SA-Asp, an inactive form of SA, to be dramatically impacted in *pbs3*. While SAG is reduced, SA-Asp is 17-fold elevated in induced *pbs3* compared to WT. However, reduction of induced SA-Asp to WT levels in *pbs3* via genetic disruption of SA-Asp synthetases does not restore WT active SA accumulation or response phenotypes. While

exogenous SA does reduce *P. syringae* growth in *pbs3*, it does not fully restore bacterial growth to WT levels. We posit that in addition to regulating induced SA metabolism downstream of ICS1, PBS3 also controls antagonism between SA and other hormone/defense pathways.

INTRODUCTION

In response to (hemi)-biotrophic pathogens and abiotic stressors including ozone and UV-C, the phytohormone salicylic acid (SA) accumulates and induces robust gene expression associated with defense and stress tolerance (Vlot et al., 2009). In *Arabidopsis*, the bulk of induced SA is synthesized from chorismate via isochorismate synthase 1 (ICS1, also known as SID2 and EDS16; AT1g74710; Garcion et al., 2008; Wildermuth et al., 2001) and induced *ICS1* expression correlates with SA accumulation (see Strawn et al., 2007). Free SA may then be modified to form SA glucosides, which act as non-toxic storage forms of SA, methyl salicylate (a more volatile form of SA involved in transporting the SA signal to distal leaves), and irreversibly to salicyloyl-L-aspartate (SA-Asp), 2,3-dihydroxybenzoic acid (2,3-DHBA) and 2,5-DHBA (Dempsey et al. 2011). SA-Asp, 2,3-DHBA, and 2,5-DHBA are very week inducers of SA responses and likely act as SA catabolites (Chen et al. 2013; Zhang et al. 2013; Zhang et al. 2017). The concentration and locale of active phytohormone is finely regulated, with multiple levels of control and integration with other phytohormone networks (Jaillais and Chory, 2010; Mackelprang et al., 2017; Robert-Seilaniantz et al., 2011; Pieterse et al., 2012; Woodward and Bartel, 2005). Despite the importance of SA, our understanding of the regulatory and biochemical mechanisms underlying its activity and function is limited, lagging behind knowledge of growth hormones such as auxin.

AvrPphB Susceptible 3 (*PBS3*; also known as *GDG1*, *WIN3*, and *GH3.12*; At5g13320) a member of the GH3 family of acyl adenylase thioester forming enzymes, is essential for total (free SA plus SA glucosides) SA accumulation and robust defense responses (e.g. expression of *pathogenesis related 1*; *PR-1;* At2g14610) when challenged with bacterial pathogens (Jagadeeswaran et al., 2007; Lee et al., 2008, 2007; Nobuta et al., 2007; Warren et al., 1999). A mechanism for this drastic effect on defense induction has not been identified. GH3 family proteins, of which there are 19 in *Arabidopsis thaliana*, conjugate acyl acid substrates to amino acids. Investigation of the biochemical activity of PBS3 identified 4-substituted benzoic acids and glutamic acid as its major substrates (Okrent et al., 2009). Neither the accumulation of 4-substituted benzoic acids in *pbs3* nor the accumulation of 4-substited benzoic acid-Glu conjugates in Col-0 (WT) are known to affect plant defense responses to an extent that would yield the *pbs3* phenotype (see Anderson et al., 2014). Enzymatic assays and analysis of the PBS3 crystal structure show that SA (2-hydroxybenzoic acid) inhibits PBS3, likely reflective of feedback to fine tune the induced SA response (Okrent et al., 2009; Westfall et al., 2012).

Identification of a protein's position in a signaling pathway can yield insight into its function. PBS3 is predicted to act upstream of ICS1, as application of exogenous SA rescues *pbs3* phenotypes of reduced *PR-1* expression (Nobuta et al., 2007) and resistance to *Pseudomonas syringae* (Jagadeeswaran et al., 2007). Wang et al. 2008 transcriptionally profiled defense-related genes 24 hpt with virulent *P. syringae* in several defense gene mutants including *pbs3*, *pad4*, *eds1*, and *ics1*. Clustering analysis placed PBS3 downstream of the SA network regulators Phytoalexin Deficient 4 (PAD4, At3g52430) and Enhanced Disease Susceptibility 1 (EDS1; At3g48090). PAD4 and EDS1 are lipase-like proteins that interact to promote SA accumulation and corresponding defense signaling (e.g. Cui et al. 2017). Wang et al. 2011 found

similar results with global transcriptional profiling, again placing PBS3 upstream of ICS1 and downstream of PAD4/EDS1 in the SA defense network.

Herein, we present a method to temporally resolve an early phase of free SA synthesis (priming) from a later phase accompanied by robust SA glucoside formation and SA-dependent defense gene expression (amplification). SA induction and metabolism is generally studied in response to pathogens, and thus plant genetic and metabolic changes are obscured by pathogen interference. Treatment with 5,000 J/m^2 UV-C enabled our exploration of controls over Arabidopsis induced SA metabolism and regulation in isolation, finding parallel biphasic *ICS1* transcription and translation. Although both early and later phases of SA accumulation are dramatically reduced in *pbs3, ICS1* transcript and protein levels are unaltered, indicating PBS3 acts downstream of ICS1 to promote SA accumulation. We use biochemical analyses and transcriptional profiling to identify potential roles of PBS3 in SA metabolism and explore the effect of an SA metabolite, SA-Asp, that accumulates in *pbs3* infected with avirulent *P. syringae* but not in WT. SA-Asp does not activate SA defense responses (i.e. *PR-1* expression) suggesting it is an SA catabolite. Furthermore, SA-Asp does not enhance pathogen growth. Taken together with previously published work of others, we propose that in the early, SA priming phase of response, PBS3, like PAD4 operates downstream of ICS1. PBS3 and PAD4, along with its binding partner EDS1 then, in the second/amplification phase of response, appear to act coordinately to promote the robust accumulation of active forms of SA (SA and SAG) and expression of SA defense genes such as *PR-1*. While PAD4/EDS1 appears to act upstream of ICS1 in this phase of response, our model suggests PBS3 functions downstream of ICS1 inhibiting SA catabolism (e.g. to SA-Asp) and SA response antagonism (e.g. by jasmonic acid; JA). Exogenous SA treatment does not limit *P. syringae* growth in *pbs3* to WT levels supporting an additional role for PBS3 in plant immunity beyond its impact on SA metabolism and response.

METHODS

All specialty reagents and chemicals were obtained from Sigma-Aldrich unless otherwise specified. HPLC-grade solvents (EMD Biosciences) were employed in all metabolite analyses.

Plant growth and treatment conditions:

Arabidopsis thaliana Columbia-0 plants *pbs3-2*, *pad4-1*, *ndr1-1*, and *eds5-1* mutants were grown in MetroMix 200 (Scott, Marysville, OH, USA) in a controlled environment chamber (22ºC, 70+% relative humidity, 100-150 µE m^{-2} sec^{-1} fluorescent illumination) on a 12-hr-light/12-hr-dark cycle. At three weeks flats were fertilized with ¼ strength Hoagland's solution. Mature rosette leaves of 4-5 week old plants were syringe-inoculated with virulent *P. syringae* pv. *maculicola* ES4326 (*Pma*) or avirulent *Pma* and *P. syringae* pv. *tomato DC3000 (*Pto*)* strains carrying *avrRpt2* as described by Volko (1998). For UV-C treatment, 4-5 week old plants were treated with UV-C by irradiation in a UV (254 nm) Stratalinker 1800 (Stratagene) with a dose of 5 kJ m^{-2}; control plants were placed in the Stratalinker for the equivalent amount of time without a dose. UV-C and infections were performed at 9 am, unless otherwise specified.

Quantitative real-time PCR analysis:

RNA from 2-3 fully expanded mature leaves was ground to a fine powder in liquid nitrogen with Trizol (Invitrogen) per manufacturer's instructions. 2 µg RNA were treated with 0.5 units of DNase I (Invitrogen) and cDNA was synthesized from oligo dT primers using 20 units of RNaseOut (Invitrogen) and 100 units of SuperScriptIII (Invitrogen) in a final volume of

20 μl per manufacturer's instructions. Real-time PCR reactions were performed using an Opticon 4 quantitative PCR instrument (MJResearch) with iQSYBR Green supermix (BioRad) for Figure 3.1 and Figure 3.S2 and ABI 7300 Prism with SYBR Premix Ex Taq (TaKaRa #RR041A) for Figure 3.S2, 3.S3, 3.5B. Three technical replicates were performed for each cDNA sample analyzed. Plasmid standard curves were used for quantification and RNA expression was normalized to ubiquitin 5. Gene-specific primers are provided in Supplemental Material.

Development of anti-ICS1 Antibody:

Purified recombinant mature ICS1 protein was obtained as described in (Strawn et al., 2007). Rabbit polyclonal anti-ICS1 antibody was made by immunizing rabbits with the purified ICS1 protein. The titer and specificity of the antibody were tested by immunoblot analysis. The antibody can detect as low as 31 pg of ICS1.

Western Blotting:

Leaves were weighed at time of sample collection, flash frozen in liquid nitrogen and stored at –80°C. Frozen leaves were ground in gel loading buffer (100 μl buffer per 100 mg fresh weight; 140 mM Tris HCl, pH 6.8 , 4.5 % SDS, 400 mM B-ME, 0.02% bromophenol blue, 23% glycerol) for Figure 3.1, 3.S2, 3.S3. For Figure 3.4 and 3.S4, frozen leaves were ground in cold PE buffer (50 mM Tris-HCl 7.5, 150 mM NaCl, 10 mM MgCl2, 5 mM EDTA, 10% glycerol, 0.6 mM PMSF, 0.6 mM NEM, 1 ug/ml Pepstatin A, 50 ug/ml TLCK, 50 ug/ml TPCK) and combined with sample loading buffer (to final concentration of 125 mM Tris-HCl pH 6.8, 5% SDS, 25% glycerol, 0.125 % bromophenol blue) prior to electrophoresis. Samples were electrophoresed on 8% polyacrylamide SDS gels and transferred to PVDF membrane (Immobilon-Psq, Millipore). Blots were probed with primary anti-ICS1 antibody (1/10,000 dilution) and secondary goat anti-rabbit conjugated horseradish peroxidase antibody (1/3,000 dilution; Bio-Rad) and developed using SuperSignal West Dura Extended Duration Substrate (Pierce). Total protein was visualized by Ponceau staining of blot.

Salicylic acid and camalexin quantitation:

Total salicylic acid (free and glucose-conjugated) and camalexin was extracted from 0.2-0.5 grams of leaves and quantified by HPLC with fluorescence detection as described (Strawn, et al 2007). Recovery was determined for each sample by spiking with *o*-anisic acid before leaf extraction.

Metabolite analysis:

Preliminary experiments included treatments included UV-C (3 hpt, 12 hpt), *Pto* (72 hpt), and *Pst avrRpt2* (24 hpt). No significant, reproducible differences in cell wall bound metabolites were identified. Extraction of cell-wall bound metabolites was performed as described in (Hagemeier et al., 2001) with a few modifications (**Supplemental Methods**). The most significant, reproducible differences in soluble metabolites were observed in response to *Pto avrRpt2* at 24 hpt; therefore, further purification of the peak of interest (B), below, used that protocol.

Mature leaves of 4.5 week plants were syringe inoculated with 0.0001 *Pto avrRpt2*. Frozen leaf samples (approximately 0.5 g) were ground to a powder in a prechilled mortar and pestle using liquid nitrogen. The ground leaf material was transferred to a glass tube and suspended in 3 mL of 90% MeOH. Samples were vortexed, sonicated in a water bath sonicator for 20 min, and centrifuged at 5,000 rpm for 15 min at 4°C. The supernatant was transferred to a new tube and the brown pellet was resuspended in 2 mL 90% MeOH with vortexing. This

suspension was sonicated for 20 min and centrifuged for 15 min at 4°C. The two supernatants from each sample were combined, vortexed to mix and transferred to a new tube. The solvent was evaporated using a dry vacuum at approximately 5 Torr. Suspensions in 2 mL 25 mM potassium phosphate (KH_2PO_4) buffer, pH 2.5, were loaded onto an solid phase extraction (SPE) column (Biotage Isolute 101, 200 mg bed, 6mL capacity), washed with 3 mL buffer plus 1% methanol, and eluted sequentially with 2 x 0.5 mL and 2 x 1mL 1% acetic acid in 80% methanol. The eluates were dried, then resuspended in 160 – 180 μL 20% MeOH or starting HPLC buffer, vortexed, sonicated for 20 min, and filtered through a 0.22 μM syringe filter (Millipore) and analyzed by HPLC. HPLC separation of leaf extracts was performed on a Shimadzu SCL-10A system with a Shimadzu RF-10A scanning fluorescence detector and a Shimadzu SPD-M10A photodiode array detector. Samples were separated on a 5-μm, 15 cm x 4.6-mm i.d. Supelcosil LC-ABZ Plus column (Supelco) preceded by a LC-ABZ Plus guard column maintained at 27°C. Prior to loading the 50-μL sample, the column was equilibrated with 5% acetonitrile in 25 mM KH_2PO_4, pH 2.5, at a flow rate of 1.0 mL/min. After 10 min, the concentration of acetonitrile was increased linearly to 43% over 25 min, followed by isocratic flow at 43% for 5 min, followed by a linear decrease from 43% to 5% over 3 min, and isocratic flow at 5% for 5 min.

Identification of Peak of Interest (Compound B):

Metabolite extraction was similar to that described above, except the starting samples were 1 – 2 g. Samples are extracted into 2 x 5 mL 90% MeOH, which was evaporated under vacuum. Extracts were prepared for injection onto the HPLC column as above. For the first round of purification, samples were separated on a 5-μm, 15 cm x 4.6-mm i.d. Supelcosil LC-ABZ Plus column (Supelco) preceded by a LC-ABZ Plus guard column maintained at 27°C. Prior to loading the 50 μL sample, the column was equilibrated with 5% acetonitrile in 25 mM ammonium formate, pH 2.8, at a flow rate of 1.0 mL/min. After 7 min, the concentration of acetonitrile was increased linearly to 48% over 23 min, followed by isocratic flow at 43% for 5 min, a linear decrease from 43% to 5% over 3 min, and isocratic flow at 5% for 5 min. For the second round of purification, samples were separated on a 5-μm, 15 cm x 4.6-mm i.d. Altech C18 column with the same buffer and method as in the first round. Fractions corresponding to the peak of interest were collected using an automatic fraction collector, pooled, and concentrated. Peaks were detected using the fluorescence detector set to 305/407. Synthesized SA-Asp, SA-Glu, 4-HBA-Glu, and 4-HBA-Asp were used as standards as detailed in Supplemental Methods. LC-Mass spectrometry (MS) analysis was performed at the Stanford Mass Spectrometry Facility (Stanford University, USA) on the purified concentrated peak of interest using a Thermo Fisher Surveyor HPLC with a Phenomenex Gemini C18 150 mm x 2.1mM, 5 μM column and 0.1% formic acid with an acetonitrile gradient elution scheme similar to that above and optimized for separation and detection of the four standards above. MS analysis was optimized for the standards using the Thermo Fisher LCQ Classic Mass Spectrometer with electrospray ionization (ESI) positive and negative ion switching, data dependent scan, and dynamic exclusion analysis.

Quantification of SA-Asp:

For quantification of SA-Asp, extraction was done as described above with methanol extraction, drying down, and extraction on SPE column. Samples were run on the HPLC with a 5 μm, 15 cm x 4.6 mm inner diameter Prevail C18 column (Alltech) preceded by a 7.5 cm x 4.6 mm guard column. The column was pre-equilibrated with 5% acetonitrile in 25 mM formic acid, pH 2.8 at a flow rate of 1.0 mL/min and run isocratically for 7 minutes after loading sample. For

23 minutes, acetonitrile was increased linearly from 5% to 52%, followed by isocratic flow for five minutes and linear decrease from 52% to 5% Can over 3 minutes, followed by isocratic flow for 4 minutes.

Measurement of bacterial growth:

4-5 week old plants were inoculated with *Pma* ES4326 with a dose of A_{600} = 0.0002. After infiltrating (0 DPI) or 72 hours later (3 DPI), two 0.7 cm leaf discs were taken from a leaf one using a cork borer, representing one replicate. Each condition/genotype represent 3 leaves from 3 plants, thus n = 9. Leaf discs were washed with ddH2O, then ground in 10 mM $MgSO_4$ using a bead beater at room temperature. Dilution series were pipetted onto King's Broth plates with Strep 100 and 36-48 hours later, colonies were counted. Data are reported as means and standard deviations of 9 replicates. Bacterial growth assays were performed at least twice with similar results.

RESULTS

UV-C induces biphasic SA response as measured by *ICS1* transcript, protein, and SA accumulation

Early and late phases of SA response to pathogens and abiotic stresses have long been reported (Horvath and Chua, 1996; Mur et al., 1997; Uquillas et al., 2004). However, most studies focus on either early or late phases of SA response, often with different systems, limiting an integrated dissection of SA metabolism and response. Ultraviolet C (UV-C) had been previously utilized as an inducer of SA metabolism and response, with early induction of the SA transporter *EDS5* by 2 hrs post treatment (hpt) and robust expression of *PR-1* at 24 hpt (e.g. Nawrath and Metraux, 2002). Building on these findings, we developed a 72 hour, 13 point time course using UV-C at a dose of 5000 J/m^2 that reproducibly results in a temporally resolved biphasic SA response.

The SA biosynthetic gene *ICS1* exhibits an early peak of expression at 1-3 hours post treatment (hpt) with UV-C (Fig. 3.1A, 3.2C). The transcriptional response is paralleled by ICS1 protein accumulation with an initial peak at 3-4 hpt (Fig. 3.1B) accompanied by a corresponding peak in the accumulation of free SA (Fig. 3.1C). The initial (early) peak of *ICS1* expression is associated with free SA synthesis followed by a return to pre-induced levels. To ensure that the observed early peak of *ICS1* expression is not due to a time-of-day effect, we examined its expression after UV-C treatment performed at 9 am (our standard treatment time; see Methods), 3:00 pm, and 9:00 pm. As shown in Figure 3.S1, the early phase of *ICS1* expression in response to UV-C is independent of the time of day and does not require light. Furthermore, there is no difference in *ICS1* expression in response to a mock treatment at any of these time points.

The second (late) peak of UV-C induced *ICS1* expression typically occurs at 18 hpt (Fig. 3.1A) with an associated sustained peak in ICS1 protein accumulation at 18-36 hpt (Fig. 3.1B). Total SA measurements include free SA and hydrolyzed SA glucosides (SAG) typically dominated by SA-2-O-B-D-glucoside (George Thompson et al., 2017). SAG appears to be a reversible non-toxic storage form of SA and the combination of free SA and SAG is taken to represent active total SA (Dempsey et al., 2011). We found free SA associated with the late peak of SA response appears to be readily converted to SAG which accumulates to >20-fold higher levels than does free SA (Fig. 3.1C,D, 3B,C). The robust expression of the SA-associated defense gene *PR-1* is only observed in this second phase of response; it is highly induced at 18 hpt and typically peaks at 24-48 hpt (Fig. 3.1E, 3.2D, 3.3D).

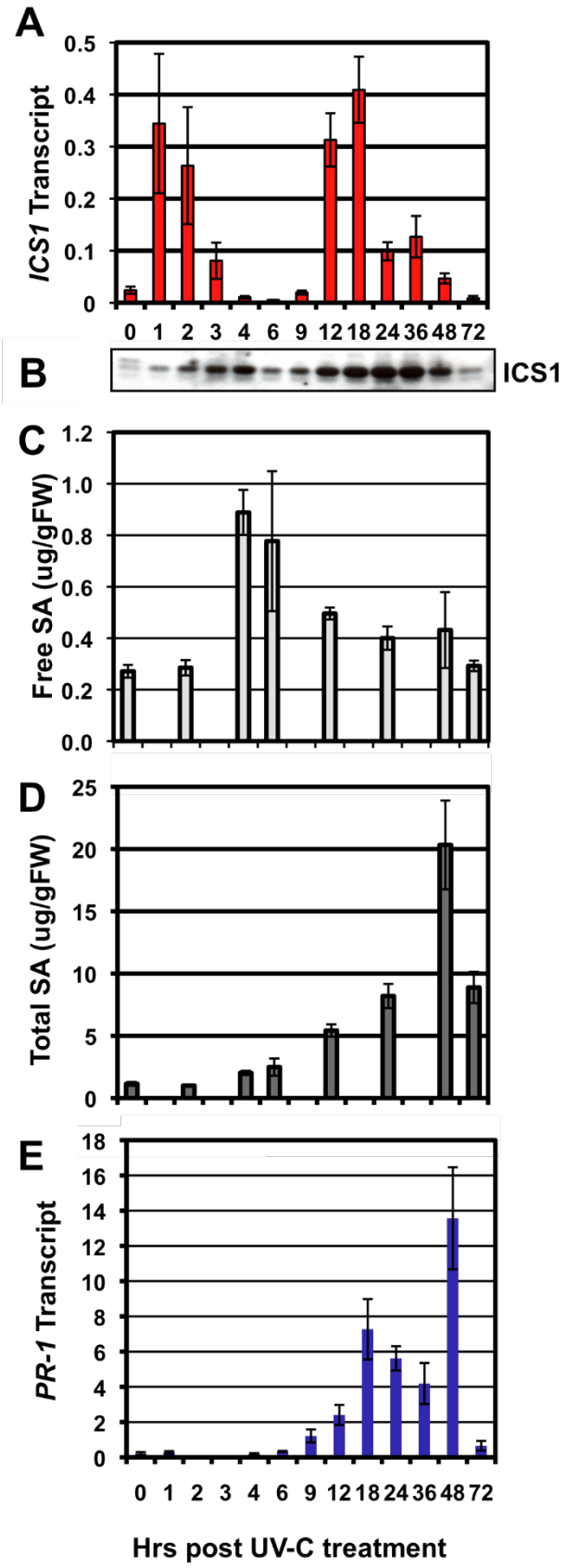

Figure 3.1. UV-C system separates initial free SA synthesis from SA glucoside formation and SA-dependent gene expression in wild type *Arabidopsis thaliana* Col-0.

ICS1 transcript (A) and protein (B) show a parallel biphasic response to UV-C. Free SA (C) and total SA (free SA plus SA glucosides) (D) in response to UV-C using HPLC with fluorescence detection. *PR-1* transcript is shown in (E). Transcripts were assessed by qPCR and normalized to *UBIQUITIN5*. Equal protein was loaded for Westerns. Mean values are shown with standard deviations, with n=3. Independent experiments gave similar results.

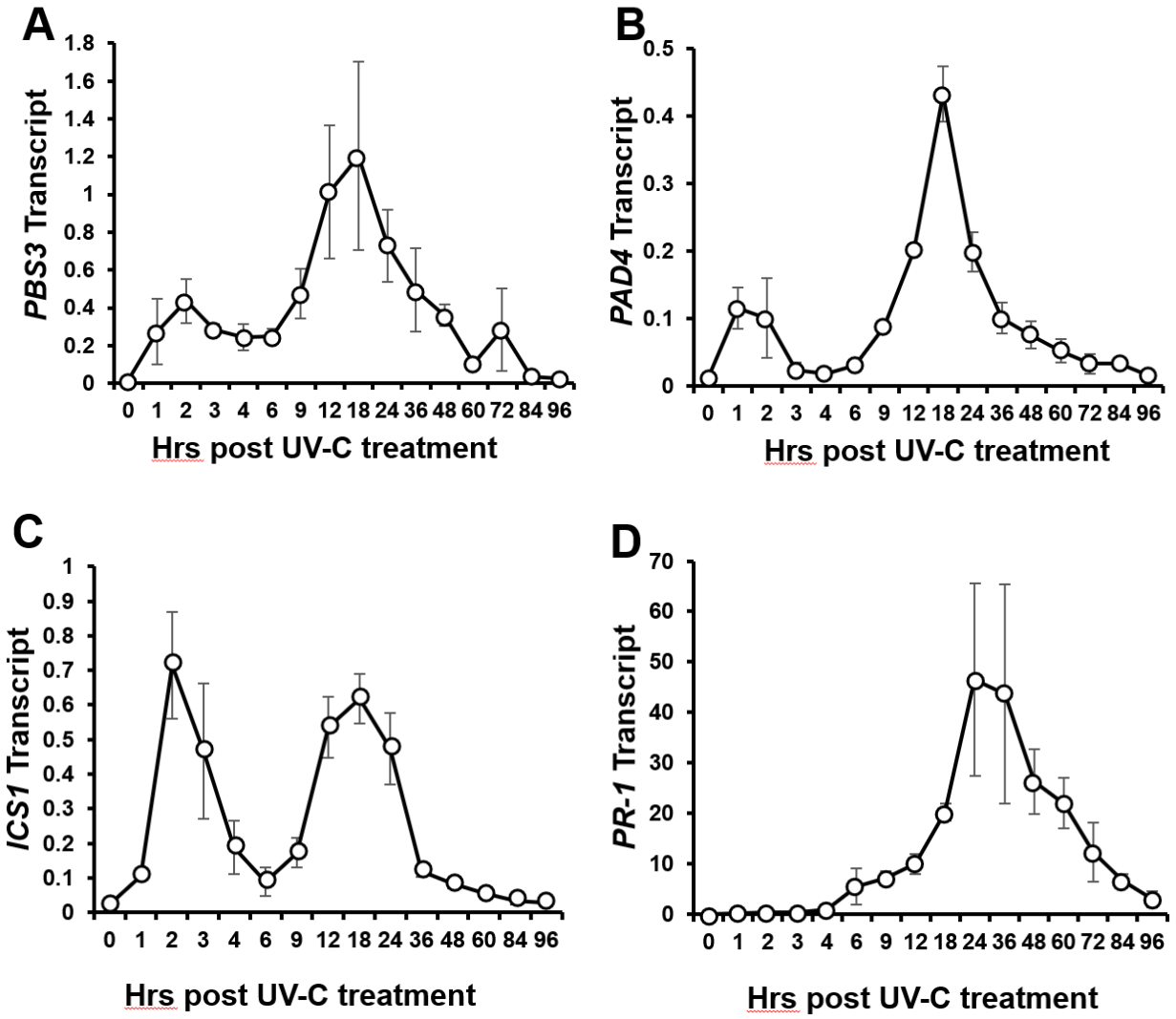

Figure 3.2. UV-C system distinguishes early and late phases of gene induction and identifies impact of mutations in genes known to mediate SA metabolism/response. qPCR analysis of *PBS3* (A) and *PAD4* (B) expression in Col-0 follows biphasic pattern. Averages shown from three independent experiments with standard error. qPCR of *ICS1* (C, E) and *PR-1* expression (D, F) in *pbs3* compared with *ics1* and *eds5* mutants that are associated with SA biosynthesis (C,D) and *pad4* and *ndr1* that regulate *ICS1* expression and SA accumulation (E,F). Transcripts were normalized to *Ubiquitin5*. Mean is shown, n≥3.

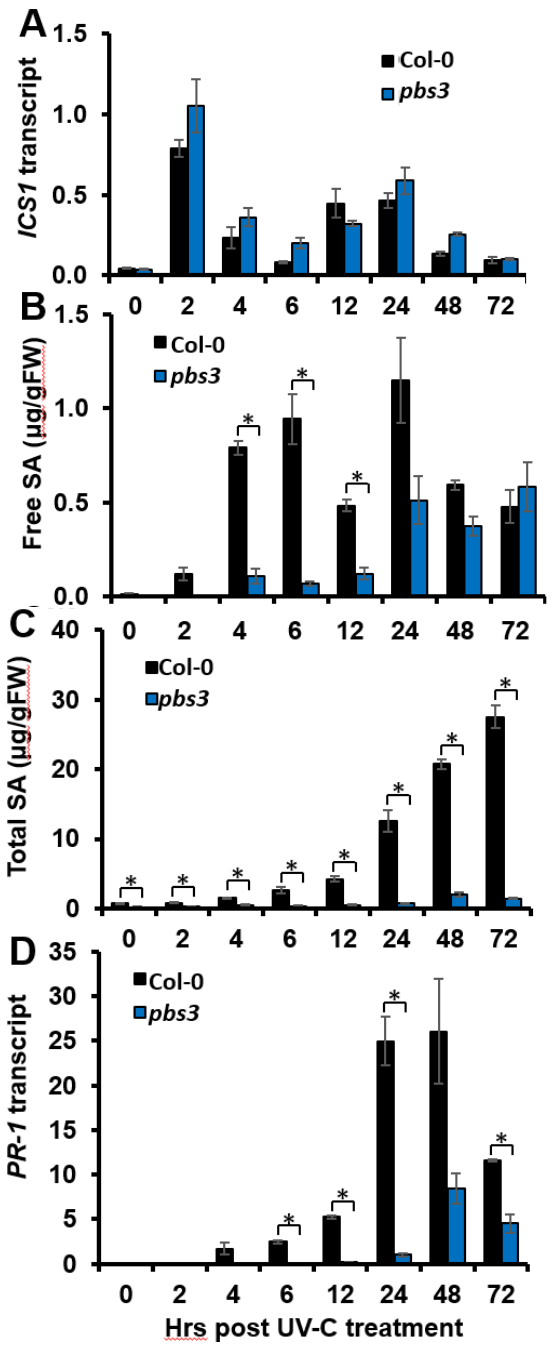

Figure 3.3. Comparison of responses to UV-C in wild type vs. *pbs3-2* null mutant plants. *ICS1* transcript (A) is similar in wt and *pbs3*. Free SA (B) and total SA (free SA plus SA glucosides, (C)) assessed using HPLC with fluorescence detection differs dramatically in *pbs3*, as does *PR-1* expression (D). Transcripts were assessed by qPCR and normalized to *Ubiquitin5*. Mean values from two experiments are shown with standard error. * indicates $p<0.05$

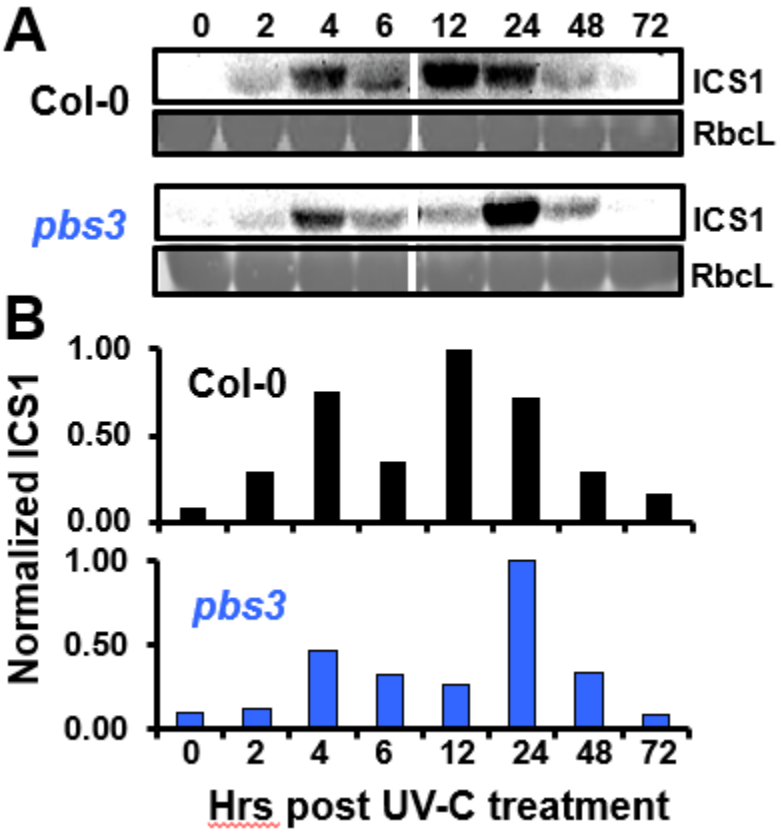

Figure 3.4. ICS1 protein expression in response to UV-C is similar in wild type and *pbs3-2* mutant plants.
(A) Western blots are shown for samples from same experiment as Figure 3.3. Equal amounts of protein (18 µg) were loaded. Western blots were adjusted in the same manner before compiling with all adjustments made to entire blot. Col-0 time points and *pbs3* time points were on separate blots, with signal normalized to each other using quantitation software in imager. RbcL is shown as an indicator of total protein. The lane between samples 6 and 12 hpt was excluded, indicated as a break. (B) Normalization by quantitation software with highest band set to 1.0. In general, ICS1 expression in *pbs3* followed the same pattern as in Col, but typically with equal or a bit more protein in *pbs3*. In the second independent experiment, shown in Fig. 3.S4, ICS1 expression peaked at 4 and 24 hpt for both Col and *pbs3*. For some replicates, subsets of the time points for Col and *pbs3* were probed in the same blot for direct comparison of protein levels. At least two biological replicates were assessed by Western; one is shown here and a repeat is shown as Supplemental Figure 3.4.

Compound	Class	Identity	UV maxima	Fluorescence	RT	Characteristics
A	Benzoate	Salicylic acid glucoside	210, 310	305/407	11.6	Reduced in *pbs3* pathogen treated
B	Unknown	Unknown	N/A	305/407	22.2	Elevated in *pbs3* pathogen treated
C	Unknown	Unknown	325	305/407	27.8	Elevated in *pbs3* pathogen treated

Set 1

Compound	Col-0		*pbs3*		Col-0 *Pto* AvrRpt2		*pbs3 Pto* AvrRpt2	
	Avg Peak Area*	STDEV†	Avg Peak Area*	STDEV†	Avg Peak Area*	STDEV†	Avg Peak Area*	STDEV†
A	10540320	8454180	1348291	778178	15848072	2031549	1463739	1106381
B	894360	13266	806836	69353	251649	39194	6189536	1923741
C	308103	73255	20563	11442	330839	282592	1105175	239142

Set 2

Compound	Col-0		*pbs3*		Col-0 *Pto* AvrRpt2		*pbs3 Pto* AvrRpt2	
	Avg Peak Area*	STDEV†	Avg Peak Area*	STDEV†	Avg Peak Area*	STDEV†	Avg Peak Area*	STDEV†
A	14705208	2476977	2130594	249863	12110812	7005030	2200320	1120670
B	275968	249384	506373	134030	880637	1045457	8206744	2893605
C	234520	277037	209499	144854	301389	426229	2611791	1425995

Table 3.1: Metabolites with reproducibly altered accumulation in Col-0 vs *pbs3* infected with *P. syringae* pv. *tomato* DC3000 AvrRpt2.
Characteristics of soluble metabolites with altered expression in *pbs3* compared with WT. Leaves were infiltrated with *Pto* AvrRpt2 at a dose of OD_{600} = 0.0001 and collected 24 hpt. Methanol extracts were analyzed by HPLC with photodiode array and fluorescence detection. Data from two independent experimental replicates is shown.

We also assessed whether a temporally resolved biphasic SA response is observed in response to a virulent *Pseudomonas syringae* pathogen (Fig. 3.S2). ICS1 protein and transcript accumulate in parallel in response to virulent *P. syringae* (Fig. 3.S2A,B). Furthermore, the pattern of SA response, with *PR-1* expression paralleling robust total active SA accumulation is maintained in response to *P. syringae* (Fig. 3.S2C-E). This suggests that coordinated *ICS1* transcription and protein synthesis also drive SA synthesis in response to *P. syringae*. Although there is likely a biphasic response, the early (initial) peak of SA response is not as reproducible as in response to UV-C (Fig. 3.1, 3.S2, 3.S3). This is likely due to variance in the timing and magnitude of bacterial growth in a given experiment, despite utilizing highly controlled conditions (see Methods). Similarly, ICS1 accumulation in response to avirulent *P. syringae* is also more variable than in response to UV-C, although an early increase in ICS1 protein is observed consistently 3-4 hpt (Fig. 3.S3).

PBS3 expression in response to UV-C is biphasic with an amplified late response, similar to *PAD4*

While PBS3 is essential for robust total active SA accumulation and defense, its location in defense signaling remains unresolved. UV-C induction of a biphasic SA response is highly reproducible and it removes the (often unknown) complexity associated with pathogen-host crosstalk. Transcriptional profiling of *PBS3* in response to UV-C found it exhibits a reproducible biphasic expression pattern with an early peak at 2 hpt and a late peak at 18 hpt similar to *ICS1* (Fig. 3.2A). However, in contrast to *ICS1*, *PBS3* reproducibly exhibits elevated expression in the late peak of SA response compared to the early peak. Because the regulator PAD4 has been implicated in amplification of the SA response (Feys et al., 2001; Jirage et al., 1999), we also profiled its expression. We found *PAD4* like *PBS3* exhibits biphasic induction in response to UV-C with timing that parallels that of *ICS1* and an amplified later peak of expression that correlates with robust SA-associated defense gene expression assessed via *PR-1* (Fig. 3.2B).

Disruption of *PBS3* dramatically limits free SA and SAG accumulation but does not alter ICS1 transcript or protein expression.

To further examine the impact of PBS3 on SA metabolism, we compared *ICS1* expression, *PR-1* expression, and free and glucose-conjugated SA levels in *pbs3* and WT plants in response to UV-C (Fig. 3.3). There is no reproducible change in ICS1 transcript or protein levels between *pbs3* and WT plants (Fig. 3.3, 3.4, 3.S4). However, free and total active SA (free SA plus SAG) are dramatically impacted. Free SA accumulation in *pbs3* is greatly reduced at early time points with no significant early peak in free SA accumulation (Fig. 3.3B). Indeed, it is not until 24 hpt that free SA levels in *pbs3* rise significantly above WT uninfected (time 0) values. Note that there is no reproducible statistically significant difference in free SA levels at later time points 24-72 hpt. However, total active SA is dramatically and consistently reduced in *pbs3* compared to WT plants for all time points. It is not until 48 hpt that total SA in *pbs3* is statistically higher than uninduced WT levels (time 0). Furthermore, the maximal average value for total SA in *pbs3* is 3 ug/gFW at 48 hpt, compared with WT values of 22 ug/gFW at 48 hpt and 27 ug/gFW at 72 hpt (Fig. 3.3C). Robust *PR-1* expression in WT plants is associated with the late peak in SA response and robust total SA accumulation (Fig. 3.3), similar to Figure 3. 1. However, *PR-1* expression is dramatically reduced and delayed in *pbs3* compared with WT (Fig. 3.3D). Taken together, these results show *pbs3* is dramatically compromised in both early and late phases of UV-C induced active SA accumulation and response. Our time course data also

explains how different labs (Nobuta et al., 2007; Lee et al., 2007; Jagadeeswaran et al., 2007) could obtain different results for free SA in *pbs3* compared to WT depending on the time-point and phase of response sampled. This alteration in induced active SA accumulation and response in *pbs3* is not due to a change in ICS1 transcript or protein expression. How then might PBS3 function to impact SA accumulation and response?

Metabolite analysis identified SA-2-O-B-D-glucoside and SA-Asp as the dominant compounds with altered expression in induced *pbs3* plants compared to WT

PBS3 is a GH3 acyl adenylase thio-ester forming enzyme that catalyzes the conjugation of favored amino acids (e.g. Glu) to 4-substituted benzoates (e.g. 4-hydroxybenzoic acid; 4-HBA) but not 2-substituted benzoates such as SA (Okrent et al., 2009). 4-HBA-Glu has not been identified in *Arabidopsis*, although 4-HBA has been shown to accumulate in the cell wall in response to pathogens (Hagemeier et al., 2001; Tan et al., 2004). 4-HBA is an intermediate in the synthesis of ubiquinone and can be incorporated into lignin (Lu et al., 2004; Okada et al., 2004; Swiezewska, 2004). Similar to SA, 4-HBA is synthesized from chorismate; however, neither the complete biosynthetic pathway for SA nor 4-HBA has been defined (Dempsey et al., 2011; Siebert et al., 1996; Smith-Becker et al., 1998). As PBS3 influences SA metabolism (free SA and SAG accumulation), it may also impact other primary and specialized metabolites, particularly those derived from chorismate.

In order to determine the impact of disruption of *PBS3* on metabolism, and particularly products derived from chorismate, leaf soluble and cell wall fractions extracted from induced and uninduced *pbs3* and WT plant leaves were analyzed by HPLC with fluorescence and photodiode array detectors. Preliminary experiments with UV-C, virulent, and avirulent *P. syringae* as inducers showed reproducible differences in chorismate-derived metabolites assessed from leaf soluble fractions. Metabolic changes were the most dramatic in response to avirulent *P. syringae* at 24 hpt, so that was chosen for further analyses (Okrent, 2010). Several classes of compounds derived from the chorismate pathway including indoles, flavonoids, anthocyanins, and benzoates were tentatively identified based on retention times and previously published fluorescence properties and UV absorption profiles (e.g., Bloor and Abrahams, 2002; Hagemeier et al., 2001; Tan et al., 2004; Veit and Pauli, 1999). Only three compounds exhibit reproducible and statistically significant differences in *pbs3* compared to WT (Table 3.1). Compound A, with an average 7.3-fold reduction in peak area for induced *pbs3* compared to WT, is the known dominant SAG, SA-2-O-B-D-glucoside. Compounds B and C are unknown. Because PBS3 disruption had the most dramatic impact on Compound B of any metabolite detected, and Compound B fluoresces at ex305/em407 similarly to SA, we focused on its identification.

Compound B is dramatically elevated (17-fold) in induced *pbs3* but not WT plants with no difference from uninduced plants (Table 3.1). We had not previously detected this compound using our standard SA extraction method in which SA is extracted into the organic layer of ethylacetate/cyclopentane. We therefore reasoned that Compound B is likely water-soluble and thus was discarded with our aqueous layer in standard SA extractions but retained in this 90% methanol extraction (see Methods). Glycosides are typically water soluble; our standard SA assay releases SA from SAGs via B-glucosidase treatment prior to extraction into the organic layer. To determine whether Compound B is a glycoside, we performed a B-glucosidase treatment on this eluted fraction and re-ran it on the HPLC; there was no difference in the HPLC chromatogram. Compound B elutes at 22.2 min, whereas SA-2-O-B-D-glucoside elutes at 11.6 min and SA elutes at 27.01 min under our run conditions. In our work characterizing the

substrate preferences and kinetic properties of PBS3 (Okrent et al., 2009), we found 4-HBA-Glu and 4-HBA-Asp to elute slightly earlier than 4-HBA. Therefore, based on the function of PBS3 and other GH3 family members as benzoate/hormone amino acid synthetases, as well as the properties of Compound B described above, we hypothesized an amino acid conjugate of SA to be a good candidate for Compound B. It should be noted that 4-HBA-Glu and 4-HBA-Asp do not fluoresce at 305ex/407em.

Salicyloyl-L-aspartate (SA-Asp) is the only SA amino acid conjugate that has been detected in plants, including *Arabidopsis* (Bourne et al., 1991; Steffan et al., 1988; Westfall et al., 2016; Zhang et al., 2007). SA-Asp would be expected to have chemical properties (fluorescence and UV absorbance) similar to SA but to be more water-soluble. While Compound B eluted without overlap from other fluorescent compounds, another highly UV absorbant compound co-eluted with Compound B preventing us from obtaining a UV aborbance profile from B at this stage. Therefore, to aid in the identification of Compound B, SA-Asp and SA-Glu were synthesized (Method S3). We found SA-Asp and SA-Glu fluoresce at 305ex/407em as does SA. As SA-Asp elutes at the same retention time with similar chemical properties as Compound B, Compound B was tentatively identified as SA-Asp.

A scaled up isolation and purification protocol employing two rounds of HPLC separation and elution using Supelco ABZ+ and Prevail C18 columns was then performed to provide sufficient and enriched Compound B for LC-MS analysis (see Methods). Compound B elutes at the same retention time as the SA-Asp standard with parent ions corresponding to those of SA-Asp (m/z= 252 (ESI -); m/z= 254 (ESI+)) consistent with an assignment of SA-Asp to Compound B (Fig. 3.S5). Quantitative comparison of SA-Asp levels (using standard curves) determined that SA-Asp is not significantly induced in WT or *ics1* mutant plants in response to avirulent *P. syringae*, but is dramatically induced in *pbs3* (Fig. 3.5A). In *pbs3*, SA-Asp accumulates to levels of ~850 ng/gFW in induced *pbs3* (Fig. 3.5A), which is in the range of induced free SA accumulation in WT (Fig. 3.1C, 3.3C). Taken together, our results show that of the range of detectable classes of compounds in our metabolite analyses, SA metabolites are specifically and dramatically altered in induced leaves of *pbs3* harvested at the later phase of SA response. SA-2-O-B-glucoside levels are dramatically decreased in *pbs3* compared to WT, while SA-Asp levels are dramatically elevated.

The standard SA extraction and HPLC quantification we used to examine the temporal response to UV-C and *P. syringae* (Fig. 3.1, 3.2, 3.S2) also allows us to quantify the indolic phytoalexin, camalexin. We found no change in camalexin levels in *pbs3* compared to WT in response to UV-C (Fig. 3.S6). This is consistent with our metabolite profiling results in response to avirulent *P. syringae* at 24 hpt.

SA-Asp does not induce robust *PR-1* expression

Previously published work suggested that SA-Asp may be a weak inducer of *PR-1* (Chen et al., 2013). To test this directly under our conditions, exogenous treatment of mature *Arabidopsis* leaves with the detergent Silwet, SA with Silwet, or SA-Asp with Silwet were compared for their ability to induce robust *PR-1* expression (Fig. 3.5B). Neither exogenous SA-Asp nor Silwet alone induce *PR-1* expression; whereas exogenous SA treatment induces robust *PR-1* expression as standardly reported (e.g. Jagadeeswaran et al., 2007; Nobuta et al., 2007; Chen et al. 2013). This suggests SA-Asp is an inactive form of SA, although we cannot exclude the possibility that SA-Asp is less effective at entering cells than SA.

SA conversion to SA-Asp is not sufficient to explain *pbs3* impact on SA response

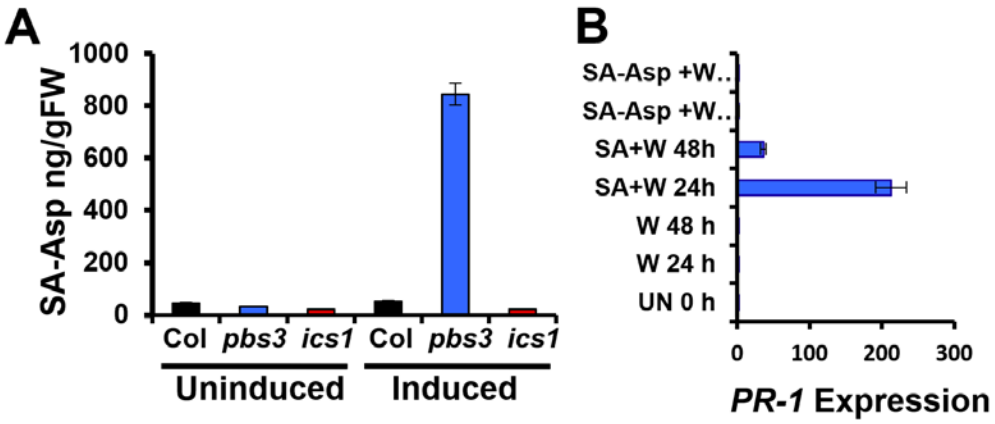

Figure 3. 5. SA-Asp is elevated in induced *pbs3* leaves but fails to induce SA-inducible *PR-1*.

(A) SA-Asp levels in uninduced or induced (24 hpt *Pst* avrRpt2) leaves of Col-0, *pbs3*, or *ics1*. Synthetic SA-Asp was used for quantitation. (B) Exogenous application of 2 mM SA with 0.01% Silwet (W), 2mM SA-Asp with 0.01% Silwet, or Silwet alone was performed on 4-5 week old plants and qPCR was performed to assess *PR-1* expression (normalized to Ubiquitin5). UN=untreated. Numbers shown are hrs post treatment when leaves were harvested. Means are shown with standard deviation, n=3. Independent experiments gave similar results.

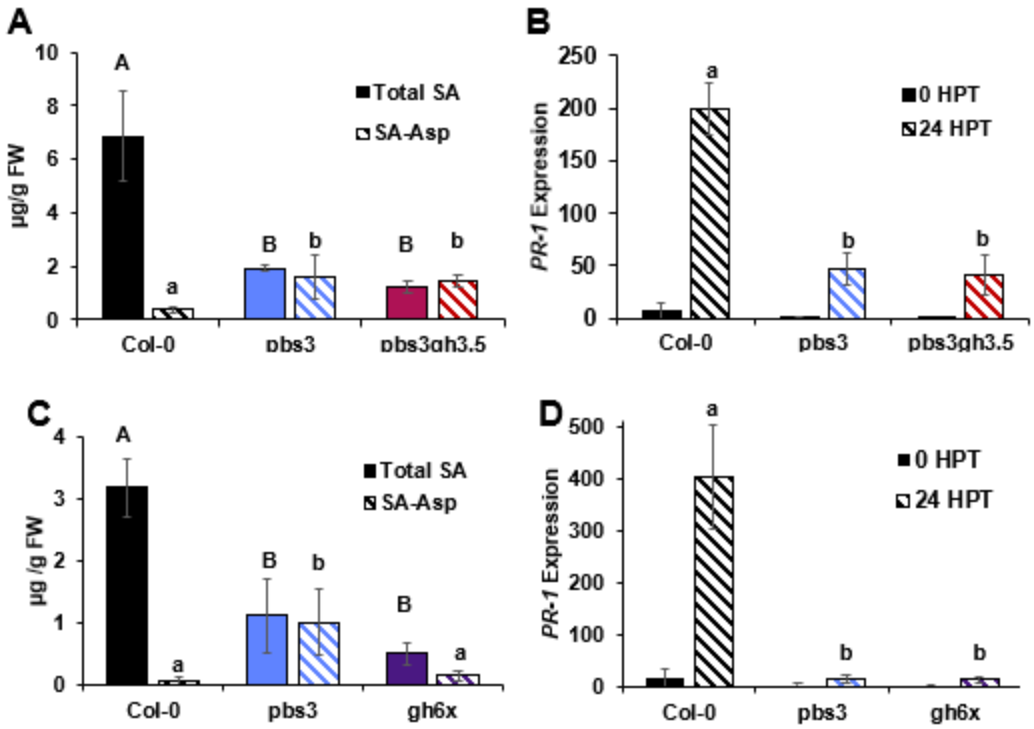

Figure 3.6. SA-Asp synthetase mutants in the *pbs3* background do not restore SA accumulation or *PR-1* expression.
P. syringae pv. *tomato* DC3000 AvrRpt2 with OD_{600} = 0.0001 was syringe infiltrated into 4-5 week old *pbs3gh3.5*, *gh6x* or control genotypes. 24 hours post infection, tissue was collected for SA metabolism analysis or *PR-1* expression. TotalSA/SA-Asp (**A**) and *PR-1* (**B**) expression were quantified in *pbs3* crossed to the known SA-Asp synthetase *gh3.5*. Putative SA-Asp synthethases (*gh3.1*, *gh3.3*, *gh3.4*, *gh3.6*) were crossed to the *gh3.5pbs3* double knockout to make the *gh6x* mutant and measured for total SA/SA-Asp (**C**) and *PR-1* expression (**D**)**.** Experiments were repeated with similar results.

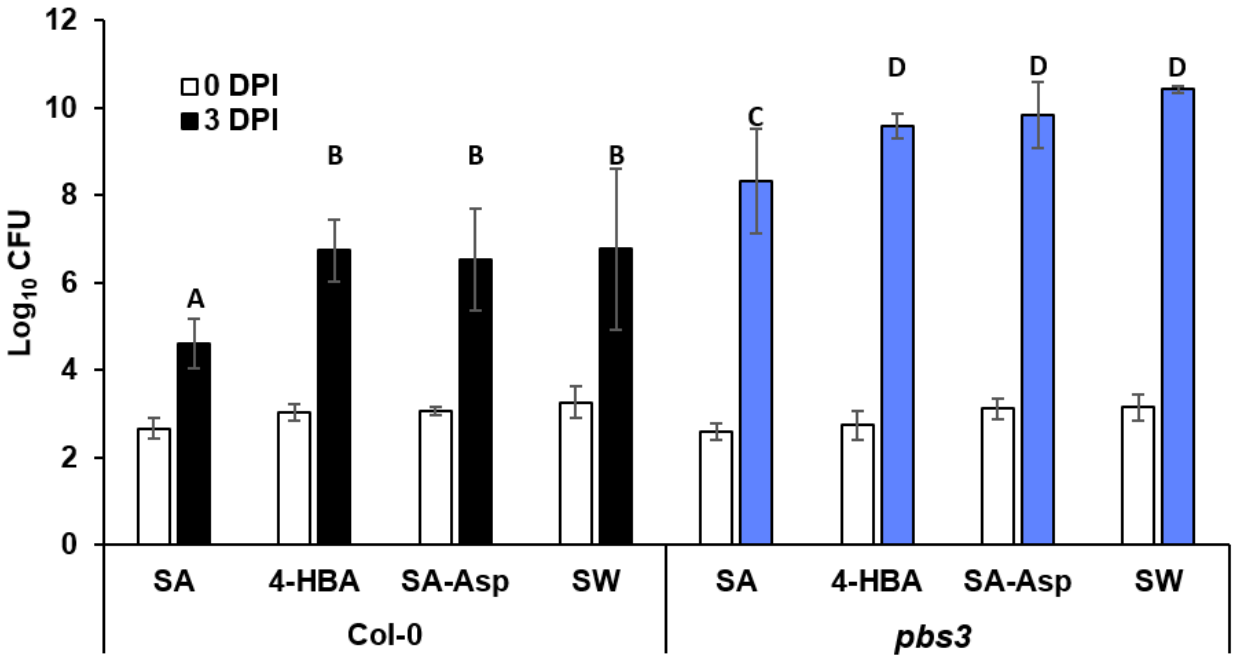

Figure 3.7. Exogenous application of SA-Asp or 4-HBA does not increase susceptibility to virulent *P. syringae*.
2 mM SA in 0.05% Silwet, 2 mM SA-Asp in 0.05% Silwet, 2 mM 4-HBA in 0.05% Silwet or 0.05% Silwet alone (SW) were exogenously applied to 4-5 week old plants 24 hours before inoculation with virulent *P. syringae* pv. *maculicola* ES4326 at inoculum level OD_{600} = 0.0002. 0 and 72 hour post infection, leaf discs were collected and bacterial growth was measured (see methods). Means are shown with standard deviation, n=9. Independent experiments gave similar results.

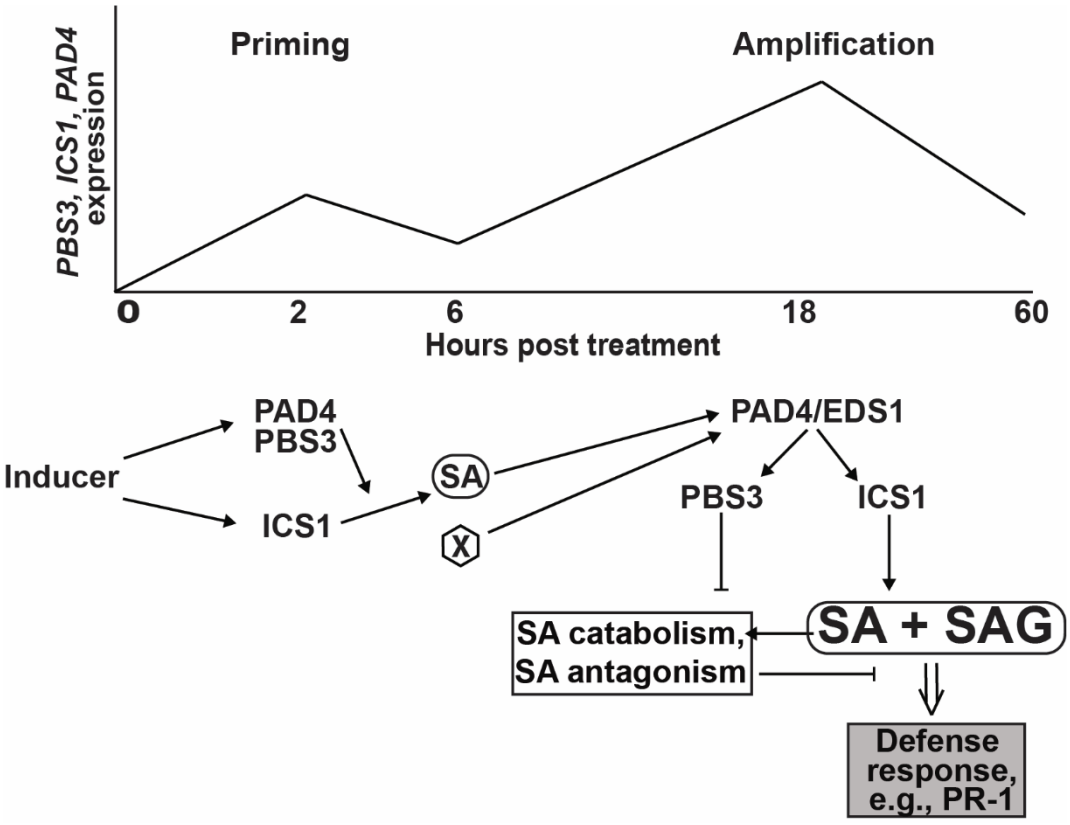

Figure 3.8: Model of biphasic SA metabolism and response.
UV-C induces the expression of *PAD4*, *ICS1*, and *PBS3*. We demonstrate that PBS3 and ICS1 are necessary for rapid accumulation of free SA, however PBS3 is not responsible for ICS1 expression. This free SA in concert with factor X primes the plant for the second phase of SA metabolism and response. An amplified peak of *PAD4* and *PBS3* expression promote high level accumulation of active total SA (free SA and SAG) and associated SA defense responses (e.g. expression of *PR-1*). *PAD4/EDS1* are necessary for *PBS3* and *ICS1* induction and SA biosynthesis. Although PBS3 is required for SA accumulation and signal amplification, it functions downstream (independent) of ICS1 likely through inhibition of SA catabolism (e.g. to SA-Asp) and SA response antagonism (e.g. via JA). As exogenous SA does not fully limit bacterial growth in *pbs3* to WT levels, we also suggest PBS3 plays a role in plant immunity beyond its impact on SA, which is not shown here. See text for more details.

Given that SA-Asp appears to be an inactive form of SA, we hypothesized that in *pbs3*, induced active SA may be shunted to inactive SA-Asp, limiting active total SA accumulation and associated defense responses. GH3.5 is the only known GH3 family member to conjugate SA to Asp (Mackelprang et al., 2017; Westfall et al., 2016). We therefore crossed *pbs3-2* and *gh3.5-2* to make the *pbs3gh3.5* double knockout (Method 3.S4) and assessed whether induced total SA, SA-Asp, and *PR-1* were restored to WT levels. Induced levels of SA-Asp remain elevated in *pbs3gh3.5* compared to WT and are not distinguishable from *pbs3* levels (Fig. 3.6A). Furthermore, induced total active SA (free SA and SAG) in *pbs3gh3.5* plants remain reduced compared to WT, similar to *pbs3*. In accordance with the results for total SA, expression of *PR-1* remains reduced in *pbs3gh3.5* similar to *pbs3*. While GH3.5 is the only known SA-Asp synthetase, SA-Asp is not fully eliminated in *gh3.5* knockout lines (Zhang et al., 2007), indicating that genetic redundancy may be responsible for the retained elevated induced SA-Asp we observe in *pbs3gh3.5*.

There are 19 *GH3* genes in *Arabidopsis thaliana*. We used previously published information about GH3 acyl and amino acid substrate preferences, induced expression and co-expression data, protein sequence identity, and insight on substrate preference derived from analysis of previously published crystal structures to identify additional SA-Asp synthetase candidates (Altschul et al., 1997; Aoki et al., 2016; Chandran et al., 2009; Mackelprang et al., 2017; Okrent and Wildermuth, 2011; Peat et al., 2012; Staswick et al., 2005, 2002, Westfall et al., 2016, 2012; Winter et al., 2007). Initial candidates focused on the GH3 group II subfamily that includes GH3.5, the only known GH3 that can utilize SA as a substrate. We also examined GH3 enzymes in group III (which contains PBS3); in particular, GH3.17, which is induced by *P. syringae* and coexpressed with *GH3.5*. GH3.1, GH3.3, GH3.4 and GH3.6 were selected as the most likely additional SA-Asp synthetases (Table 3.S1). GH3.2 (group II) and GH3.17 (group III) were ultimately excluded because they prefer amino acid substrates other than Asp (Staswick et al., 2005). We therefore created the *gh3.1gh3.3gh3.4gh3.5gh3.6pbs3(gh3.12)* sextuple mutant, which we refer to as *gh6x* (Method S4).

Induced SA-Asp is restored to WT levels in *gh6x*; however, induced total active SA and *PR-1* expression remain low and similar to *pbs3* (Fig. 3.6C, 3.6D). It therefore appears that the conversion of active SA to SA-Asp by GH3 SA-Asp synthetase enzymes is not sufficient to explain the impact of disruption of *PBS3* on SA metabolism and response.

Exogenous application of SA-Asp or 4-HBA does not alter *P. syringae* growth

Plant benzoates and their derivatives have the capacity to regulate both plant and pathogen responses. Therefore, we wondered if either elevated SA-Asp or 4-HBA might impact *P. syringae* growth on *pbs3*. Wild type and *pbs3* plants were sprayed with 2 mM SA, SA-Asp, 4-HBA or water in 0.05% Silwet 24 hours before infection with virulent *P. syringae*. Zero and three days post inoculation, leaf discs were collected and bacterial growth was measured (see Methods). While SA pre-treatment decreases bacterial growth in both WT and *pbs3*, SA-Asp and 4-HBA have no effect compared to the Silwet control (Fig. 3.7). For SA-Asp application in WT, this result supports our finding in Figure 3.5 that exogenous SA-Asp did not induced robust SA defense, assessed as *PR-1* expression. Our result also suggests SA-Asp does not itself have a significant direct impact on pathogen virulence as there was no difference in bacterial growth with SA-Asp pre-treatment compared with the Silwet control on WT plants (Fig. 3.7).

In the *pbs3* mutant, 4-HBA would presumably not be converted to 4-HBA-Glu which could result in elevated 4-HBA accumulation. Although we did not identify altered accumulation

of 4-HBA or 4-HBA-Glu in induced *pbs3* or WT samples, it could be that selected time points did not capture such changes (Okrent, 2010). 4-HBA is a known inducer of the type III secretion system of *P. syringae* (Anderson et al., 2014). However, we found no impact of exogenous 4-HBA pre-treatment on *P. syringae* growth in WT or *pbs3* (Fig. 3.7).

Under all conditions tested, *pbs3* supports dramatically more bacterial growth (~1000-fold) than the parallel WT samples at 3 days post inoculation; the initial inoculum was similar across all genotypes and treatments (0 dpi, Fig. 3.7). *Pbs3* also supports significantly more bacterial growth in response to all pre-treatments than the WT control (Silwet only). We had anticipated that exogenous SA pre-treatment would restore bacterial growth in *pbs3* to WT levels as previously reported (Jagadeeswaran et al., 2007); however, bacterial growth in *pbs3* at 3 dpi, following SA pre-treatment is reproducibly ~35-fold higher than the WT control, and ~5000-fold higher than WT pre-treated with SA (Fig. 3.7). There are slight differences in our protocols. The most likely explanation for the different outcomes is that our SA pretreatment results in a higher intracellular concentration of SA that limits bacterial growth in WT by 2 logs (100-fold); whereas, bacterial growth in WT was only reduced by 0.5 log by SA pretreatment in Jagadeeswaran et al. (2007). Therefore, because we observed a larger impact of SA pretreatment on bacterial growth for WT, we were better able to resolve a difference with *pbs3* compared to WT. Our result indicates that the impact of PBS3 on bacterial growth extends beyond its impact on active SA accumulation.

DISCUSSION

We used UV-C to reproducibly temporally resolve early (priming) and late (amplification) phases of SA accumulation and response (Fig. 3.1, 3.2, 3.3). *P. syringae* also appears to induce a biphasic SA response, but the results were less reproducible (Fig. 3.S2) and have the added complexity of (unknown) pathogen effector impacts. Here we integrate results reported herein with previously studies to generate a model of PBS3 function in priming and amplification phases of SA metabolism and response (Fig. 3.8). These findings also suggest a larger role for PBS3 beyond its impact on SA metabolism and response.

After treatment with an inducer such as UV-C, *PAD4*, *PBS3*, and *ICS1* are rapidly induced, peaking at 1-2 hpt (Fig. 3.2). The rapid induction of *ICS1* is independent of the treatment time-of-day (Fig. 3.S1) and returns to uninduced levels prior to the second amplification phase of response (Fig. 3.1). This early peak of ICS1 transcript and protein, which accumulate in parallel, is accompanied by an early peak in free SA accumulation in WT plants (Fig. 3.1). In the *pbs3* mutant, early free SA accumulation is dramatically reduced; however, ICS1 transcript and protein expression are not altered (Fig. 3.3, 3.4). SA priming in response to MAMPs showed that while *ICS1* is required for rapid early induced SA synthesis associated with priming, mutants in *PAD4* exhibit reduced rapid free SA accumulation with only a minimal impact on *ICS1* transcription (Tsuda et al., 2008), similar to our findings with *pbs3* mutants (Fig. 3.3). Therefore, PBS3 and PAD4 are shown to act independent of ICS1 to promote free SA accumulation associated with the priming phase of response (Fig. 3.8). This positioning does not imply that PBS3 and PAD4 promote early free SA accumulation via a biosynthetic route other than through ICS1. In Arabidopsis, the biosynthesis of SA via ICS1 is well established (Garcion et al., 2008; Wildermuth et al., 2001). *ics1* mutants exhibit <10% of wild type induced SA accumulation and *ics1ics2* double mutants completely abrogate induced SA accumulation (Garcion et al., 2008). Instead, we suggest that PBS3 and PAD4 act downstream of ICS1 to

regulate early free SA accumulation associated with priming. This could occur via regulation of a yet undetermined SA biosynthetic enzyme responsible for the conversion of isochorismate to SA, the SA plastid transporter EDS5 which is required for free SA accumulation, and/or proteins involved in SA catabolism.

As shown in Figure 3.8, following free SA accumulation, the second phase of induction of *PAD4, PBS3,* and *ICS1* occurs, peaking at 18-24 hpt (Fig. 3.2). Wang et al., (2008) focused on this amplification phase of the SA response, comparing the transcriptional response of *WT, ics1, pbs3, and pad4* mutants to *P. syringae* at 24 hpt using a miniarray of 571 selected defense/pathogen-altered genes. *PBS3* expression associated with the amplification phase of SA response is tightly coupled to *PAD4* expression. Wang et al., (2008) found *PBS3* expression was 39% of WT in the *pad4* background 24 hpt with *P. syringae*. *PAD4* was expressed to 85% of WT levels in *pbs3* in Wang et al., 2008, and consistently, 84% of WT in a separate, independent microarray experiment (Wang et al., 2011), also with *P. syringae*. This suggests that PBS3 has a minor, but repeatable effect on *PAD4* expression while PAD4 has a strong impact on *PBS3* expression. Furthermore, in *eds1pad4* double mutants, *PBS3* expression 24 hpt requires both estradiol-induced PAD4 and EDS1; with only estradiol-induced PAD4, *PBS3* expression remained at background levels (Cui et al., 2017). This indicates that PAD4 and its interaction partner, EDS1, are required for *PBS3* expression. Therefore, we place PBS3 downstream of PAD4/EDS1 in this phase of SA response (Figure 3.8), in agreement with Wang et al. 2008, 2011.

PAD4, PBS3, and *ICS1* are all induced by exogenous application of SA (Hunter et al., 2013; Jagadeeswaran et al., 2007; Jirage et al., 1999) suggesting a threshold of free SA could be sufficient for their induction in the amplification phase. However, *PBS3* expression was unchanged and *PAD4* decreased to 62% of wildtype in the *ics1* background, suggesting that free SA is only partially responsible for the amplified induction of *PAD4* and *PBS3* in the second phase of response. This indicates that another factor(s) (X in Fig. 8) is required for the amplified induction of *PAD4* and *PBS3* expression. X may be a small molecule such as ROS or NO which have been previously implicated in amplification of the SA response (Green and Fluhr, 1995; Klessig et al., 2000), a regulatory protein, or a small RNA.

ICS1 expression is 26% of WT in *pad4* 24 hpt with *P. syringae* (Wang et al., 2008). It is reduced to background levels in *pad4eds1* mutants with restored expression requiring both estradiol-induced PAD4 and EDS1 (Cui et al., 2017). Therefore, ICS1 is placed downstream of PAD4/EDS1 in Figure 3.8, consistent with previous findings. In contrast, we found ICS1 transcript and protein expression were similar in *pbs3* and WT in association with the second (amplification) phase of SA response to UV-C, despite the dramatic reduction in total active SA accumulation in *pbs3* (Fig. 3.3, 3.4). Similarly, *ICS1* expression was not reduced in *pbs3* in response to *P. syringae* at 24 hpt, but elevated (Wang et al., 2008). Taken together, these findings indicate that PAD4/EDS1 regulate *PBS3* and *ICS1* expression to impact the amplification phase of total active SA accumulation. While PBS3 does not affect *ICS1* expression, *pbs3* mutants are dramatically compromised in SA accumulation, suggesting significant activity downstream of ICS1.

During this second (amplification) phase of SA response, total active SA accumulates to very high levels (e.g. 25-30 ug/gFW), dominated by SAG, and robust expression of the SA-defense gene *PR-1* is observed (Fig. 3.1, 3.3). In *pbs3*, metabolic profiling found not only SAG to be dramatically reduced, but SA-Asp to be 17-fold elevated (Fig. 3.5A, Table 3.1). Exogenous application of SA-Asp did not induce robust *PR-1* expression and did not affect susceptibility to

P. syringae in *pbs3* (Fig. 3.5, 3.7). The possibility remains that this is due to a lack of SA-Asp uptake or molecular change before uptake. However, Chen et al., (2013) exogenously applied ^{2}H-labeled SA-Asp and measured its levels 9 to 51 hours later via UPLC/ESI-QtOF-MS. SA-Asp had entered leaves and some had travelled to systemic leaves. It thus seems that SA-Asp, similar to the conjugate IAA-Asp, is an inactive form destined for catabolism (Woodward and Bartel, 2005). This indicates PBS3 negatively regulates SA catabolism to SA-Asp. However, genetic disruption of induced SA-Asp formation in *pbs3* did not restore either WT levels of active total SA nor expression of the SA defense gene *PR-1* (Fig. 3.6). It is possible that PBS3 limits SA catabolism more broadly, for example to 2,3-DHBA/2-3-DHBA-xyloside, (Bartsch et al., 2010; Zhang et al., 2013), 2,5-DHBA (Zhang et al., 2017) or other less well-defined potential SA catabolites (e.g. Dempsey et al., 2011).

However, as repeated independent experiments found exogenous SA did not fully reduce *P. syringae* growth to WT levels in *pbs3* (Fig. 3.7), it is likely that PBS3 function is broader than controlling total active SA. For example, PBS3 may promote activated NPR1 and SA-associated defense gene expression downstream of SA (not shown in Fig. 3.8). Wang et al. (2008) found NIMIN1, which interacts with nuclear-localized NPR1 and the transcription factor TGA to promote *PR-1* expression (Johnson et al., 2003; Weigel et al., 2005, 2001), has reduced expression in induced *pbs3.* Similarly, expression of *WRKY70*, which promotes SA-responsive gene expression and negatively regulates JA-associated gene expression (Li et al., 2006, 2004), is reduced in *pbs3* compared to WT (Wang et al., 2008). Interestingly, of the 144 genes with differential expression in *pbs3* compared to WT in the miniarray study, 73 genes exhibited enhanced expression in *pbs3* suggesting their expression is negatively regulated by PBS3 (Fig. 3.S7). Many of these genes are associated with responses mediated by JA, which typically antagonize SA-associated defenses (Fig. 3.8), including the JA biosynthetic genes *LOX3* and *OPR3* (*At2g06050*), JA responsive genes jacalin lectin family protein *JR1, COR13* transaminase, the defensin *PDF1.2* (*At5g44420*), vegetative storage protein (VSP) *VSP1,* and the ERF transcription factor *RAP2.3.*

Differentially expressed genes in the *ics1* mutant are fewer in number (40 total), with only 20% exhibiting enhanced expression compared with the 51% in *pbs3* (Wang et al., 2008). Furthermore, 34 of these 40 genes with differential regulation in *ics1* also show differential regulation in *pbs3.* Therefore, while PBS3 promotes SA metabolism and response similar to ICS1, it plays a much broader regulatory role than ICS1 that includes limiting SA catabolism (e.g. to SA-Asp) and SA response antagonism (e.g. via the JA pathway). This is consistent with our finding that exogenous SA did not reduce *P. syringae* growth in *pbs3* to WT levels (Fig. 3.7).

Of the 144 genes differentially expressed in *pbs3,* 77 were also differentially expressed in *pad4*. This highlights the closely associated role PBS3 and PAD4 play in induced SA metabolism and response as suggested in Figure 3.8. However, 67 genes with altered expression in *pbs3* were not altered in *pad4*, and 89 genes with altered expression in *pad4* were not altered in *pbs3* (Wang et al., 2008), indicating that PBS3 and PAD4 each play distinct regulatory roles beyond that discussed here. One obvious example is the impact of PAD4 but not PBS3 on induced accumulation of the phytoalexin camalexin. We found induced camalexin levels to be unchanged in *pbs3* compared to WT in response to UV-C (Fig. 3.S6), whereas *pad4* mutants were identified based on their dramatically reduced accumulation of camalexin in response to *P. syringae* pathogens (Glazebrook et al., 1997; Zhou et al., 1998).

Our model provides important insights on the PBS3 node of plant immunity and suggests a mechanistic link between PBS3 and PAD4/EDS1 in regulation of SA metabolism and response

that should be further explored. For example, as PAD4/EDS1can also regulate SA catabolism and JA-SA antagonism, this component of PAD4/EDS1 function could occur via PBS3 as shown in Figure 8. A role for PBS3 in plant immunity that extends beyond its impact on SA is also indicated.

CONCLUSIONS

This work adds valuable new insight into the function and mechanism of salicylic acid-mediated resistance. First, we characterize UV-C as a reliable inducer of the biphasic SA metabolism and response pathway that separates rapid free SA accumulation associated with priming from robust total active SA (free SA plus SAG) accumulation and SA defense gene expression. We find for the first time that ICS1 protein and transcript accumulation occur in parallel and independent of PBS3. *PBS3* and *PAD4* exhibit biphasic expression similar to *ICS1*. However, PAD4 (with EDS1) directly regulates SA accumulation in the second (amplification) phase of response via ICS1; whereas PBS3 acts downstream of ICS1 to promote SA accumulation. PBS3 functions in part by inhibiting SA catabolism (e.g. to SA-Asp); however this is not sufficient to explain its impact on SA or SA defense gene expression. Similarly, PAD4/EDS1 inhibits SA catabolism (to 2,3-DHBA). Both PBS3 and PAD4/EDS1 also appear to limit antagonism of SA responses (e.g. via JA) and play additional independent roles in defense beyond SA. Our model suggests a mechanistic link between PBS3 and PAD4/EDS1 in regulation of SA metabolism and response that should be further explored.

ACKNOWLEDGEMENTS

We thank Ludmila Alexandrova and Allis Chien of the Stanford Mass Spectrometry Facility for LC-MS analysis of the Peak of Interest. This work was supported in part by NSF MCB-04202267 and NSF IOS-1449110 to M.C.W, NSF GRFP to R.M., UC Berkeley William Carroll Smith graduate fellowship in plant pathology to R.A.O, and Undergraduate Research Apprenticeship Program funds for A.W. and Y. H.

AUTHOR CONTRIBUTION

M.C.W directed the research, designed and performed experiments. M.C.W. and R.M. wrote the manuscript. R.A.O, R.M., S.K.M., and D.R. designed and performed experiments. M.C., A.W., and Y. H. performed experiments. P. S. created the *gh3* pentuple mutant and E.S. synthesized and purified reagents SA-Asp and 4-HBA-Glu.

SUPPLEMENTAL FIGURES AND METHODS

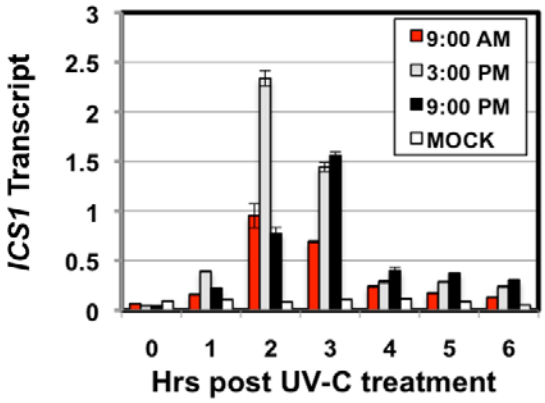

Figure 3.S1. Initial phase of *ICS1* expression is independent of time-of-day.

ICS1 transcript normalized to *Ubiquitin5* was obtained using qPCR analysis on cDNA from UV-C treated wild type plants, with UV-C treatment performed at different times. Note that 9 am is "standard" start time in all experiments. Mean is shown with standard deviation, n=3. An independent experiment gave similar results.

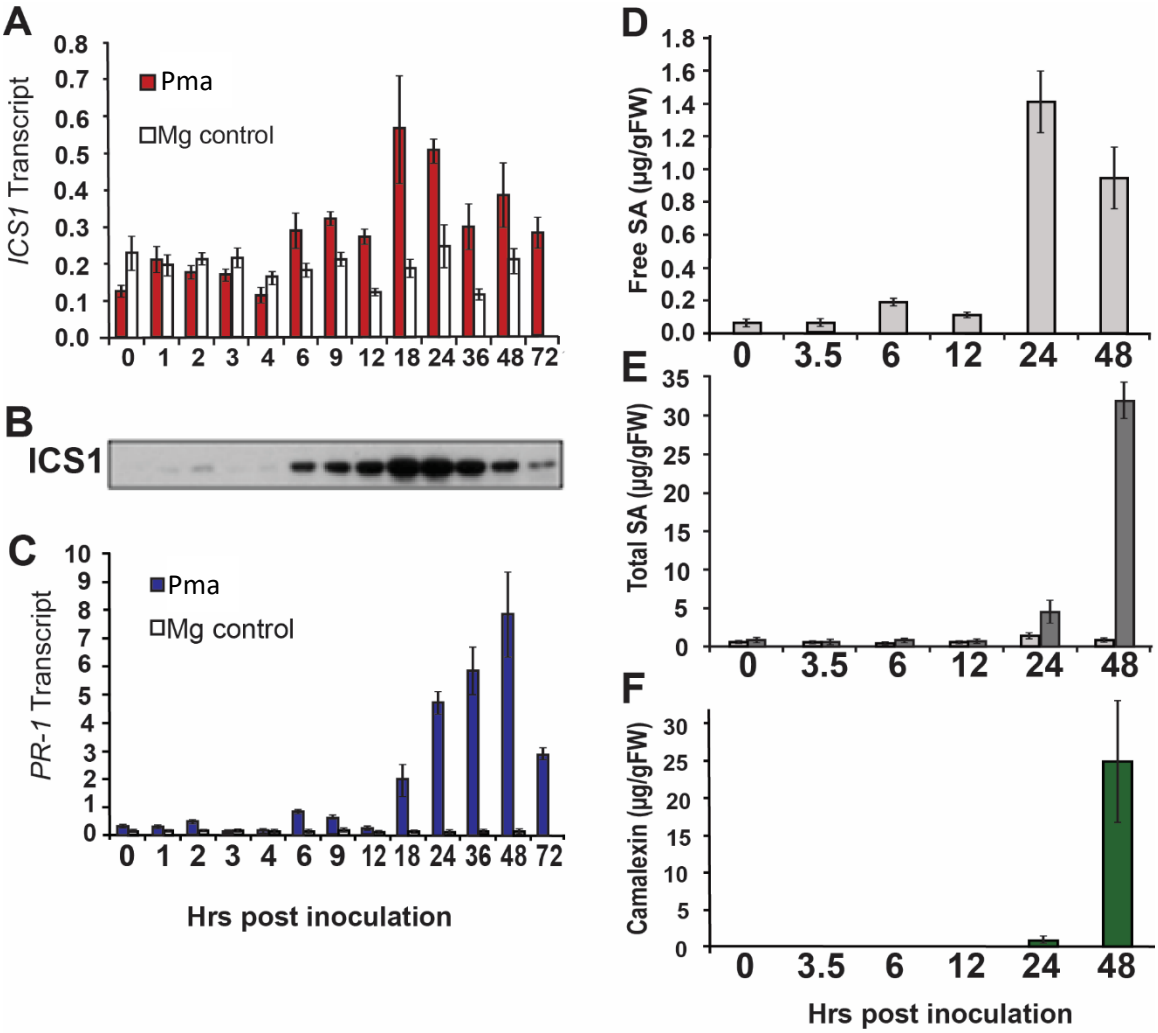

Figure 3.S2. *P. syringae* induced SA metabolism and response. *ICS1* transcript (A), ICS1 protein (B), and *PR-1* transcript following inoculation with *P. syringae* pv. *maculicola* ES4326 at a dose of OD_{600}= 0.002 in 10 mM $MgSO_4$ or 10mM $MgSO_4$. A subset of time points were analyzed for free SA (D), total SA (E; free SA (light grey) and SA glucosides (dark grey)), and camalexin (F), assessed using HPLC with fluorescence detection. Transcript levels were determined by qPCR and normalized to *Ubiquitin5*. Equal protein was loaded for Westerns. Mean values are shown with standard deviations, with n=3. See Methods for additional detail.

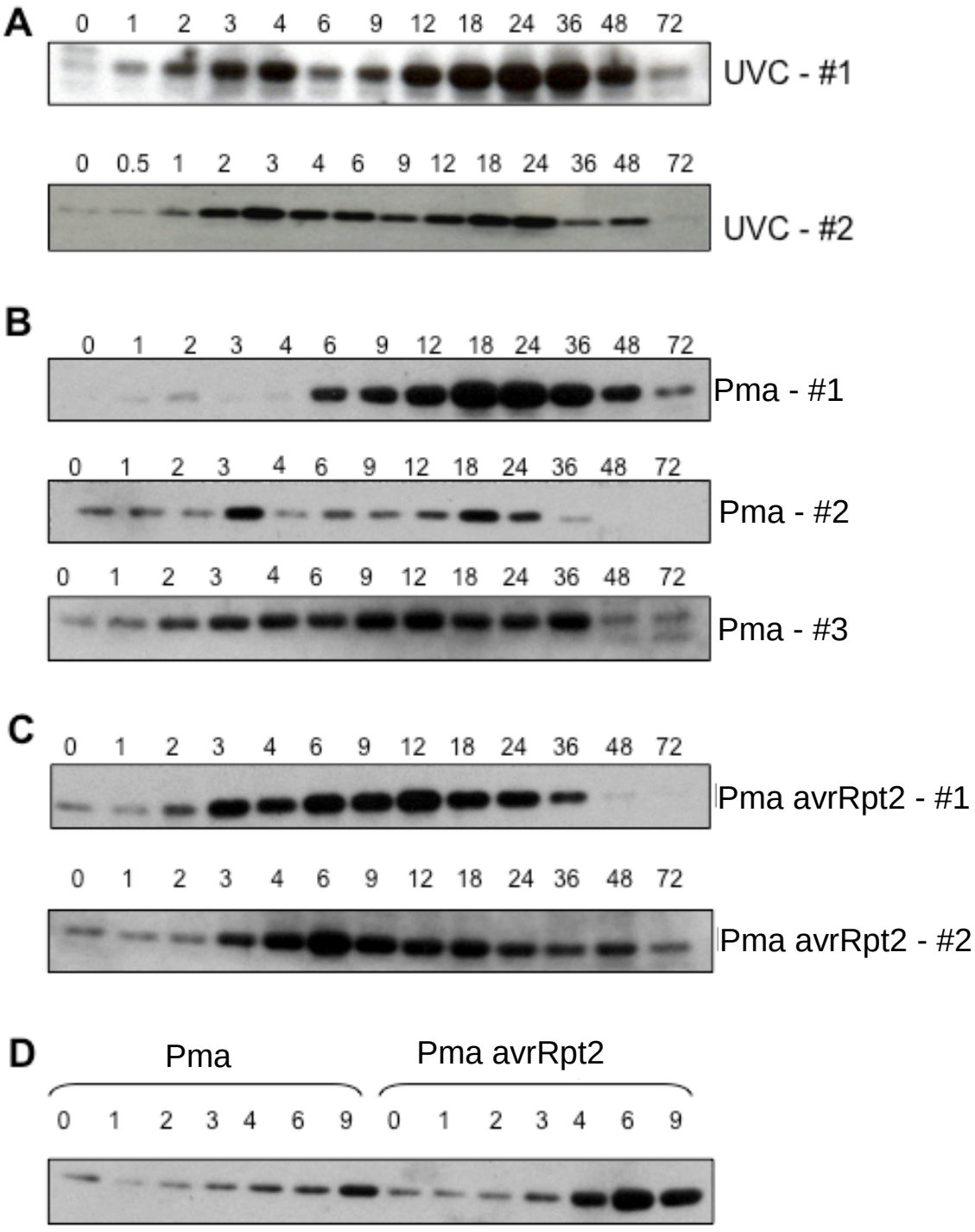

Figure 3.S3. ICS1 protein levels in response to UV-C (A), virulent (B,D) or avirulent (C,D) *P. syringae*. Mature leaves were inoculated with virulent or avirulent *P. syringae* pv. *maculicola* (*Pma*) ES4326 at a dose of OD_{600}= 0.002 in 10 mM $MgSO_4$. Equal protein was loaded for Westerns. Data for independent experiments (numbered) are shown for comparison. See Methods for details.

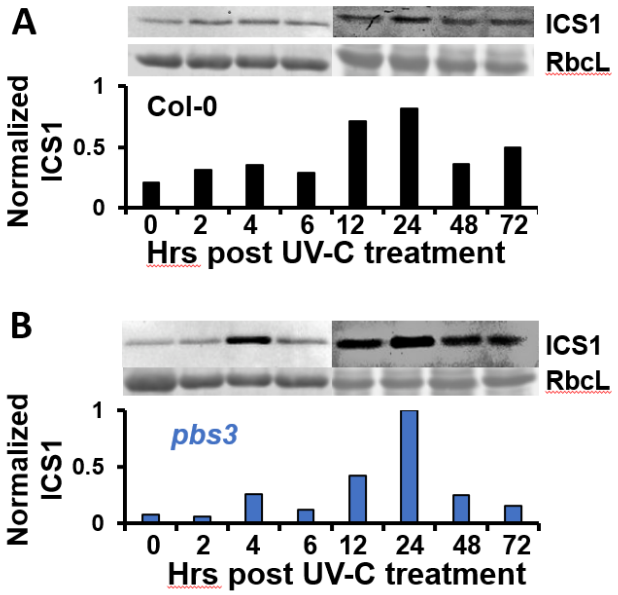

Figure 3.S4. ICS1 protein expression in response to UV-C is similar in Col-0 and *pbs3* mutant plants (independent experimental repeat of Fig. 3.4).
Western blot and protein quantification of ICS1 in (A) Col-0 and (B) *pbs3* are shown over 72-hour time-course. Equal amounts of protein were loaded. Col-0 time points and *pbs3* time points were on separate blots, with signal normalized to each other using quantitation software in imager. RbcL is shown as an indicator of total protein. The lane between samples 6 and 12 hpt was excluded, indicated as a break. Quantitation software normalized to the highest band.

Figure 3.S5: LC-MS identifies Compound B to be Salicyloyl-L-Aspartate
Extracts from *pbs3* plants treated with *Pst* AvrRpt2 were combined, enriched and purified for Compound B, which was analyzed by LC-MS. As shown, Compound B eluted at the same retention time as synthetic Salicyloyl-L-Aspartate (SA-Asp), with the SA-Asp parent ions of ESI- m/z= 252 and ESI+ m/z=254. See Methods for details.

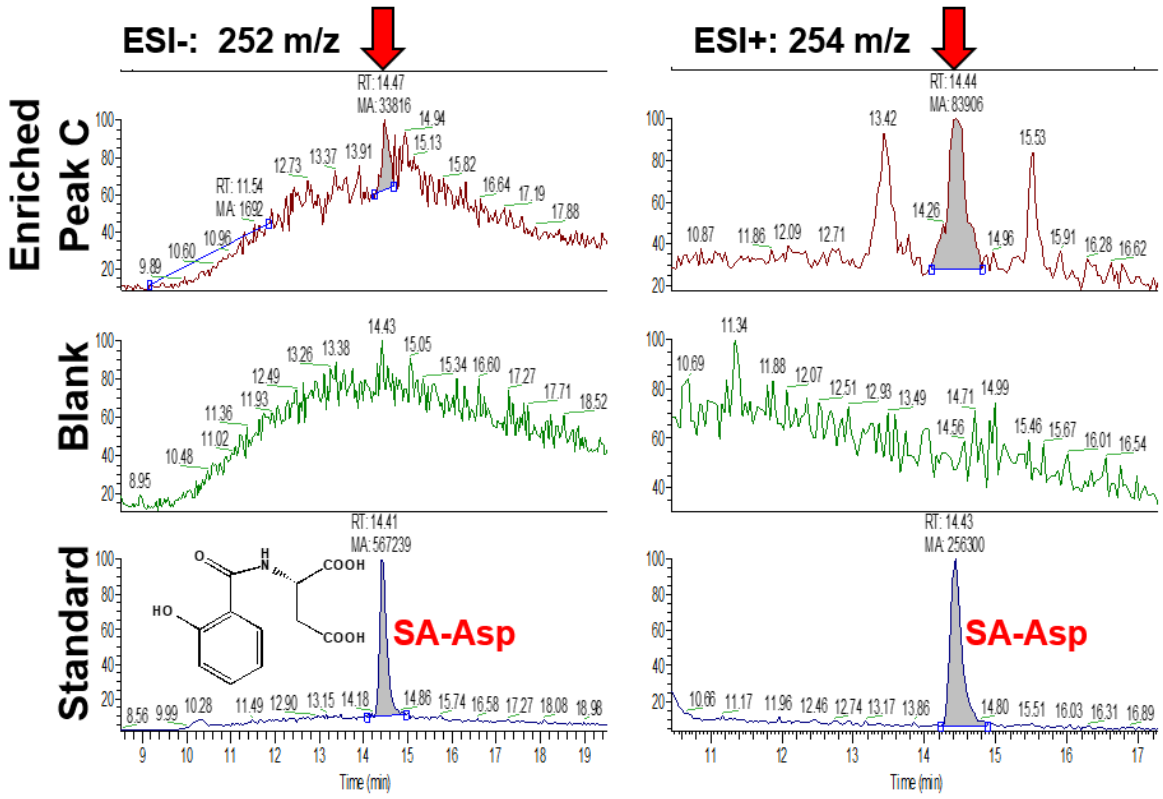

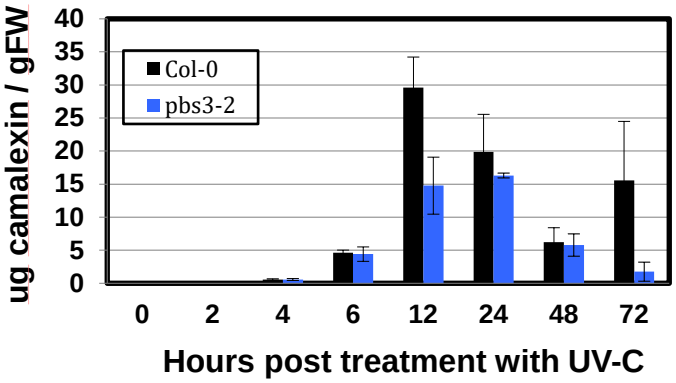

Figure 3.S6. Induced camalexin accumulation is not significantly altered in *pbs3* compared with wild type plants in response to UV-C. Camalexin levels were assessed by HPLC (see Methods). Results are shown for the experiment presented in Figure 4. Unlike SA, camalexin accumulation is not reproducibly different in *pbs3* in response to UV-C compared with wt. Mean is shown with standard deviation, n=3. Independent experiments show similar results, but without the difference at 12 hpt

	Total DE	# Genes up	# Genes down
pbs3	**144**	**73**	**71**
pad4	**166**	**49**	**117**
ics1	**40**	**8**	**32**

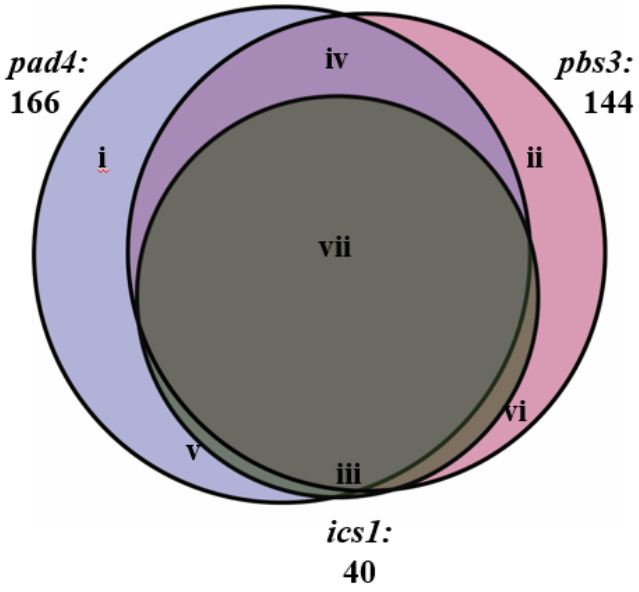

Figure 3.S7 Analysis of differentially expressed genes in *pad4*, *pbs3*, and *ics1* as compared to WT 24 hpt *P. syringae* (Data from Wang et al., 2008, Supplemental Table 3.8).

(A) Number of genes differentially expressed, along with breakdown of up vs down regulation, in each mutant background compared to WT out of 571 gene miniarray.
(B) Clustering of differentially expressed genes shows that nearly all *ICS1*-dependent genes are also dependent upon *PAD4* and *PBS3*.

Section	Expression category	# of genes
i	*pad4* only	85
ii	*pbs3* only	58
iii	*ics1* only	2
iv	*pad4* and *pbs3*	52
v	*pad4* and *ics1*	*4*
vi	*pbs3* and *ics1*	9
vii	*pad4, pbs3, ics1*	*25*

						Expression induced by		
Locus	Gene Name	Syntenic Group[a]	amino acid % identity with GH3.5[b]	Hormone Acyl substrate activity	Activity with Asp[c]	G. orontii[g]	Virulent Pto DC3000[h]	CoExpressed with GH3.5[i]
At2G14960	***GH3.1***	**IIA**	**67%**	**N.D.**	**N.D.**	**-**	**+**	**Yes**
At4G37390	*GH3.2/YDK1*	IIA	65%	IAA[c]	-	-	+	N/A
At2G23170	***GH3.3***	**IIA**	**64%**	**IAA[c,d]**	**+**	**++**	**++**	**Yes**
At1G59500	***GH3.4***	**IIA**	**60%**	**IAA[c]**	**+**	**-**	**+**	**N/A**
At4G27260	***GH3.5***	**IIB**	**100%**	**IAA, SA[c-f]**	**+[c,e,f]**	**++**	**++**	
At5g54510	***GH3.6/DFL1***	**IIB**	**90%**	**IAA[c]**	**++**	**-**	**+**	**Yes**
At1G28130	*GH3.17*	IIIA	58%	IAA[c]	-	-	+	Yes

Table 3.S1: SA-Asp synthetase candidates

To prioritize potential SA-Asp synthetases, we analyzed members of the *GH3* family for similar sequence, activity, and expression patterns as *GH3.5* based on previously published work and databases. We prioritized the strongest SA-Asp synthetase candidates and ones without sufficient data to eliminate (bolded) and created a sextuple knockout with these genes in the *pbs3* (*gh3.12*) background. We predicted this *gh3.1*/*gh3.3*/*gh3.4*/*gh3.5*/*gh3.6*/*gh3.12* (*pbs3*) mutant, referred to as *gh6x*, would eliminate or significantly diminish SA-Asp accumulation. "-" = minimal expression or activity. "+" = some expression or activity. "++" = strong expression or activity. N.D. = not determined. References: a = Okrent & Wildermuth, 2011; b = Altschul et al., 1997; c = Staswick et al., 2005; d = Staswick et al., 2002; e = Mackelprang et al., 2017; f = Westfall et al., 2016; g = Chandran et al., 2009; h = Winter et al., 2007

Method 3.S1. Primers for real time quantitative PCR.
Gene-specific primers for *A. thaliana* ecotype Columbia Ubiquitin5 (*UBQ5*, At3g62250), Pathogenesis-Related protein 1 (*PR-1*, AT2g14610), and Isochorismate Synthase 1 (*ICS1*, At1g74710) for Figure 3. 1 and Supplemental Figure 3. 1 follow: UBQ5 (forward (F), 5'-GTGGTGCTAAGAAGAGGAAGA-3'; reverse (R), 5'-TCAAGCTTCAACTCCTTCTTT-3'), *PR-1* (F, 5'-GTAGGTGCTCTTGTTCTTCCC-3'; R, 5'-CACATAATTCCCACGAGGATC-3'), and ICS1 (F, 5'-ACTCCAGCTGTTTGTGGGCT-3'; R, 5'-TCAATTAATCGCCTGTAGAGATG-3'). For Figure 3.s 2, 4, and 6D, *UBQ5* (F, 5'-GAAGACTTACACCAAGCCGAAG-3'; R, 5'-TTCTGGTAAACGTAGGTGAGTCC-3'), *PR-1* (F, 5'-GAAAACTTAGCCTGGGGTAGC-3'; R, 5'-TTCATTAGTATGGCTTCTCGTTCA-3') and *ICS1* (F, 5'-GAATTTGCAGTCGGGATCAG-3'; R, 5'-AATTAATCGCCTGTAGAGATGTTG-3') were employed.

Method 3.S2. Extraction of Cell Wall Metabolites
Extraction of cell wall bound metabolites was performed as described in (Hagemeier et al., 2001)[1] with a few modifications. Frozen leaf tissue (2.5 g) was homogenized in 90% MeOH (20 mL), shaken at RT for 15 min and centrifuged 15 min at 4000 g. The supernatant was removed, and the residue was washed sequentially with: MeOH, water, 0.5% SDS, 1 M NaCl, water, MeOH, acetone and n-hexane (2 x 8 mL, shaken, and centrifuged). The white crystalline residues were evaporated using a dry vacuum at approximately 5 Torr and stored at -20º. Cell wall samples (~25mg/sample) were transferred to serum bottles, suspended under N_2 in 3 ml 1 M NaOH, and incubated in darkness for 24 h at 80º C. Mixtures were acidified to ~ pH 3 with concentrated HCl and extracted 2 times with ethyl acetate. Organic layers were combined and dried as above. Residues were redissolved in 160 µL 20% MeOH for HPLC analysis as described for soluble metabolites (in text).

Method S3. Synthesis of SA-Asp, SA-Glu, 4-HBA-Asp, and 4-HBA-Glu.
Please note that synthesis of 4-hydroxybenzoyl-L-glutamic acid was previously described in (Okrent et al., 2009)[2], but is also included here for completeness.

Dichloromethane (CH_2Cl_2) and triethylamine (Et_3N) were distilled over calcium hydride. All other solvents and reagents were used as received. Thin layer chromatography was performed using SiliCycle silica gel 60 F-254 precoated plates (0.25 mm) and visualized by UV irradiation and anisaldehyde stain. ^1H and ^{13}C NMR spectra were recorded on Bruker DRX-500 and AV-500 MHz spectrometers with a ^{13}C operating frequency of 125 MHz. Chemical shifts (δ) are reported in ppm relative to the residual solvent signal (δ = 7.26 for $CDCl_3$ and δ = 3.31 for CD_3OD (for ^1H NMR) and δ = 49.05 for CD_3OD (for ^{13}C NMR)). Data for ^1H NMR spectra are reported as follows: chemical shift (multiplicity, coupling constants,

[1] Hagemeier, J., Schneider, B., Oldham, N.J., and Halhlbrock., K. (2001) Accumulation of soluble and wall-bound indolic metabolites in Arabidopsis thaliana leaves infected with virulent or avirulent Pseudomonas syringae pathovar tomato strains. *Proc. Natl. Acad. Sci. USA* 98: 753-758.
[2] Okrent, R.A., Brooks, M.D., and Wildermuth, M.C. (2009) Arabidopsis GH3.12 (PBS3) conjugates amino acids to 4-substituted benozates and is inhibited by salicylate. *J. Biol. Chem.* 284: 9742-9754.

number of hydrogens). Abbreviations are as follows: s (singlet), d (doublet), t (triplet), q (quartet), m (multiplet).

Synthesis of Diethyl *4*-acetoxybenzoyl-L-glutamate: The procedure of Magerlein[3] and co-workers was followed with slight modifications. To a suspension of 4-acetoxybenzoic acid (5.00 g, 27.8 mmol) in CH_2Cl_2 (50 mL) at 0 °C was added oxalyl chloride (2.42 mL, 27.8 mmol) over 3 min. DMF (3 drops) was then added, and resulting mixture was allowed to warm to rt. After stirring for 4 h, TLC analysis indicated complete consumption of the acid. The resulting clear solution was concentrated on the rotovap, and the crude acid chloride was redissolved in CH_2Cl_2 (40 mL) and cooled to 0 °C. A solution of diethyl L-glutamate hydrochloride (6.65 g, 27.8 mmol) in CH_2Cl_2 (36 mL) was then added, followed by a solution of Et_3N (8.49 mL, 61.1 mmol) in CH_2Cl_2 (24 mL), which caused the immediate formation of a white precipitate. The resulting suspension was allowed to warm to rt and was stirred for 1.5 h. The mixture was then transferred to a separatory funnel and washed successively with 100 mL water, 100 mL 1 N HCl, 100 mL sat. aq. $NaHCO_3$ and 100 mL brine. The organic layer was dried ($MgSO_4$) and concentrated to give 9.47 g (ca. 25.9 mmol, 93%) of crude diethyl *p*-acetoxybenzoyl-L-glutamate as a white solid, which was used without further purification. $\mathbf{R_f}$ 0.18 (2:1 hexanes/EtOAc); **^{1}H NMR** (500 MHz, $CDCl_3$) δ 7.86 (d, *J* = 8.7 Hz, 2H), 7.18 (d, *J* = 8.6 Hz, 2H), 7.04 (d, *J* = 7.0 Hz, 1H), 4.77 (m, 1H), 4.30-4.19 (m, 2H), 4.17-4.06 (m, 2H), 2.51 (m, 1H), 2.42 (m, 1H), 2.32 (s, 3H), 2.35-2.27 (m, 1H), 2.20-2.09 (m, 1H), 1.30 (t, *J* = 7.1 Hz, 3H), 1.23 (t, *J* = 7.2 Hz, 3H); **^{1}H NMR** (500 MHz, CD_3OD) δ 7.90 (d, *J* = 8.6 Hz, 2H), 7.23 (d, *J* = 8.6 Hz, 2H), 4.62 (dd, *J* = 9.5, 5.2 Hz, 1H), 4.21 (q, *J* = 7.1 Hz, 2H), 4.12 (q, *J* = 7.1 Hz, 2H), 2.49 (t, *J* = 7.3 Hz, 2H), 2.30 (s, 3H), 2.34-2.24 (m, 1H), 2.15-2.05 (m, 1H), 1.28 (t, *J* = 7.1 Hz, 3H), 1.23 (t, *J* = 7.2 Hz, 3H).

4-Hydroxybenzoyl-L-glutamic acid (4-HBA-Glu): To a solution of crude diethyl *4*-acetoxybenzoyl-L-glutamate (2.00 g, ca. 5.47 mmol) in EtOH (20 mL) at 0 °C was added NaOH (1.09 g, 27.4 mmol). The resulting mixture was allowed to warm to rt and stirred for 1 h before the addition of water (4 mL) to effect complete dissolution of the NaOH. The resulting mixture was stirred at rt for 18 h, at which point the EtOH was removed on the rotovap. The resulting solution was diluted with water (ca. 5 mL) and extracted with Et_2O (2 x 15 mL). The Et_2O layers were discarded, and the aq. layer was acidified to pH = 0 with 4 N HCl (10 mL) and extracted with EtOAc (30 mL, then 5 x 15 mL). The combined EtOAc layers were dried ($MgSO_4$) and concentrated to give 1.38 g of a thick gummy solid. Azeotropic drying with MeOH, followed by extended drying on hi-vac (ca. 60 h), yielded 1.24 g (ca. 4.64 mmol, 85%) of crude 4-hydroxybenzoyl-L-glutamic acid as a fine white crystalline solid. **^{1}H NMR** (500 MHz, CD_3OD) δ 7.75 (d, *J* = 7.7 Hz, 2H), 6.83 (d, *J* = 7.8 Hz, 2H), 4.67-4.55 (m, 1H), 2.55-2.41 (m, 2H), 2.37-2.22 (m, 1H), 2.16-2.04 (m, 1H); **^{13}C NMR** (125 MHz, CD_3OD) δ 176.7, 175.3, 170.2, 162.3, 130.6, 125.9, 116.1, 53.7, 31.5, 27.6.

2-Hydroxybenzoyl-L-glutamic acid (SA-Glu): Following the general procedure for the synthesis of diethyl *4*-acetoxybenzoyl-L-glutamate, coupling of 1.00 g (5.55 mmol) of acetylsalicylic acid and 1.33g (5.55 mmol) of diethyl L-glutamate hydrochloride gave 1.78 g (4.87 mmol, 80%) of diethyl *o*-acetoxybenzoyl-L-glutamate as a colorless oil. $\mathbf{R_f}$ 0.23 (2:1

[3] Fairburn, E. I., Magerlein, B. J., Stubberfield, L., Stapert, E., and Weisblat, D. I. (1954) Oxygen analogs of pteroic acid. *Journal of the American Chemical Society* **76**: 676-679.

hexanes/EtOAc). Saponification of this material with NAOH according to general procedure gave 1.19 g (4.36 mmol, 92%) of the title compound as a white solid. **^{1}H NMR** (500 MHz, CD_3OD) δ 7.85 (d, *J* = 8.4, 1.6 Hz, 1H), 7.41-7.36 (m, 1H), 6.94-6.86 (m, 2H), 4.68 (dd, *J*= 8.8, 5.1 Hz, 1H), 2.52-2.42 (m, 2H), 2.36-2.27 (m, 1H), 2.16-2.07 (m, 1H).

4-Hydroxybenzoyl-L-aspartic acid (4-HBA-Asp): Following the general procedure for the synthesis of diethyl *4*-acetoxybenzoyl-L-glutamate, coupling of 1.00 (5.5 mmol) of 4-acetoxybenzoic acid and 1.10 g (5.55 mmol) of dimethyl L-aspartate hydrochloride gave 1.76 g (4.89 mmol, 88%) of dimethyl p-acetoxybenzoyl-L-aspartate as a colorless oil. **R_f** 0.06 (2:1 hexanes/EtOAc). Saponification of this material with NAOH according to the general procedure gave 856 mg (2.96 mmol, 61%) of the title compound as a sticky pale yellow solid. **^{1}H NMR** (500 MHz, CD_3OD) δ 7.72 (d, *J* = 8.8 Hz, 2H), 6.83 (d, *J*= 8.8 Hz, 2H), 4.93 (dd, *J*= 7.2, 5.4 Hz, 1H), 2.99 (dd, *J*= 16.7, 5.4 Hz, 1H), 2.90 (dd, *J*= 16.7, 7.1 Hz, 1H).

2-Hydroxybenzoyl-L-aspartic acid (SA-Asp): Following the general procedure for the synthesis of diethyl *4*-acetoxybenzoyl-L-glutamate, coupling of 1.00 g (5.55 mmol) of acetylsalicylic acid and 1.10g (5.55 mmol) of dimethyl L-aspartate hydrochloride gave 1.68 g (4.67 mmol, 84%) of dimethyl *o*-acetoxybenzoyl-L-aspartate as a colorless oil. **R_f** 0.10 (2:1 hexanes/EtOAc). Saponification of this material with NAOH according to general procedure gave 1.16 g (4.01 mmol, 86%) of the title compound as a pale Pink solid. **^{1}H NMR** (500 MHz, CD_3OD) δ 7.84 (d, *J* = 8.2, 1.7 Hz, 1H), 7.38 (ddd, *J*= 8.4, 7.3,1.7 Hz, 1H), 6.93-6.88 (m, 2H), 4.98 (t, *J*= 5.7 Hz, 1H), 2.98 (d, *J*= 5.7 Hz, 2H).

Method 3.S4. Creation of *gh3.1gh3.3gh3.4gh3.5gh3.6pbs3* sextuple mutant

The *gh3* pentuple mutant (*gh3.1,3,4,5,6*) was derived by crossing between the single-gene insertion mutants or their double- or triple-mutant derivatives. All single mutants were verified to be gene knockouts by analyzing mRNA from IAA treated plants using Northern blot hybridizations. *gh3.1* is a Ds transposon line in the *Landsberg erecta* background and was previously described (Staswick et al., 2005). All other mutants were in the Col-0 background. *gh3.5/wes1* was also described previously (Park et al., 2007), *gh3.4* and *gh3.6* are T-DNA insertion lines (Salk_102549 and Salk_013458, respectively), and *gh3.3* is an Spm transposon line (SM.37350). Homozygous mutant genotypes were identified by PCR using the forward and reverse primers shown in Table 3.1, along with Lba1 (for gh3.4, gh3.5, and gh3.6) or 3′dSpm (for gh3.3).

To make the *gh3.1gh3.3gh3.4gh3.5gh3.6pbs3*(*gh3.12*) sextuple mutant (*gh6x*), the *gh3* pentuple mutant (*gh3.1gh3.3gh3.4gh3.5gh3.6*) was crossed to the t-DNA insertion mutant *pbs3-2* (Salk_018225) and genotyped as described above, using the same or different primers as indicated.

Used for pentuple or sextuple	Gene	Forward primer	Reverse primer
sextuple	Pbs3	CAAATCAATTGAACCAAA CCC	TAACTGGGTCACAGACTTGG G
sextuple	Gh3.3	CCG TTG ATT CAG CTC TGC GA	AACCTCAGCATTTAGTCTTC ACG
pentuple	Gh3.3	GTGACAGGCAG AG TCACAAG C	TTTTAACGTATTAATC TTGGC ACG
both	Gh3.4	CAATGACGGGATTTTGATC AC	TGTGGAGCGGAATTATG AAAC
both	Gh3.5	AGGCCAGTGTTG TTGTC TTTG	TGGTCTTGAGCATAG ATTCCG
sextuple	Gh3.6	AAACCTAAACGATGCCTG AGG	CTCAGGCCAATGTTTCTCAA G
pentuple	Gh3.6	GCAAAAACAGC ACC AAC ACG A	CGCAGCTTTGGAG GTTTC TG A
pentuple	Lba1	TGGTTCACGTAG TG GGCC ATCG	
sextuple	LBb1.3	ATTTTGCCGATTTCGGAAC	
both	3′dSpm	TACGAATAAGAGCG TCC ATTTTAG AGT	

REFERENCES

Altschul, S.F., Madden, T.L., Schäffer, A.A., Zhang, J., Zhang, Z., Miller, W., Lipman, D.J., 1997. Gapped BLAST and PSI-BLAST: a new generation of protein database search programs. Nucleic Acids Res. 25, 3389–402.

Anderson, J.C., Wan, Y., Kim, Y.-M., Pasa-Tolic, L., Metz, T.O., Peck, S.C., 2014. Decreased abundance of type III secretion system-inducing signals in Arabidopsis mkp1 enhances resistance against Pseudomonas syringae. Proc. Natl. Acad. Sci. U. S. A. 111, 6846–51. doi:10.1073/pnas.1403248111

Aoki, Y., Okamura, Y., Tadaka, S., Kinoshita, K., Obayashi, T., 2016. ATTED-II in 2016: A Plant Coexpression Database Towards Lineage-Specific Coexpression. Plant Cell Physiol. 57, e5–e5. doi:10.1093/pcp/pcv165

Bartsch, M., Bednarek, P., Vivancos, P.D., Schneider, B., von Roepenack-Lahaye, E., Foyer, C.H., Kombrink, E., Scheel, D., Parker, J.E., 2010. Accumulation of Isochorismate-derived 2,3-Dihydroxybenzoic 3- *O* -β-d-Xyloside in *Arabidopsis* Resistance to Pathogens and Ageing of Leaves. J. Biol. Chem. 285, 25654–25665. doi:10.1074/jbc.M109.092569

Bloor, S.J., Abrahams, S., 2002. The structure of the major anthocyanin in Arabidopsis thaliana. Phytochemistry 59, 343–6.

Bourne, D.J., Barrow, K.D., Milborrow, B. V., 1991. Salicyloylaspartate as an endogenous component in the leaves of Phaseolus vulgaris. Phytochemistry 30, 4041–4044.

Chandran, D., Tai, Y.C., Hather, G., Dewdney, J., Denoux, C., Burgess, D.G., Ausubel, F.M., Speed, T.P., Wildermuth, M.C., 2009. Temporal global expression data reveal known and novel salicylate-impacted processes and regulators mediating powdery mildew growth and reproduction on Arabidopsis. Plant Physiol. 149, 1435–51. doi:10.1104/pp.108.132985

Chen, Y., Shen, H., Wang, M., Li, Q., He, Z., 2013. Salicyloyl-aspartate synthesized by the acetyl-amido synthetase GH3 . 5 is a potential activator of plant immunity in Arabidopsis. Acta Biochim Biophys Sin 45, 827–836. doi:10.1093/abbs/gmt078.Advance

Cui, H., Gobbato, E., Kracher, B., Qiu, J., Bautor, J., Parker, J.E., 2017. A core function of EDS1 with PAD4 is to protect the salicylic acid defense sector in Arabidopsis immunity. New Phytol. 213, 1802–1817. doi:10.1111/nph.14302

Dempsey, D.A., Vlot, a C., Wildermuth, M.C., Klessig, D.F., 2011. Salicylic Acid biosynthesis and metabolism. Arabidopsis Book 9, e0156. doi:10.1199/tab.0156

Feys, B.J., Moisan, L.J., Newman, M.A., Parker, J.E., 2001. Direct interaction between the Arabidopsis disease resistance signaling proteins, EDS1 and PAD4. EMBO J. 20, 5400–5411. doi:10.1093/emboj/20.19.5400

Garcion, C., Lohmann, A., Lamodière, E., Catinot, J., Buchala, A., Doermann, P., Métraux, J.-P., 2008. Characterization and biological function of the ISOCHORISMATE SYNTHASE2 gene of Arabidopsis. Plant Physiol. 147, 1279–87. doi:10.1104/pp.108.119420

George Thompson, A.M., Iancu, C. V, Neet, K.E., Dean, J. V, Choe, J.-Y., 2017. Differences in salicylic acid glucose conjugations by UGT74F1 and UGT74F2 from Arabidopsis thaliana. Sci. Rep. 7, 46629. doi:10.1038/srep46629

Glazebrook, J., Zook, M., Mert, F., Kagan, I., Rogers, E.E., Crute, I.R., Holub, E.B., Hammerschmidt, R., Ausubel, F.M., 1997. Phytoalexin-deficient mutants of Arabidopsis reveal that PAD4 encodes a regulatory factor and that four PAD genes contribute to downy mildew resistance. Genetics 146, 381–92.

Green, R., Fluhr, R., 1995. UV-B-Induced PR-1 Accumulation is Mediated by Active Oxygen

Species. Plant Cell 7, 203–212.
Hagemeier, J., Schneider, B., Oldham, N.J., Hahlbrock, K., 2001. Accumulation of soluble and wall-bound indolic metabolites in Arabidopsis thaliana leaves infected with virulent or avirulent Pseudomonas syringae pathovar tomato strains. Proc. Natl. Acad. Sci. 98, 753–758. doi:10.1073/pnas.98.2.753
Horvath, D.M., Chua, N.-H., 1996. Identification of an immediate-early salicylic acid-inducible tobacco gene and characterization of induction by other compounds. Plant Mol. Biol. 31, 1061–1072. doi:10.1007/BF00040724
Hunter, L.J.R., Westwood, J.H., Heath, G., Macaulay, K., Smith, A.G., MacFarlane, S.A., Palukaitis, P., Carr, J.P., 2013. Regulation of RNA-Dependent RNA Polymerase 1 and Isochorismate Synthase Gene Expression in Arabidopsis. PLoS One 8, e66530. doi:10.1371/journal.pone.0066530
Jagadeeswaran, G., Raina, S., Acharya, B.R., Maqbool, S.B., Mosher, S.L., Appel, H.M., Schultz, J.C., Klessig, D.F., Raina, R., 2007. Arabidopsis GH3-LIKE DEFENSE GENE 1 is required for accumulation of salicylic acid, activation of defense responses and resistance to Pseudomonas syringae. Plant J. 51, 234–46. doi:10.1111/j.1365-313X.2007.03130.x
Jaillais, Y., Chory, J., 2010. Unraveling the paradoxes of plant hormone signaling integration. Nat. Struct. Mol. Biol. 17, 642–5. doi:10.1038/nsmb0610-642
Jirage, D., Tootle, T.L., Reuber, T.L., Frost, L.N., Feys, B.J., Parker, J.E., Ausubel, F.M., Glazebrook, J., 1999. Arabidopsis thaliana PAD4 encodes a lipase-like gene that is important for salicylic acid signaling. Proc. Natl. Acad. Sci. U. S. A. 96, 13583–8.
Johnson, C., Boden, E., Arias, J., 2003. Salicylic acid and NPR1 induce the recruitment of trans-activating TGA factors to a defense gene promoter in Arabidopsis. Plant Cell 15, 1846–58. doi:10.1105/TPC.012211
Klessig, D.F., Durner, J., Noad, R., Navarre, D.A., Wendehenne, D., Kumar, D., Zhou, J.M., Shah, J., Zhang, S., Kachroo, P., Trifa, Y., Pontier, D., Lam, E., Silva, H., 2000. Nitric oxide and salicylic acid signaling in plant defense. Proc. Natl. Acad. Sci. U. S. A. 97, 8849–55. doi:10.1073/PNAS.97.16.8849
Lee, M.W., Jelenska, J., Greenberg, J.T., 2008. Arabidopsis proteins important for modulating defense responses to Pseudomonas syringae that secrete HopW1-1. Plant J. 54, 452–65. doi:10.1111/j.1365-313X.2008.03439.x
Lee, M.W., Lu, H., Jung, H.W., Greenberg, J.T., 2007. A key role for the Arabidopsis WIN3 protein in disease resistance triggered by Pseudomonas syringae that secrete AvrRpt2. Mol. Plant. Microbe. Interact. 20, 1192–200. doi:10.1094/MPMI-20-10-1192
Li, J., Brader, G., Kariola, T., Tapio Palva, E., 2006. WRKY70 modulates the selection of signaling pathways in plant defense. Plant J. 46, 477–491. doi:10.1111/j.1365-313X.2006.02712.x
Li, J., Brader, G., Palva, E.T., 2004. The WRKY70 transcription factor: a node of convergence for jasmonate-mediated and salicylate-mediated signals in plant defense. Plant Cell 16, 319–31. doi:10.1105/tpc.016980
Lu, F., Ralph, J., Morreel, K., Messens, E., Boerjan, W., Busson, R., Herdewijn, P., Devreese, B., Beeumen, J. Van, Marita, J.M., Ralph, J., Chen, C., Burggraeve, B., Montagu, M. Van, Messens, E., Boerjan, W., 2004. Preparation and relevance of a cross-coupling product between sinapyl alcohol and sinapyl p-hydroxybenzoate. Org. Biomol. Chem. 2, 2888–2890. doi:10.1039/b411428k
Mackelprang, R., Okrent, R.A., Wildermuth, M.C., 2017. Preference of Arabidopsis thaliana

GH3.5 acyl amido synthetase for growth versus defense hormone acyl substrates is dictated by concentration of amino acid substrate aspartate. Phytochemistry 143, 19–28. doi:10.1016/j.phytochem.2017.07.001

Mur, L.A., Bi, Y.M., Darby, R.M., Firek, S., Draper, J., 1997. Compromising early salicylic acid accumulation delays the hypersensitive response and increases viral dispersal during lesion establishment in TMV-infected tobacco. Plant J. 12, 1113–26.

Nobuta, K., Okrent, R. a, Stoutemyer, M., Rodibaugh, N., Kempema, L., Wildermuth, M.C., Innes, R.W., 2007. The GH3 acyl adenylase family member PBS3 regulates salicylic acid-dependent defense responses in Arabidopsis. Plant Physiol. 144, 1144–56. doi:10.1104/pp.107.097691

Okada, K., Ohara, K., Yazaki, K., Nozaki, K., Uchida, N., Kawamukai, M., Nojiri, H., Yamane, H., 2004. The AtPPT1 gene encoding 4-hydroxybenzoate polyprenyl diphosphate transferase in ubiquinone biosynthesis is required for embryo development in Arabidopsis thaliana. Plant Mol. Biol. 55, 567–77. doi:10.1007/s11103-004-1298-4

Okrent, R.A., 2010. Biochemical and Functional Characterization of the GH3 Amino Acid-Conjugase PBS3 of Arabidopsis thaliana. Dissertation.

Okrent, R. a, Brooks, M.D., Wildermuth, M.C., 2009. Arabidopsis GH3.12 (PBS3) conjugates amino acids to 4-substituted benzoates and is inhibited by salicylate. J. Biol. Chem. 284, 9742–54. doi:10.1074/jbc.M806662200

Okrent, R. a, Wildermuth, M.C., 2011. Evolutionary history of the GH3 family of acyl adenylases in rosids. Plant Mol. Biol. 76, 489–505. doi:10.1007/s11103-011-9776-y

Peat, T.S., Böttcher, C., Newman, J., Lucent, D., Cowieson, N., Davies, C., 2012. Crystal structure of an indole-3-acetic acid amido synthetase from grapevine involved in auxin homeostasis. Plant Cell 24, 4525–38. doi:10.1105/tpc.112.102921

Robert-Seilaniantz, A., Grant, M., Jones, J.D.G., 2011. Hormone crosstalk in plant disease and defense: more than just jasmonate-salicylate antagonism. Annu. Rev. Phytopathol. 49, 317–43. doi:10.1146/annurev-phyto-073009-114447

Siebert, M., Sommer, S., Li, S.M., Wang, Z.X., Severin, K., Heide, L., 1996. Genetic engineering of plant secondary metabolism. Accumulation of 4-hydroxybenzoate glucosides as a result of the expression of the bacterial ubiC gene in tobacco. Plant Physiol. 112, 811–9. doi:10.1104/PP.112.2.811

Smith-Becker, J., Marois, E., Huguet, E.J., Midland, S.L., Sims, J.J., Keen, N.T., 1998. Accumulation of salicylic acid and 4-hydroxybenzoic acid in phloem fluids of cucumber during systemic acquired resistance is preceded by a transient increase in phenylalanine ammonia-lyase activity in petioles and stems. Plant Physiol. 116, 231–8. doi:10.1104/PP.116.1.231

Staswick, P.E., Serban, B., Rowe, M., Tiryaki, I., 2005. Characterization of an Arabidopsis Enzyme Family That Conjugates Amino Acids to Indole-3-Acetic Acid. Plant Cell 17, 616–627. doi:10.1105/tpc.104.026690.1

Staswick, P.E., Tiryaki, I., Rowe, M.L., 2002. Jasmonate Response Locus JAR1 and Several Related Arabidopsis Genes Encode Enzymes of the Firefly Luciferase Superfamily That Show Activity on Jasmonic , Salicylic , and Indole-3-Acetic Acids in an Assay for Adenylation. Plant Cell 14, 1405–1415. doi:10.1105/tpc.000885.defect

Steffan, H., Ziegler, A., Rapp, A., 1988. N-salicyloyl-aspartic acid: A new phenolic compound in grapevines. Vitis 27, 79–86.

Strawn, M. a, Marr, S.K., Inoue, K., Inada, N., Zubieta, C., Wildermuth, M.C., 2007.

Arabidopsis isochorismate synthase functional in pathogen-induced salicylate biosynthesis exhibits properties consistent with a role in diverse stress responses. J. Biol. Chem. 282, 5919–33. doi:10.1074/jbc.M605193200
Swiezewska, E., 2004. Ubiquinone and plastoquinone metabolism in plants. Methods Enzymol. 378, 124–31. doi:10.1016/S0076-6879(04)78007-6
Tan, J., Bednarek, P., Liu, J., Schneider, B., Svatoš, A., Hahlbrock, K., 2004. Universally occurring phenylpropanoid and species-specific indolic metabolites in infected and uninfected Arabidopsis thaliana roots and leaves. Phytochemistry 65, 691–699. doi:10.1016/j.phytochem.2003.12.009
Tsuda, K., Sato, M., Glazebrook, J., Cohen, J.D., Katagiri, F., 2008. Interplay between MAMP-triggered and SA-mediated defense responses. Plant J. 53, 763–775. doi:10.1111/j.1365-313X.2007.03369.x
Uquillas, C., Letelier, I., Blanco, F., Jordana, X., Holuigue, L., 2004. NPR1-Independent Activation of Immediate Early Salicylic Acid-Responsive Genes in *Arabidopsis*. Mol. Plant-Microbe Interact. 17, 34–42. doi:10.1094/MPMI.2004.17.1.34
Veit, M., Pauli, G.F., 1999. Major Flavonoids from *Arabidopsis thaliana* Leaves †. J. Nat. Prod. 62, 1301–1303. doi:10.1021/np990080o
Vlot, a C., Dempsey, D.A., Klessig, D.F., 2009. Salicylic Acid, a multifaceted hormone to combat disease. Annu. Rev. Phytopathol. 47, 177–206. doi:10.1146/annurev.phyto.050908.135202
Wang, L., Mitra, R.M., Hasselmann, K.D., Sato, M., Lenarz-Wyatt, L., Cohen, J.D., Katagiri, F., Glazebrook, J., 2008. The genetic network controlling the Arabidopsis transcriptional response to Pseudomonas syringae pv. maculicola: roles of major regulators and the phytotoxin coronatine. Mol. Plant-Microbe Interact. 21, 1408–20. doi:10.1094/MPMI-21-11-1408
Wang, L., Tsuda, K., Truman, W., Sato, M., Nguyen, L. V., Katagiri, F., Glazebrook, J., 2011. CBP60g and SARD1 play partially redundant critical roles in salicylic acid signaling. Plant J. 67, 1029–1041. doi:10.1111/j.1365-313X.2011.04655.x
Warren, R.F., Merritt, P.M., Holub, E., Innes, R.W., 1999. Identification of three putative signal transduction genes involved in R gene-specified disease resistance in Arabidopsis. Genetics 152, 401–12.
Weigel, R.R., Bäuscher, C., Pfitzner, A.J.P., Pfitzner, U.M., 2001. NIMIN-1, NIMIN-2 and NIMIN-3, members of a novel family of proteins from Arabidopsis that interact with NPR1/NIM1, a key regulator of systemic acquired resistance in plants. Plant Mol. Biol. 46, 143–160. doi:10.1023/A:1010652620115
Weigel, R.R., Pfitzner, U.M., Gatz, C., 2005. Interaction of NIMIN1 with NPR1 modulates PR gene expression in Arabidopsis. Plant Cell 17, 1279–91. doi:10.1105/tpc.104.027441
Westfall, C.S., Sherp, A.M., Zubieta, C., Alvarez, S., Schraft, E., Marcellin, R., Ramirez, L., Jez, J.M., 2016. Arabidopsis thaliana GH3.5 acyl acid amido synthetase mediates metabolic crosstalk in auxin and salicylic acid homeostasis. Proc. Natl. Acad. Sci. U. S. A. 113, 13917–13922. doi:10.1073/pnas.1612635113
Westfall, C.S., Zubieta, C., Herrmann, J., Kapp, U., Nanao, M.H., Jez, J.M., 2012. Structural basis for prereceptor modulation of plant hormones by GH3 proteins. Science 336, 1708–11. doi:10.1126/science.1221863
Wildermuth, M.C., Dewdney, J., Wu, G., Ausubel, F.M., 2001. Isochorismate synthase is required to synthesize salicylic acid for plant defence. Nature 414, 562–5.

doi:10.1038/35107108
Winter, D., Vinegar, B., Nahal, H., Ammar, R., Wilson, G. V, Provart, N.J., 2007. An "Electronic Fluorescent Pictograph" browser for exploring and analyzing large-scale biological data sets. PLoS One 2, e718. doi:10.1371/journal.pone.0000718
Woodward, A.W., Bartel, B., 2005. Auxin: regulation, action, and interaction. Ann. Bot. 95, 707–35. doi:10.1093/aob/mci083
Zhang, K., Halitschke, R., Yin, C., Liu, C.-J., Gan, S.-S., 2013. Salicylic acid 3-hydroxylase regulates Arabidopsis leaf longevity by mediating salicylic acid catabolism. Proc. Natl. Acad. Sci. U. S. A. 110, 14807–12. doi:10.1073/pnas.1302702110
Zhang, Y., Zhao, L., Zhao, J., Li, Y., Wang, J., Guo, R., Gan, S., Liu, C.-J., Zhang, K., 2017. S5H/DMR6 Encodes a Salicylic Acid 5-Hydroxylase That Fine-Tunes Salicylic Acid Homeostasis. Plant Physiol. 175, 1082–1093. doi:10.1104/pp.17.00695
Zhang, Z., Li, Q., Li, Z., Staswick, P.E., Wang, M., Zhu, Y., He, Z., 2007. Dual regulation role of GH3.5 in salicylic acid and auxin signaling during Arabidopsis-Pseudomonas syringae interaction. Plant Physiol. 145, 450–64. doi:10.1104/pp.107.106021
Zhou, N., Tootle, T.L., Tsui, F., Klessig, D.F., Glazebrook, J., 1998. PAD4 functions upstream from salicylic acid to control defense responses in Arabidopsis. Plant Cell 10, 1021–30. doi:10.1105/TPC.10.6.1021

CHAPTER IV: Forward genetic suppressor screen in the *pPR1::GUSpbs3* background identifies mutants that restore PBS3-mediated salicylic acid accumulation

ABSTRACT

Mutations in the *PBS3* gene of *Arabidopsis thaliana* compromise plant defense responses such as accumulation of the defense phytohormone salicylic acid (SA), expression of defense related genes such as *pathogenesis related 1* (*PR1*), and resistance to virulent and avirulent bacterial pathogens. Previous efforts to identify the mechanism by which PBS3 mediates plant defense have not yielded definitive results. Therefore, we used a genetic suppressor screen in the SA-deficient *pPR1::GUSpbs3* background to identify additional components of the PBS3-signaling pathway. Not all mutants with restored *GUS* expression had restored SA, and so a secondary screen was used and identified six mutant lines with both restored *PR1* expression and SA accumulation. Two of these lines, *suppressor of pbs3 susceptibility 19* (*sops19*) and *sops101*, were selected for further analysis. High throughput sequencing of *sops19* and *sops101* identified several candidate causal mutants which were analyzed and ranked based on a number of criteria and are currently being introduced into the clean *pPR1::GUSpbs3* background for confirmation. These results, coupled with RNA-sequencing of Col-0 (WT) and *pbs3*, suggest that PBS3 may be a higher order regulator of not only SA induction and accumulation, but also of inhibition of the jasmonic acid response, coordinating these mutually antagonistic pathways.

INTRODUCTION

The phytohormone salicylic acid (SA) is critical for plant defense against biotrophic and hemibiotrophic pathogens. In *Arabidopsis thaliana,* SA is synthesized through conversion of chorismate to isochorismate by *isochorismate synthase 1* (ICS1; At1g74710), likely followed by conversion of isochorismate to SA by an as yet unknown isochorismate pyruvate lyase (Strawn et al., 2007; Wildermuth et al., 2001). Synthesized free SA can be converted to different forms such as SA-glucosides, which serve as hydrolysable storage forms of SA, or SA-amino acid conjugates such as SA-Asp (see Chapters II, III, Dempsey et al., 2011; Mackelprang et al., 2017; Westfall et al., 2016).

Mutations in *Arabidopsis thaliana PBS3* (*Pseudomonas syringae* pv *tomato* DC3000 avrPphB susceptibility; *GH3.12*; At5g13320) are more susceptible to bacterial pathogens and accumulate lower levels of SA and downstream SA-inducible genes such as *Pathogenesis Related 1* (*PR1*; At2g14610) (Jagadeeswaran et al., 2007; Lee et al., 2008, 2007; Nobuta et al., 2007). While PBS3 enzymatic activity has been characterized, a direct mechanism by which this activity influences SA accumulation remains unknown (Okrent et al., 2009). PBS3 is a member of the *Gretchen Hagan 3* (*GH3*) family of adenylating enzymes which conjugate small acyl acids to amino acids, but its enzymatic activity is actually inhibited by SA (Okrent et al., 2009; Westfall et al., 2012). PBS3 preferentially conjugates 4-substituted benzoic acids such as 4-hydroxybenzoic acid (4-HBA) and *para*-aminobenzoic acid (pABA) to glutamic acid (Glu) (Okrent et al., 2009). Hyperaccumulation of the PBS3 substrate 4-HBA does not seem to cause *pbs3*-mediated susceptibility, as exogenous application of 4-HBA did not cause increased susceptibility in Col-0 (WT) plants infected with virulent *Pseudomonas syringae* pv. *maculicola*

(*Pma*) (Chapter III). It remains unclear how or if the enzymatic activity of PBS3 is responsible for the lack of SA accumulation in *pbs3*.

Extensive metabolite analyses (see Chapter III; Okrent, 2010) identified higher levels of SA-Asp in *pbs3* plants 24 hours post infection with avirulent *Pseudomonas syringae* pv. *tomato* (*Pto*) DC3000 AvrRpt2. Interestingly, SA-Asp is the product of the enzymatic activity of another GH3 family protein, GH3.5 (Chapter II; Mackelprang et al., 2017; Staswick et al., 2002; Westfall et al., 2016). We hypothesized that in Col-0, PBS3 or one of its products inhibits GH3.5 conversion of SA to SA-Asp. In *pbs3* mutants, SA would be shunted to SA-Asp, decreasing the pool of available active SA. However, crossing of *pbs3* to *gh3.5* did not rescue the *pbs3* phenotype, and mutants still accumulated significant SA-Asp (Chapter III). I therefore further crossed *pbs3gh3.5* to make the *pbs3gh3.1gh3.3gh3.4gh3.5gh3.6* sextuple mutant, called *gh6x*. SA-Asp did not accumulate in *gh6x*, however this did not rescue the low SA and increased susceptibility (Chapter III). In addition, exogenous application of SA-Asp to WT plants did not increase their susceptibility to pathogen growth. While the metabolic change resulting in dramatically elevated SA-Asp in *pbs3* is striking, it is insufficient to explain *pbs3* susceptibility.

Given previous work on PBS3, there remain three likely mechanisms by which PBS3 increases plant resistance. First, *pbs3* may facilitate a shift in metabolism that alters flux to SA precursors such as chorismate or could pull from the pool of SA or SAG as SA-Asp appears to do. Either an overabundance of the PBS3 substrate or a dirth of PBS3 product in *pbs3* mutants could be enough to cause this metabolic shift. However, based on the metabolic profiling performed by Rachel Okrent (see Chapter III; Okrent, 2010), this does not seem likely. Using both absorbance and fluorescence detection, no changes in cell wall components were observed, and only three leaf soluble compounds were altered between *pbs3* vs Col-0. Two of these three were SA metabolites, namely an SA glucoside and SA-Asp (Chapter III, Okrent, 2010). While there are limits to such an analysis by HPLC, a broad metabolic shift in metabolism surrounding the SA precursor chorismate should be visible through the variety of extractions and analyses tested. It is possible that an entirely different class of compounds, undetected by our analyses, is altered, or that PBS3-mediated metabolic reprogramming is not the cause of *pbs3*-susceptibiliy.

A second mechanism by which PBS3 may affect defense induction is through the production of a regulatory ligand. A regulatory ligand produced by PBS3 could interact with and alter a protein's activity and/or protein/protein interactions to cause broad downstream cellular changes. For example, the hormone jasmonic acid (JA) must be conjugated to isoleucine by GH3.11/JAR1 to be activated and to bind to the JA receptor (Staswick and Tiryaki, 2004). The JA receptor COI1 is the F-Box of an SCF E3 ligase. Upon JA-Ile binding, COI1 ubiquitinates the JAZ transcriptional repressors, allowing JA-induced transcriptional changes to occur (Chini et al., 2007; Thines et al., 2007; Yan et al., 2007). If this hypothesis is correct, the identification of the biologically relevant product/regulatory ligand and its interaction partner(s) would be critical to our understanding of PBS3. 4-HBA-Glu and pABA-Glu, *in vitro* products of PBS3, have not been tested for such activity, and broad screening for a biologically relevant secondary messenger product of PBS3 would be difficult based on the lack of 4-subsituted benzoate-amino acid conjugates for purchase. However, when exogenous 4-HBA was applied to WT plants, it did not result in increased pathogen growth, as would be expected if 4-HBA accumulation was responsible for the *pbs3* phenotype (Chapter III). As such, a preferable mechanism to metabolite screening for elucidating this type of activity may be through identification of a regulatory ligand binding protein.

Finally, PBS3 could interact with another protein to affect downstream changes. While there are no predicted protein-protein interaction domains in PBS3 (Marchler-Bauer et al., 2017), it was identified in a yeast-two-hybrid screen for targets of the bacterial effector HopW1-1 (Lee et al., 2008). HopW1-1 is a relatively rare effector found in *Pma* ES4326 but is absent from *Pto* DC3000 (Lee et al., 2008). When added to *Pto*, *HopW1-1* decreases *Pto* virulence; however this is partially compromised in *pbs3*, suggesting that PBS3 is involved in effector triggered immunity in the presence of HopW1-1 (Lee et al., 2008). Amino acids 335-575 of PBS3 were sufficient for binding to HopW1-1. The PBS3 protein's active site is at the interface between the N- and C- terminal domains (Westfall et al., 2012). A flexible hinge loop near amino acids 420-432 allows the C terminus to pivot during catalysis (Westfall et al., 2012). PBS3 interaction with another protein(s) at amino acids 335-575 could alter this pivot, changing PBS3 enzyme activity. Identification of such an interaction partner would quickly move our understanding of PBS3 and induced SA forward.

Given the body of research around PBS3 and the lack of clarity as to its effect on SA, I used a forward genetic suppressor screen to identify additional proteins involved in PBS3-mediated SA accumulation. I created a *pPR1*::*GUSpbs3* mutant line through crossing *pPR1::GUS* to *pbs3-2*. Screening of M2 plants after EMS mutagenesis identified several mutant lines with restored GUS staining in response to SA-inducible UV-C treatment. After being secondarily screened for restored total SA, two lines, designated *suppressors of pbs3 susceptibility 19* (*sops19*) and *sops101* were chosen for further characterization. In addition to characterization in response to UV-C, responses to both avirulent and virulent *P. syringae* were assayed. Candidate causal mutations were identified through high-throughput sequencing of mutant gDNA with the Illumina HiSeq 4000 platform. After ranking of candidate causal mutations, the $RAP2.6^{A93V}$ and $PAD4^{S135F}$ emerged as top candidates for causing the *sops19* and *sops101* phenotypes, respectively. Furthermore, RNA-Seq was used to interrogate transcriptional reprogramming between Col-0 and *pbs3*, which identified not only broad changes in SA-associated transcriptional output, but also transcriptional differences associated with other hormones, particularly JA. Through this work, valuable insight about PBS3 has been gained. I provide further evidence for activity of PBS3 beyond promoting SA accumulation; it may functionally inhibit the JA pathway, which antagonizes SA and is involved in defense against necrotrophic pathogens and insects.

METHODS

Plant growth conditions and UV-C treatment:
Arabidopsis thaliana Col-0, *pbs3-2*, *pPR1::GUS*, *pPR1::GUSpbs3-2*, EMS-mutagenized lines, and *sops* lines for characterization were grown in MetroMix 200 (Scott, Marysville, OH, USA). Plants for *sops* characterization or NGS were grown with 12:12 light:dark in a controlled growth chamber at 22°C, 70% relative humidity, 100-115 µE $m^{-2}sec^{-1}$ fluorescent illumination. Plants for screening were grown at 22-25°C without humidity control and 100 µE $m^{-2}sec^{-1}$ fluorescent illumination. At three weeks old, all plants were treated with ¼ strength Hoagland's solution. Plants in initial screen were UV-C treated at 3 weeks old with 5 kJ/m^2 UV-C, and secondary screen and further characterized lines were treated at 4-5 weeks old with 5 kJ/m^2 UV-C irradiation in a UV (254 nm) Stratalinker 1800 (Stratagene) or with pathogen as described.

Creation of pPR1::GUSpbs3 EMS-mutagenized lines:
Arabidopsis thaliana transformants with the *pPR1::GUS* construct were crossed to the T-DNA insertional knockout *pbs3-2*. Both lines were in the Col-0 ecotype. F1s were allowed to self and

F2s were genotyped for *pbs3* homozygosity and presence of GUS. As the location of the *pPR1::GUS* insert is not precisely known, zygosity was not determined in the F2 generation. Homozygous *pbs3-2* lines with GUS were selfed and in the F3 generation, if all progeny were positive for GUS, the line was considered homozygous for *pPR1::GUS* as well.

2.5 grams (approximately 125,000 seeds) of *pPR1::GUSpbs3* seeds were incubated in 40 mL of 100 mM potassium phosphate, pH = 7.5, overnight rocking at 4°C. The buffer was switched for 0.4% ethyl methanesulfonate (EMS) in 40 mL potassium phosphate buffer, pH=7.5 and rocked gently at room temperature for 8 hours. Seeds were washed to remove EMS and stratified for 4 days. 3500 M1 seeds were planted. After germination, they were thinned to approximately 2000 M1 plants, which were grown in 12:12 light:dark conditions and allowed to self. One silique from each plant was harvested, and siliques from 100 plants constituted one pool. 20 pools were generated.

Screening of EMS mutagenized lines:
M2 plants were grown in 12:12 light:dark and were treated with 5 kJ/m^2 UV-C at 3-4 weeks post germination. One *PR1::GUS* and one *PR1::GUSpbs3* plant were included in each treatment as controls. One leaf from each plant was harvested 24 hours later and vacuum infiltrated for 20 minutes at 200 Torr with GUS staining solution (0.1 M $NaPO_4$, pH=7, 10 mM EDTA, 0.1% Triton X, 1 mM $K_3Fe(CN)_6$, 2 mM X-Gluc). Leaves were incubated in GUS staining solution at 37°C for 24 hours, then put in 50% EtOH at room temperature to destain. Destain was changed once 24 hours later, then leaves were mounted on slides for best visualization of *GUS* induction. GUS positive leaves were designated as “dark blue,” “medium blue,” or “pale blue,” with “full,” “most,” or “some” coverage. This created nine subcategories. Leaves that were dark or medium blue that were fully or mostly covered were prioritized for further characterization.

Free and total salicylic acid quantification:
0.2-0.5 grams of mature, fully expanded leaves were collected and extracted with methanol as described in Nobuta et al., 2007. Total SA samples were treated with B-glucosidase to hydrolyze SA glucosides. Samples were run on Shimadzu SCL-10A HPLC system with a Shimadzu RF-10A scanning fluorescence detector and a Shimadzu SPD-M10A photodiode array detector with a 5-µm, 15 cm x 4.6-mm Supelcosil LC-ABZ Plus column (Supelco) with LC-ABZ Plus guard column. Before loading sample, the column was equilibrated with 15% acetonitrile in 25 mM KH_2PO_4, pH=2.5 at a 1.0 mL/min flow rate. The concentration of acetonitrile was raised linearly from 15% to 20% over the course of 10 minutes, then increased linearly over 12 minutes from 20% to 43% acetonitrile, increased linearly from 43% to 66% acetonitrile over 2 minutes, isocratic flow at 66% for 5 minutes, linear decrease from 66% to 15% over 5 minutes, and isocratic flow at 15% for 3 minutes. Known quantities of SA and an internal standard, *o*-Anisic acid, were run to generate a standard curve for quantification. SA and *o*-ANI were detected with a fluorescence detector at 305-nm excitation / 405 nm-emission.

Quantitative Real-time PCR analysis of PR1 *expression:*
4-5 week old plants were treated with 5 kJ/m2 of UV-C, or syringe inoculated with *Pseudomonas syringae* pv. *tomato* DC 3000 AvrRpt2 at A_{600} = 0.0001. Three leaves from a single treated or control plant were collected and frozen immediately in liquid nitrogen, constituting one replicate. Samples were ground to powder with Mini-Beadbeater-96 (Biospec Products). RNA was extracted with Spectrum™ Plant Total RNA Kit (Sigma-Aldrich) according to manufacturer’s instructions. RNA was treated with DNase I (RNase-free) (NEBiolabs) before

cDNA synthesis. cDNA was synthesized with High Capacity cDNA Reverse Transcription Kit (Applied Biosystems) as per manufacturer's instructions with RiboLock RNase Inhibitor (ThermoFisher Scientific). Quantitative real-time PCR reactions were done on CFX ConnectTM Real-Time PCR Detection System (Bio-Rad) using iTaq™ Universal SYBR® Green Supermix (Bio-Rad). Three technical replicates were performed for each sample and expression is relative to ubiquitin5 or actin2, as indicated.

Primers for quantitative real-time PCR:
Primers for qPCR of *Arabidopsis thaliana UBQ5, PR1*, and *Act2* are as follows: *UBQ5* Forward: GAAGACTTACACCAAGCCGAA, *UBQ5* Reverse: TTCTGGTAAACGTAGGTGAGT, *PR1* Forward: GAAAACTTAGCCTGGGGTAGC, *PR1* Reverse: TTCATTAGTATGGCTTCTCGTT, *Actin2* Forward: GGTAACATTGTGCTCAGTGGTGG, *Actin2* Reverse: AACGACCTTAATCTTCATGCTGC

Semi-quantitative flowering time:
24 days after planting 12 plants of each genotype grown under 16:8 light:dark, the % of plants bolting for each genotype was calculated. Based on germination, most genotypes had n = 5-12 plants. This assay was done in two batches; half the genotypes grown and tested at one time and the other half grown and tested at a later date. Because of this, and the growth of plants in an uncontrolled temperature and humidity setting, there was variation in flowering between the two sets. For each set, the difference in percent bolting between *PR1::GUS* and *PR1::GUSpbs3* was calculated, and plants with a percent germinating closer to *PR1::GUS* were classified as *PR1::GUS*-like and those with a percent germinating closer to *PR1::GUSpbs3* were classified as *PR1::GUSpbs3*-like. Genotypes that were within three percentage points of the mid-way point between the two were classified as "ambiguous."

Bacterial virulence assays:
4-5 week old *Arabidopsis* leaves were inoculated with *Pseudomonas syringae* pv. *maculicola* ES4326 at an OD_{600} = 0.0002. Tissue was collected immediately after infection or 72 hours later. For collection, a cork borer was used to punch two leaf discs of 0.7 cm diameter from a single leaf. These leaf discs constituted one replicate, and each condition had 3 replicates from each of 3 plants for a total of 9 replicates. Leaf discs were washed with 500 µL sterile ddH_2O, then reconstituted in 300 µL of 10 mM MgSO4. Tissue was ground with Mini-Beadbeater-96 (Biospec Products) at room temperature. Suspensions were serially diluted and 10 µL were pipetted onto plates with King's B medium and appropriate antibiotic. Plates were incubated at 28°C for 36-48 hours, and the number of colonies was counted from two different dilutions per rep for two technical replicates. Data presented are the means and standard deviations of the log colony forming units per cm^2 from 9 replicates. Experiments were repeated and gave similar results.

Quantitative flowering time measurement:
At least 21 plants per genotype were grown as described in "*plant growth conditions*." Beginning around 3 weeks, plants were monitored daily for the appearance of initial buds. The day of appearance was recorded as well as the number of leaves on the plant at that time. Date of bolting and date of flowering were also recorded. In an independent experiment, the number of leaves at bolting and flowering were also recorded. Data shown are means with standard deviations. Experiment repeated with similar results.

Plant growth and DNA extraction for High Throughput Sequencing

Sops19 was backcrossed to *pPR1::GUSpbs3* and one leaf from each of 92 three-week old F2s was collected and frozen in liquid nitrogen. Plants were UV-C treated (5kJ/m^2) and 24 hpt, one leaf was collected from each plant and stained for GUS (see above). 24 hours later, the frozen leaves from the 20 plants with the most robust GUS staining were ground and combined to make a pool of tissue for *sops19* DNA extraction. Leaf tissue from unbackcrossed *sops101* and from *pPR1::GUSpbs3* were also ground. CTAB DNA extraction was used with DNase free and Protease-free RNase A (Thermo Scientific EN0531) and submitted to the Functional Genomics Laboratory (UC Berkeley) for library preparation and Vincent J. Coates Genomics Sequencing Laboratory at University of California, Berkeley for sequencing. Sequencing was done with Illumina HiSeq 4000 with 50 base pair single end reads.

Analysis of high throughput sequencing to identify candidate causal mutations:
CLC Genomics Workbench Version 10.0.1 (CLC Bio, https://www.qiagenbioinformatics.com/) was used to identify candidate causal mutations. *Sops19* and *sops101* were aligned to the Arabidopsis TAIR10 genome. The "Filter against known variants" function was used to filter out mutations in common between *sops* lines and *pPR1::GUSpbs3*, identifying 2420 unique variants in *sops19* and 893 unique variants in *sops101*. All variants except for G/C to A/T transitions were filtered, followed by filtering of any mutation not in a coding region or that caused a synonymous mutation. The remaining mutants were categorized based on gene identity, BLOSUM score for amino acid change, domain of protein with mutation, and (co-)expression data.

Modeling of PAD4 interaction with EDS1
The EDS1/SAG101 heterodimer and PAD4 model were downloaded from Protein Data Base, Accession 4NFU (Wagner et al., 2013). PAD4 and SAG101 amino acid sequences were aligned and amino acids 150-195 from SAG101 and their homologous residues (122-167) in PAD4 were used to align the two structures using the MatchMaker function of UCSF Chimera (Pettersen et al., 2004).

Genome wide transcriptional analyses (RNA-Seq):
4-5 week old Col-0 and *pbs3* plants were either treated with UV-C or kept as controls. 24 hours later, 3 leaves from each of 3 plants per treatment and genotype were collected and frozen in liquid nitrogen. RNA was extracted using the Spectrum^{TM} Plant Total RNA Kit from Sigma-Aldrich and treated with RNase-free DNase (NEBiolabs) on column. Fragment size and RNA integrity were assessed with Bioanalyzer 2100 (Agilent). Library preparation was performed at the Functional Genomics Laboratory (UC Berkeley) and next generation sequencing on Illumina Hi-Seq2500 Rapid sequencing system was done at the Vincent J. Coates Genomics Sequencing Laboratory (UC Berkeley). 12 samples (3 each for Col-0 Control, Col-0 24 hpt UV-C, *pbs3* Control, *pbs3* 24 hpt UV-C) were multiplexed and run on one lane with 50 bp single end reads resulting in ~141,000,000 reads.
Reads were aligned to the Arabidopsis TAIR 10 genome with HiSat2 using Galaxy (Afgan et al., 2016; Kim et al., 2015). Reads were counted with HTSeq (Anders et al., 2015) and differential expression was determined in edgeR using Fisher's exact test to perform pair-wise tests. Genes were considered significantly differently expressed if their False Discovery Rate (FDR) < 0.05 and Log_2 FC ≥ |1.5|. Overrepresented gene ontology categories were identified by entering gene lists into Virtual Plant's BioMaps using GO Biological Process assignments by TAIR/TIGR (Katari et al., 2010).

RESULTS

EMS mutagenesis and pooling of M2 lines

We identified *suppressor of pbs3 susceptibility* (*sops*) mutants using a forward genetics suppressor screen in the *pPR1::GUSpbs3* background. As *pPR1::GUSpbs3* plants lack functional PBS3, they do not accumulate SA in response to an inducer or show expression of the SA-inducible *PR1* when treated with GUS staining solution (Fig. 4.1a). Approximately 125,000 *pPR1::GUSpbs3* seeds were subject to ethyl methanesulfonate (EMS) mutagenesis by gentle shaking at room temperature in 0.4% EMS solution. Approximately 3,200 EMS mutagenized seeds were planted to create an M1 generation with about 2000 viable plants (extra seeds planted to account for failed germination and/or lethality of mutations). The M1 generation was not tested for suppression of the *pbs3* phenotype as recessive mutations would not yield a phenotype. Therefore, one silique from each of 2000 M1 plants was collected. The contents of 100 siliques constituted one pool, yielding 20 pools.

Suppressor screen of *pbs3* in *pPR1::GUS* background

3-4 week old M2 plants were treated with 5 kJ/m^2 UV-C. UV-C treatment is a robust inducer of the SA response, causing an increase in *PBS3* and *ICS1* expression within a few hours and subsequent SA accumulation (Chapter III; Nawrath et al., 2002; Okrent, 2010; Yalpani et al., 1994). 24 hours post treatment (hpt), one leaf from each plant was harvested and stained with x-gluc staining solution (see methods). Of the 5,112 plants screened, 163 were positive for GUS staining, although the extent of GUS coloration varied.

To prioritize GUS positive plants, we used a classification system to describe the darkness of blue staining and the coverage of the leaf. Leaves were designated as dark, medium, or pale blue, and designated as fully, mostly, or lightly covered (Fig. 4.1b). This created nine classifications. All *sops* lines chosen for further characterization were dark or medium blue and fully or mostly covered.

Characterization of *sops1, sops2, sops3,* and *sops4* does not show restored induced SA accumulation

The first four mutants selected for further characterization were *sops1, sops2, sops3,* and *sops4*. As *PR1* is induced by SA, the levels of total SA in *sops1-sops4* at 24 hpt with UV-C were assayed first. Surprisingly, none of these mutants accumulated statistically higher levels of total SA than *pbs3* (Fig. 4.2a). I next wondered if the causal mutations for *PR1* expression in *sops1-sops4* were downstream of SA, causing defense responses in the absence of SA accumulation. I therefore tested the virulence of *Pma* in *sops1* and *sops2* mutants. 3 days post inoculation, *pbs3*-associated susceptibility was not suppressed in *sops1* or *sops2* as measured by bacterial titers (Fig. 4.2b).

These results indicate that *PR1* may be minimally expressed in response to an unknown SA-independent inducer. Indeed, *PR1* was induced in *sops1* and *sops2*, but to levels much lower than Col-0 (data not shown). It is therefore likely that these mutants induce *PR1* in an SA-independent manner, below a threshold required for induction of further defense responses. The use of GUS to measure gene expression may sometimes yield false positives as low level gene expression can be transient, while GUS protein is highly stable, with a half-life of around three days (Jefferson, 1987; Weinmann et al., 1994).

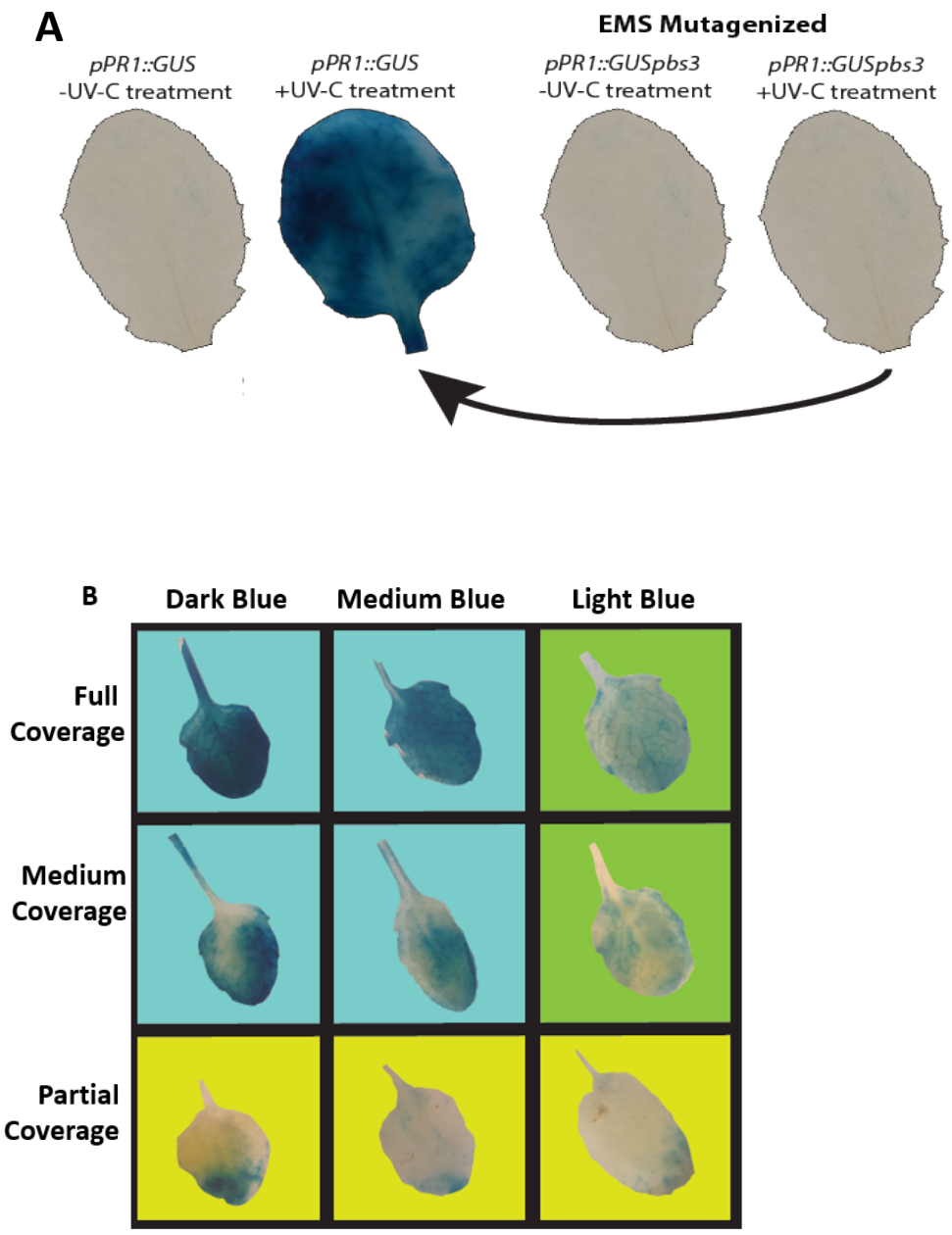

Figure 4.1: Forward genetic suppressor screen in *pPR1::GUSpbs3* background to identify mutants with restored *PR1* expression

(A) Approximately 125,000 *pPR1::GUSpbs3* seeds were EMS mutagenized. Without functional PBS3, the *PR1* promoter should not be activated and thus no *GUS* induction and blue staining should be seen. We screened for *pPR1::GUSpbs3* mutagenized lines that suppressed the non-blue *pbs3* phenotype (i.e., for *pPR1::GUSpbs3* leaves that turned blue).

(B) Classification of M2 leaves based on darkness of blue staining and coverage of staining across leaf. Dark and medium blue leaves with full or medium coverage were considered for further classification.

Secondary screen identifies mutants with restored SA

Because *sops1*, *sops2*, *sops3*, and *sops4* mutants failed to suppress the *pbs3* phenotype, I next conducted a secondary screen to identify *sops* mutants with restored total SA accumulation. 35 lines with dark or medium blue staining and fully or mostly covered after staining in the M2 generation were selected for secondary screening. Approximately 12 M3 plants from each of those 35 lines were grown to four weeks old, then treated with 5 kJ/m^2 UV-C. 24 hpt, a single leaf from each plant was collected and stained for *PR1*-driven GUS. 48 hpt, additional leaves from plants positive for GUS staining were harvested for SA analysis. This extra step was taken because in the M3 generation, the causal mutation should be segregating and inclusion of plants negative for GUS would skew SA quantification. For SA analysis, we measured total SA because it is consistently compromised in *pbs3*, whereas free SA in *pbs3* vs Col-0 has varied based on experimental conditions and time point (Jagadeeswaran et al., 2007; Lee et al., 2008, 2007; Nobuta et al., 2007). Six of the 35 lines had greater than 70% of wildtype SA (Fig. 4.3a).

As *pbs3* has an early flowering phenotype, we also made semi-quantitative measurements of flowering time of the 35 lines in the secondary screen. Plants were grown under 16:8 light:dark. On day 25, I measured the percent of plants in each genotype that had bolted and compared that to the *PR1::GUS* and *PR1::GUSpbs3* controls. Mutant genotypes were designated as *PR1::GUS*-like or *PR1::GUSpbs3*-like based on the percent of plants bolting. The number of plants measured was between 5 and 12 based on the germination rate of that genotype. Four of the six lines with restored SA also had restored flowering time. The final two lines with restored SA were intermediate between the flowering time phenotypes, likely due to segregation of traits. Overall, 12 of the 35 lines in the secondary screen were positive for restored flowering time (Fig. 4.3b). Two lines, *sops19* and *sops101*, which are from different pools and both have restored total SA and flowering time, were chosen for further analysis (Table 4.1). However, it would be interesting at a later date to attempt to uncouple the PBS3 disease related and PBS3 flowering time related phenotypes.

***Sops101* is a dominant mutation and *sops19* shows non-Mendelian segregation**

To determine the dominance of the mutations causing the *sops19* and *sops101* phenotypes, they were backcrossed to *pPR1::GUS* and F1s were allowed to self. In the F2 generation, plants were treated with 5 kJ/m^2 UV-C and 24 hours later, a single leaf from each was collected and stained with x-gluc stain. 24 hours later, the number of leaves stained blue vs those without blue were counted to obtain a segregation ratio. *Sops101* plants were blue at the ratio of 3:1, indicating that the *sops101* mutation is dominant. A dominant mutation in a screen is more likely to be from an hyper-activated mutant whereas a recessive mutation is more likely to be from a loss-of-function mutant, therefore it is likely that *sops101* is a hyper-activated mutant in the SA-signaling pathway.

Segregation of *sops19* interestingly was 1:1 with n = 25. Deviation from the expected 3:1 ratio could be explained by a few different underlying causes. It is possible that the mutation is dominant and the initial backcross was done with a heterozygous *sops19*, which would yield an F2 segregation ratio of 3:5. It is also possible that the *sops19* phenotype is the result of multiple mutations with unknown dominance, or that a homozygous lethal mutation is obscuring ratios (although we'd expect an F2 segregation ratio of 2:5 in that case).

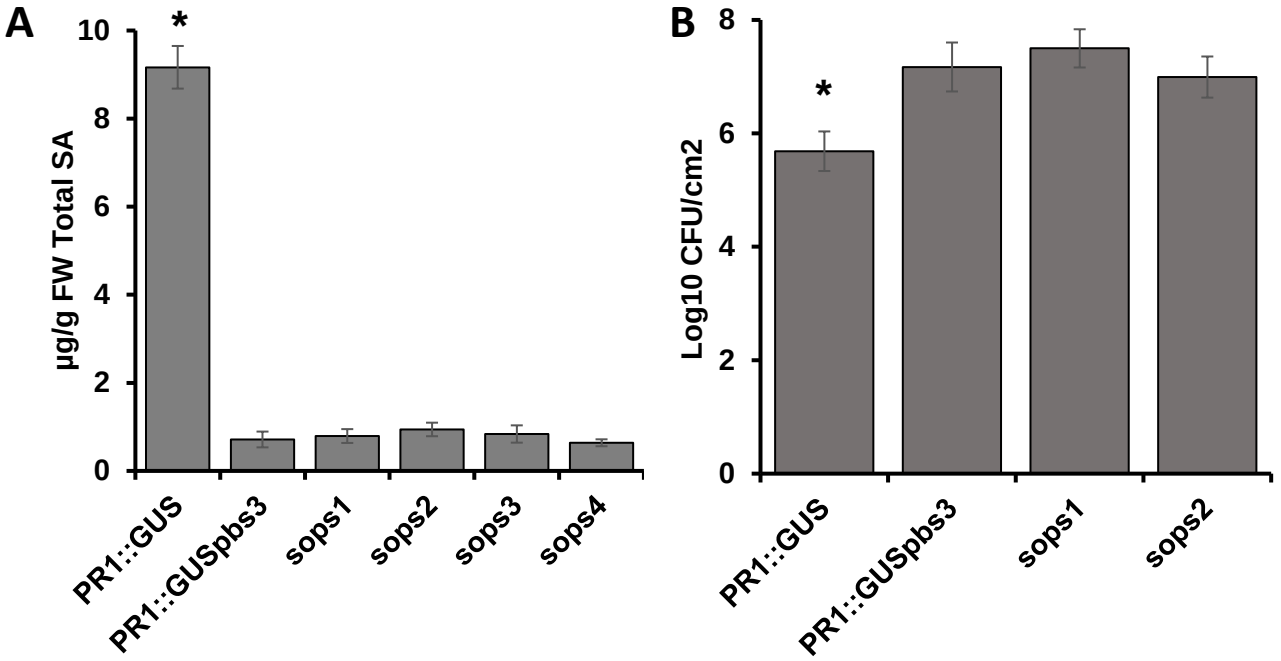

Figure 4.2: Initial *sops* mutants fails to restore total SA or resistance to virulent *Pseudomonas syringae* pv. *maculicola* ES4326

(A) *Sops1*, *sops2*, *sops3*, and *sops4* mutants were tested for restoration of total SA 24 hpt UV-C treatment. None were significantly different from the *pPR1::GUSpbs3* control. Experiment done once, in triplicate.
(B) *Sops1* and *sops2* were further tested for resistance to virulent *Pseudomonas syringae* pv *maculicola* ES4326. Resistance was not restored in *sops1* or *sops2*. Experiment done once, n=9.

Statistical significance (*) determined by student's *t* - test, $p<0.05$

***pPR1::GUSpbs3-2* Suppressor Screen**	
M2 Plants Screened	5112
M2 Plants with restored GUS	163
# of lines chosen for secondary screening	35
# from 2° screen with restored SA (70% or greater than WT)	6
# from 2° screen with restored FT	12
# with restored SA and FT	4
# with NGS results	2

Table 4.1: Number of plant lines at each step of *pPR1::GUSpbs3* Suppressor Screen
5112 M2 plants were screened for restoration of GUS in response to UV-C treatment. Of the 163 identified, 35 were secondarily screened and six of those had restored SA and 12 showed *pPR1::GUS*-like flowering time. Four demonstrated restored SA and flowering time, and two of those were chosen for further characterization.

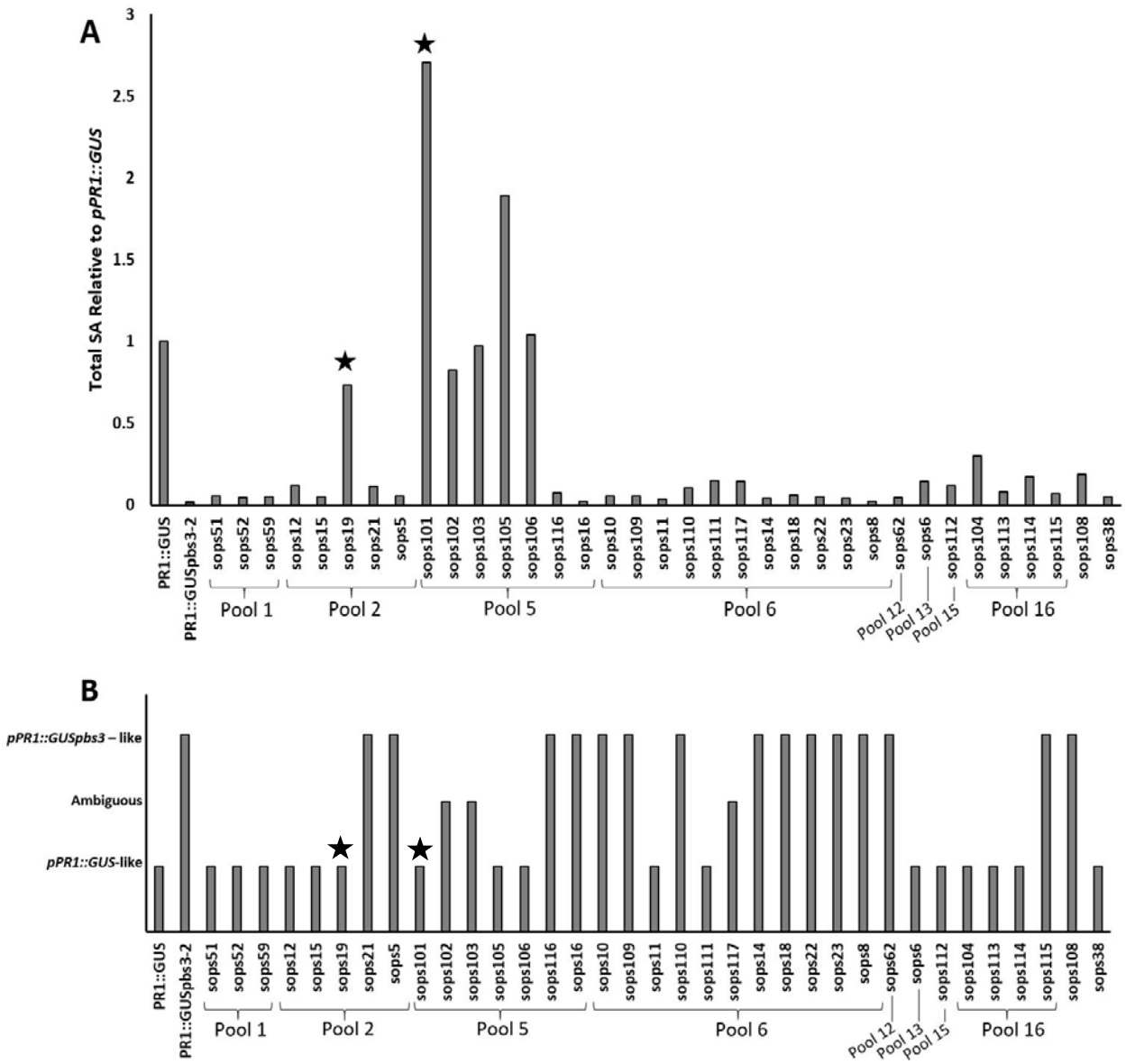

Figure 4.3: Secondary screen identifies mutants with restored SA

(A) 35 lines identified in the primary screen were selected for further analysis in a secondary screen. 5 to 12 plants of each genotype were treated with UV-C at 4 weeks old. 24 hpt, a single leaf was harvested and stained for GUS. At 48 hpt, further leaf tissue was collected only from plants with a GUS positive stained leaf. These samples were extracted for total SA and run on HPLC. We identified 6 lines with total SA > 70% of Col-0. Experiment had one replicate comprised of tissue from multiple plants. (B) As *pbs3* plants transition from vegetative to reproductive growth earlier than Col-0, we counted the % of bolting plants from each line 25 days post planting. Plants with intermediate flowering times were designated ambiguous, and all others were designated to be "*PR1::GUS* - like" or "*PR1::GUSpbs3* – like".
Lines with ★ were selected for further characterization.

Sops19 and *sops101* have restored SA accumulation and *PR1* expression in response to UV-C

In the secondary screen, SA was measured from a single sample for each line, and there were no untreated replicates to identify if SA accumulation was constitutive. I therefore quantified the total and free SA before and after UV-C treatment in *sops19* and *sops101* to better characterize SA metabolism in these lines. *Sops101* had higher total SA than *pPR1::GUS* in one experimental replicated, but in an independent experiment it had total SA that was statistically the same as *pPR1::GUS*. Total SA accumulation in *sops19* is equal to WT (Fig. 4.4a). Free SA has been measured with varied results in *pbs3* lines in the past; in response to virulent pathogens, free SA remained at WT levels or decreased (Lee et al., 2008, 2007) while in response to avirulent pathogens it was compromised (Jagadeeswaran et al., 2007; Lee et al., 2008) or slightly elevated in *pbs3* (Lee et al., 2007; Nobuta et al., 2007). As shown in Chapter III, this is likely due to the specific time point measurement and stochastic variation. In our assays, free SA is lower in *pPR1::GUSpbs3* than *PR1::GUS*, but the difference is not always statistically significant. *Sops19* accumulated significantly more free SA than *PR1::GUSpbs3* but was not statistically greater than *PR1::GUS* (Figure 4b). The varied amount of free SA may reflect the flux of interconversion between SA and SA glucosides. Thus, measurement of free SA and SA glucosides (total SA) is a much more reliable indicator of the SA response. Neither *sops19* nor *sops101* show constitutive SA activation.

To confirm and quantify *PR1* induction visualized with GUS, I treated *sops19* and *sops101* with UV-C and collected leaf tissue 24 hpt for quantitative real-time PCR analysis. Both showed restored induction of *PR1*, as expected (Fig. 4.4c)

Sops101 has restored *PR1* accumulation in response to *Pseudomonas syringae* pv. *tomato* DC3000 AvrRpt2

While UV-C is an effective inducer of the SA pathway and associated defense responses (see Chapter III, Molinier et al., 2005; Nawrath et al., 2002; Yalpani et al., 1994), we next investigated the response of *sops19* and *sops101* to a pathogen, *Pto* AvrRpt2. The AvrRpt2 effector targets *Arabidopsis thaliana* RIN4, an immune response regulator, for degradation. This targeting is sensed by RPS2 and RPM1 which initiate effector triggered immunity (Axtell and Staskawicz, 2003; Kim et al., 2005; Mackey et al., 2003). This defense induction results in *PR1* expression 24 hours post infection in WT that is compromised in *pbs3* (Nobuta et al., 2007). We therefore tested the induction of *PR1* in *sops19* and *sops101* 24 hours post syringe infiltration with *Pto* AvrRpt2 using qRT-PCR and found WT *PR1* expression (Fig. 4.5). However, *PR1* induction was only statistically significant in *sops101* and this was due to large variation between biological replicates in *sops19*. This variation is likely the result of sampling of a plant without the *sops19* mutation(s) due to the difficulty in identifying a homozygous line in this non-Mendelian segregating line. I expect additional experimental replicates and confirmation of a homozygous *sops19* line will allow confirmation of *PR1* induction in *sops19* in response to an avirulent biotic inducer.

Sops19 and *sops101* show restored resistance to virulent *Pseudomonas syringae* pv. *maculicola* ES4326

I next measured the restoration of PBS3-mediated resistance to virulent *Pma*. 4-5-week-old plants were infiltrated with $OD_{600} = 0.0002$ *Pma* in 10 mM $MgSO_4$. Bacterial titers were determined 0 and 3 days post infection. *Sops19* and *sops101* fully restored the *pPR1::GUS* phenotype, and *sops19* had even less bacterial growth than *pPR1::GUS*, although this was only

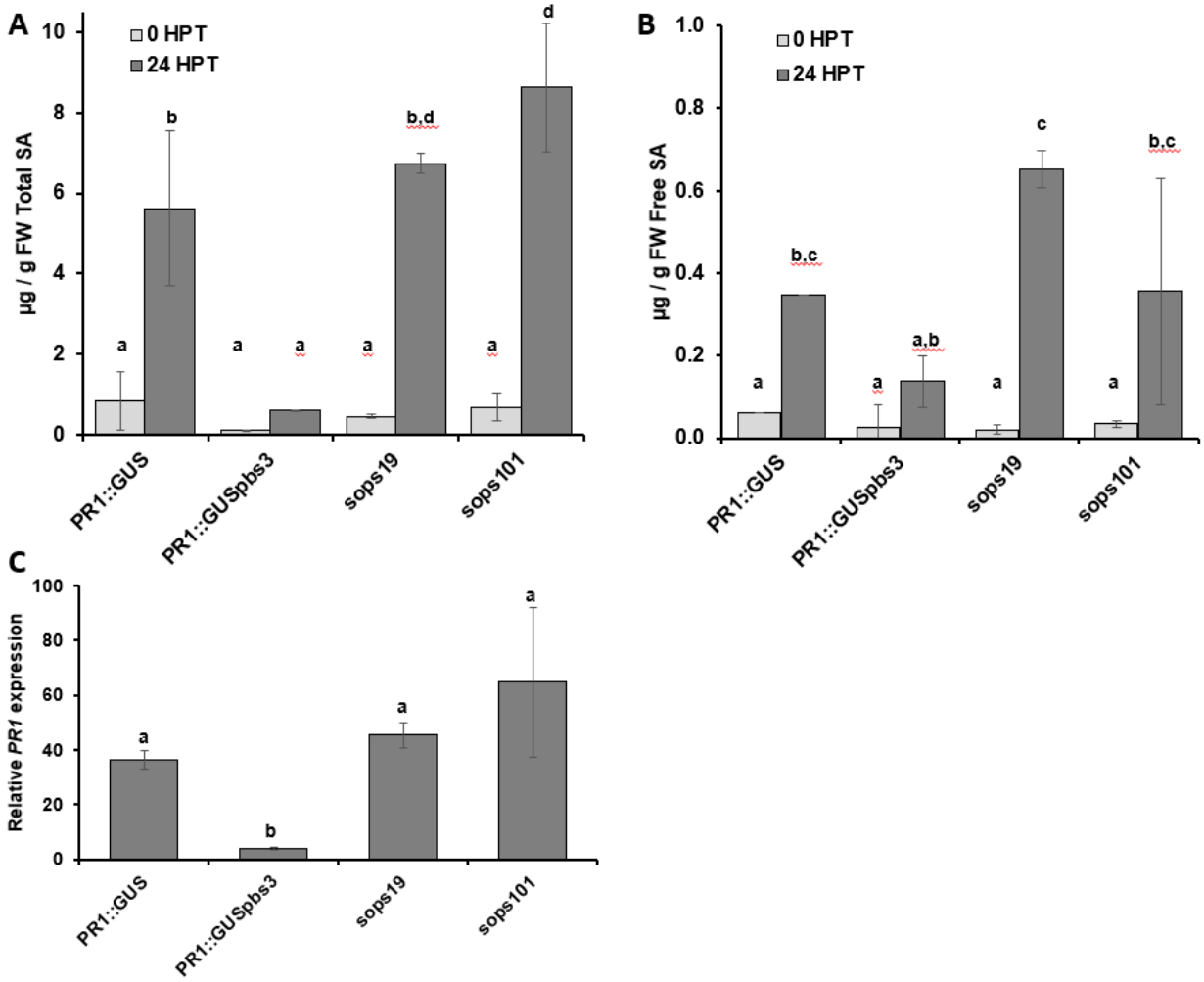

Figure 4.4: *Sops19* and *sops101* have restored total SA and *PR1* expression in response to UV-C.

(A) Total SA (free + SAG) was restored in *sops19* and *sops101* 24 hpt UV-C. *Sops101* had greater total SA than WT in the experiment shown, however in an independent experiment, the total SA of *sops101* was statistically equivalent to WT.

(B) Free SA measurements showed average free SA to be increased from *pPR1::GUSpbs3* in *sops19* and *sops101* 24 hpt UV-C, however the increase in *sops101* was not statistically significant. Free SA has been measured with varied results in *pbs3*, potentially reflecting changes in time points and/or inducers (see text).

(C) qRT-PCR analysis confirms GUS staining experiments, showing that *sops19* and *sops101* have significantly induced *PR1* expression 24 hpt UV-C.

Significance in A & B determined by 2-way ANOVA with Tukey-Kramer post-hoc test.
Significance in C determined with Fisher's exact test.
Experiments repeated with similar results.

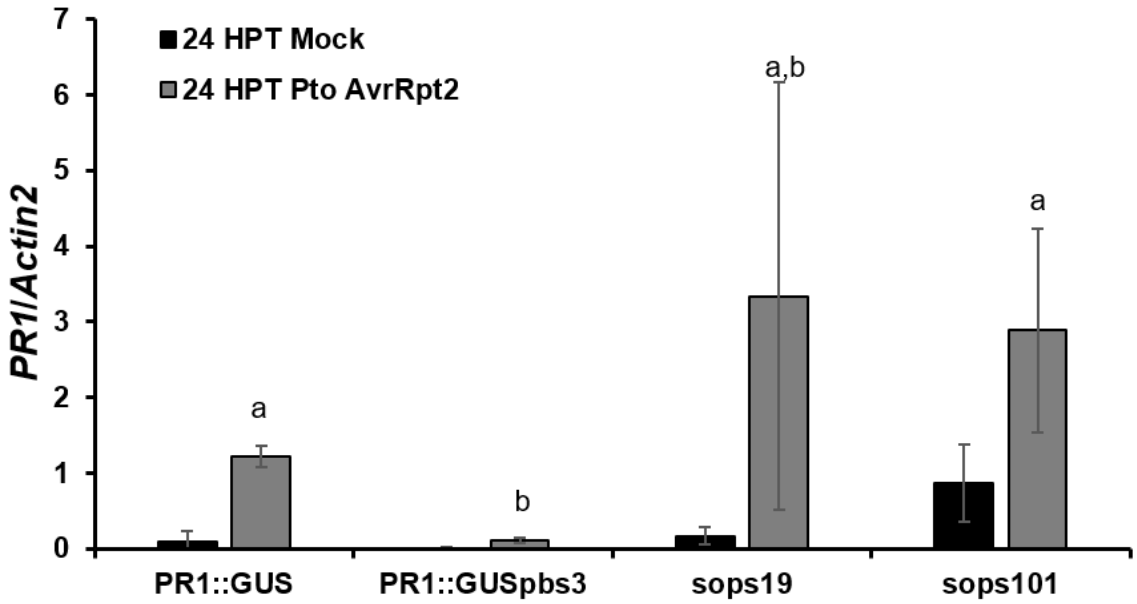

Figure 4.5: *Sops101* rescues *PR1* expression after infiltration of *P. syringae* pv. *tomato* DC3000 AvrRpt2.

4-5 week old plants were inoculated with OD_{600}=0.0001 *Pto* AvrRpt2. 24 hpt, leaves were harvested for RNA extractionand qRT-PCR analyses. *Sops101* rescued *PR1* expression. *Sops19* appears to rescue *PR1* expression, but this was not statistically significant due to large error bars. These error bars may be the result of segregation in this non-Medelian line. Data represent the averages of 3 biological replicates.

Statistical significance determined by Student's *t*-test.

statistically significant in one experimental replicate (Fig. 4.6). Thus *sops19* and *sops101* restore PBS3-mediated pathogen resistance to both virulent and avirulent pathogens.

Sops19 and *sops101* have restored flowering time

Several SA-associated genetic knockouts have developmental/flowering time-associated phenotypes. Both *pbs3* and *npr1* flower earlier than WT (Wang et al., 2011). While semi-quantitative measurements were made to assess this in mutants during the secondary screen (Fig. 4.3b), more quantitative experiments were later performed. I measured the number of days to budding, bolting, and flowering, and the number of leaves at budding in *PR1::GUS*, *PR1::GUSpbs3*, *sops19*, and *sops101* with 12/12 light/dark (Fig. 4.7). As expected, *pPR1::GUSpbs3* reaches each stage before *pPR1::GUS* and has fewer leaves when it begins budding. For all measures, *sops19* and *sops101* flowering phenotype were restored to WT. SA contributes to plant development, including plant size and seed production, although a mechanism for the early flowering in *pbs3* and *npr1* is unknown (Abreu and Munne-Bosch, 2009). Here I focus on *sops* mutants with both SA and flowering time restored to WT phenotypes. In the future, we could pursue the uncoupling of SA and flowering time responses using other mutants.

Identification of potential causal mutations of *sops19* and *sops101*

To identify the causal mutations for restored SA in *sops19* and *sops101*, DNA from *pPR1::GUSpbs3*, *sops19*, and *sops101* was sequenced using the Illumina HiSeq 4000 platform with 50 bp single end reads. Reads were aligned to the TAIR 10 genome. Over 100,000,000 reads were generated for each line, creating greater than 35x coverage. Any mutations in *sops19* and *sops101* that were in common with *PR1::GUSpbs3* were filtered out using CLC Genomics Workbench. All variants except for SNPs representing nonsynonymous G/C to A/T transitions in a coding region were also filtered out. It is possible that this filtering caused us to discard a causal A/T to G/C transition or a transversion, or an important mutation in a regulatory element. However, EMS preferentially causes G/C to A/T transitions and with several candidate causal mutations identified, we are focusing first on the candidates identified with these filters. 12 candidates remained in *sops101* and 121 candidates in *sops19*. I narrowed these lists of candidates into "likely causal mutant" groups with 4 candidates for *sops101* and 11 candidates for *sops19* based on the location within the gene (e.g., active site) of the mutation, the magnitude of the amino acid change as determined by BLOSUM score, published (co-)expression data in response to pathogens and hormones, and likelihood of being dominant for *sops101* (Aoki et al., 2016; Austin et al., 2011) (Table 4.2).

Sops101

As *phytoalexin-deficient 4* (*PAD4*; At3g52430) is already known to be essential for SA signaling, we hypothesized that $PAD4^{S135F}$ causes the *sops101* phenotype. PAD4 has an EDS1/PAD4 (EP) domain and a lipase-like domain, but lipase activity is dispensable for PAD4 function (Fig. 4.8a; Feys et al., 2001; Wagner et al., 2013). The S135F mutation occurs near the putative protein-protein interaction site with enhanced disease susceptibility 1 (EDS1; At3g48090) (Feys et al., 2005; Wagner et al., 2013). Alignment of *PAD4* homologues from various species shows some variation at this residue, however in most cases the amino acids at this locus have polar uncharged R groups (Fig. 4.8b; Altschul et al., 1997). $PAD4^{S135}$ is in a region with high homology overall. Wagner and colleagues crystalized the heterodimer of EDS1 and interaction partner senescence-associated gene 101 (SAG101; At5g14930), which has high sequence similarity with PAD4 (Fig. 4.8b; Feys et al., 2001; Wagner et al., 2013). They

identified a hydrophobic pocket of SAG101 to which an alpha helix of EDS1 binds. As SAG101 and PAD4 do not interact with EDS1 at the same time and appear to interact via homologous regions, Wagner and colleagues used SAG101 as a template to build a homology model of PAD4 and identified a similar hydrophobic pocket. Mutations in three of these hydrophobic pocket residues of PAD4 (M16A, L21S and F143A) had little effect individually but together compromised EDS1/PAD4 heterodimerization in yeast two hybrid assays (Wagner et al., 2013). I used this crystal structure, accession 4NFU, from Protein Data Bank and visualized using UCSF Chimera (Pettersen et al., 2004). PAD4 was overlaid onto SAG101 using the MatchMaker function, allowing for visualization of putative PAD4 interactions with EDS1. As expected based on Wagner and colleagues' yeast two hybrid assays, PAD4^{M16}, PAD4^{L21} and PAD4^{F143} appear to contribute to EDS1 binding with PAD4^{M16} and PAD4^{L21} holding the EDS1 alpha helix from the side of the binding pocket, and PAD4^{F143} further in the binding pocket in a ß-sheet. PAD4^{S135} is just outside the active site, at the beginning of an alpha helix behind the ß-sheet (Fig. 4.8c). Based on these structural data, the proximity of *PAD4^{S135F}* to the putative EDS1 binding site likely affects the interaction of these two proteins, promoting downstream SA accumulation.

Sops19

We hypothesize that the mutation in the DNA binding domain of the *ethylene response factor/apetala2* (ERF/AP2) transcription factor *RAP2.6* causes the *sops19* phenotype (Okamuro et al., 1997). *RAP2.6* is induced by the hormones SA and JA as well as abiotic stressors including salt, heat, and drought (Krishnaswamy et al., 2011). AP2 transcription factors are unique to plants and are grouped into the ERF-like or AP2-like classes based on having one or two 68-amino acid AP2 domains, respectively (Riechmann and Meyerowitz, 1998). AP2 domains contain a RAYD and an YRG element (Fig. 4.9a; Okamuro et al., 1997). It is likely that these elements are important for DNA binding and perhaps protein-protein interaction. RAP2.6 is ERF-like, with one AP2 domain, and the *RAP2.6^{A93V}* mutation is in an invariant position of the RAYD domain (Fig. 4.9b; Allen et al., 1998; Okamuro et al., 1997). We therefore predict that *RAP2.6^{A93V}* is compromised in DNA binding and/or that its transcriptional activity is altered.

At the writing of this dissertation, *RAP2.6^{A93V}* and *PAD4^{S135F}* in the pUC57 vector are ready for *Agrobacterium*-mediated transformation into *pPR1::GUSpbs3* mutants. At least two independent insertion lines will be used for each vector, and experiments will be done to confirm that these mutations caused the restoration of SA-associated plant defense in the *pbs3* background. If these are not the causal mutations, the Wildermuth laboratory is ready to move forward with other lines.

Transcriptome analyses identify additional factors in PBS3-mediated plant defense

I next performed transcriptome profiling of Col-0 and *pbs3* to gain insight into the mechanism of PBS3 defense signal integration. Leaves from Col-0 and *pbs3* plants were collected untreated (UT) and 24 hpt with UV-C for RNA-Sequencing. Reads were aligned to the *Arabidopsis* genome using HiSat2 (Kim et al., 2015). In multidimensional scaling, samples clustered by treatment and genotype as expected with greater distinction between UV-C treated samples than controls (Fig. 4.10a). False discovery rate (FDR) and differential expression were determined by Fisher's exact test using R. Genes with an FDR of less than 0.05 and $\log_2$ fold change greater than 1.5 were considered differentially expressed. We identified 2,758 genes differentially expressed between Col-0 24 hpt UV-C and Col-0 UT (see Fig. 4.10b). These genes were entered into BioMaps from Virtual Plant (Katari et al., 2010) and analyzed for overly represented gene ontology (GO) groups. As expected, genes involved in the response to salicylic

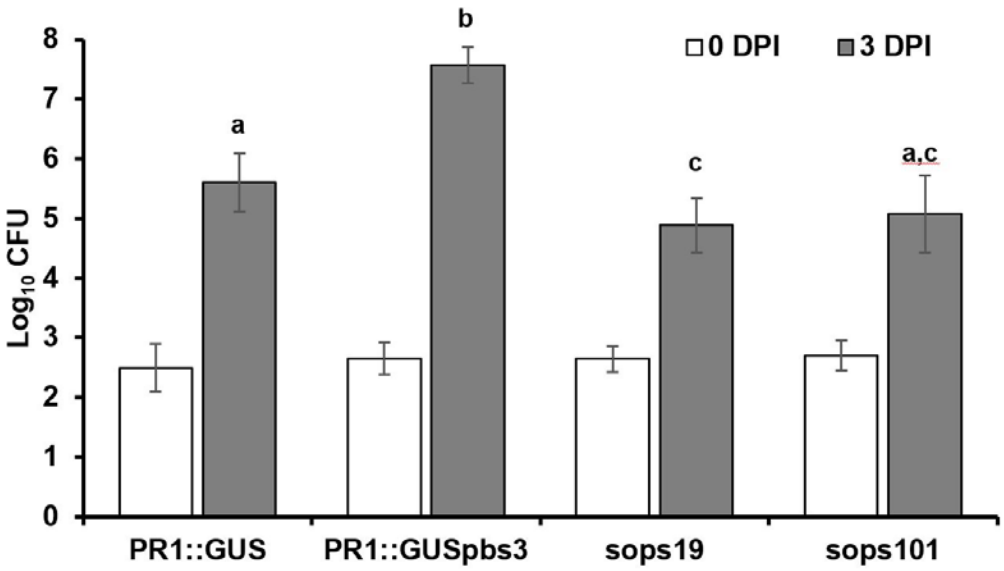

Figure 4.6: *Sops19* and *sops101* rescue *pbs3*-mediated susceptibility to *Pseudomonas syringae* pv. *maculicola* ES4326
4-5 week old plants were inoculated with OD_{600}=0.0002 *Pma*. Leaf discs were collected at 0 and 3 DPI and bacterial titers were measured. Data represent the averages of 9 replicates, 3 each from three plants.
Statistical significance determined by Student's *t*-test. Experiment repeated with similar results.

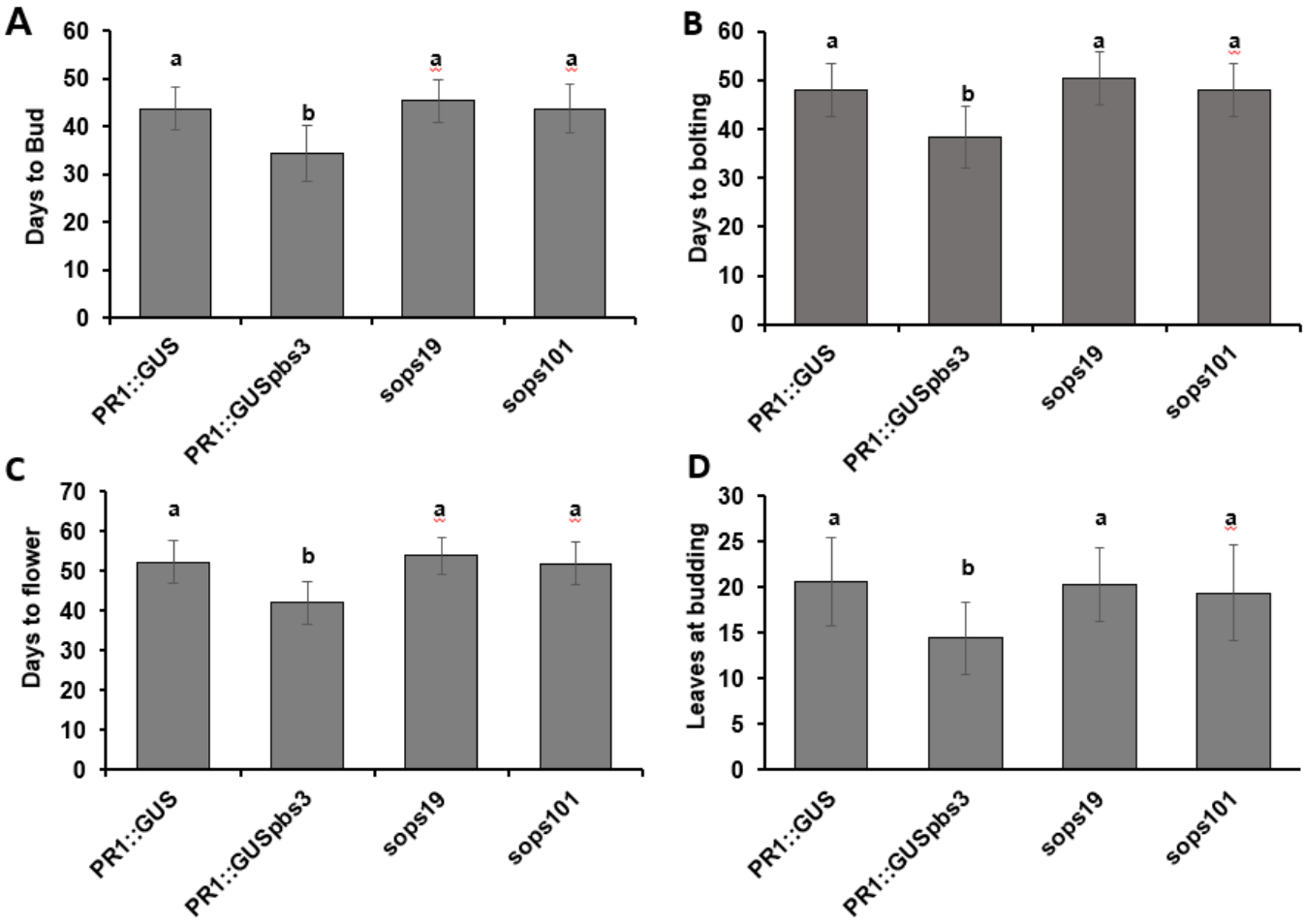

Figure 4.7: Timing of transition from vegetative to reproductive growth rescued in *sops19* and *sops101*
For n ≥ 21 plants per genotype, the number of days post planting of the appearance of buds (A), bolting (B), flowering (C), and the number of leaves at budding (D) was recorded.
Statistical significance was determined with one way ANOVA with Tukey-Kramer post-hoc test.

	Atg number	Short name	Description	AA position (mutated aa/total # of aa)	BLOSSUM62	Domain of mutation	DE between pbs3 UV-C and pbs3 UT
sops101	AT2G29880	Myb/SANT-like DNA-binding domain protein		0.06	-4	MYB/SANT like domain: aa 21-118	
sops101	AT2G32920	PDI9/PDIL9	Encodes a protein disulfide isomerase-like (PDIL) protein, a member of a multigene family within the thioredoxin (TRX) superfamily.	0.94	1	non cytoplasmic domain: aa 28-440	
sops101	**AT3G52430**	**PAD4**	**Encodes a lipase-like gene that is important for salicylic acid signaling and function in resistance (R) gene-mediated and basal plant disease resistance.**	**0.25**	**-3**	**alpha/beta hydrolase fold: aa 78-246**	3.97
sops101	AT4G34710	ADC2	encodes a arginine decarboxylase (ADC), a rate-limiting enzyme that catalyzes the first step of polyamine (PA) biosynthesis via ADC pathway	0.06	-5	arginine decarboxylase	
sops19	AT3G63200	PLP9	Patatin-like portein 9. lipid catabolic process0	0.52	0	Patatin/Phospholipase A2-related: aa 33-233. AND acyl transferase/acyl hydrolase/lysophospholipase: 26-360	-4.47
sops19	AT1G27120	GALT4	golgi-localized hydroxyproline-O-galactosyltransferase0	0.67	STOP	Glycosyl transferase aa 440-620	-2.97
sops19	AT5G46570	BSK2	Encodes BR-signaling kinase 2 (BSK2), one of the three homologous BR-signaling kinases. Mediates signal transduction from receptor kinase BRI1 by functioning as the substrate of BRI1. Plasma membrane localized.	0.84	-3	tetratricopeptide-like helical aa 376-482	-1.79
sops19	AT3G53230	CDC48B	CDC48 is induced upon oilseed rape mosaic tobamovirus infection and appears to be involved in controlling virus movement.	0.79	-1	ATPase aa: 518-651	2.57
sops19	**AT1G43160**	**RAP2.6**	**encodes a member of the ERF (ethylene response factor) subfamily B-4 of ERF/AP2 transcription factor family (RAP2.6). The protein contains one AP2 domain. There are 7 members in this subfamily.**	**0.48**	**0**	**pathogenesis-related transcriptional factor/ERF, DNA-binding aa 83-99**	2.99
sops19	AT4G34950	MFS1	MFS1: Major facilitator superfamily	0.44	0	Nodulin-like aa 16-262	
sops19	AT1G78100	AUF1	AUF1: Auxin up-regulated F-Box protein 1	0.46	0	none	
sops19	AT5G18610	PBL27	PBL27: Receptor like kinase that is an immediate downstream component of the chitin receptor CERK1 and contributes to the regulation of chitin-induced immunity.	0.95	0	none	
sops19	AT5G53160	PYL8/RCAR3	PYL8/RCAR3: Regultory component of ABA receptor. Interacts with protein phosphatase 2Cs ABI1 and ABI2. Stimulates ABA signalling, cell-to-cell mobile	0.47	-4	Polyketide cyclase/dehydrase aa 32-173	
sops19	AT5G54010	UGT79B6	UGT79B6: Encodes a flavonoid 3-O-glucoside: 2"-O-glucosyltransferase that determines pollen-specific flavonol structure	0.18	-1	UDP-glucuronosyl/UDP-glucosyltransferase aa 2-383	
sops19	AT5G36150	PEN3	PEN3: Putative pentacyclic triterpene synthase 3	0.57	1	terpenoid cyclases/protein prenyltransferase alpha-alpha toroid aa 388-758	

Table 4.2: Candidate causal mutations of *sops19* and *sops101* phenotypes
PR1::GUSpbs3, *sops101*, and *sops19* were sequenced using Illumina HiSeq 4000. Mutations were kept as candidates if they 1) were unique from *PR1::GUSpbs3*, 2) represented a G/C to A/T transition, 3) were nonsynonymous, and 4) were in a coding region. Of those 121 (*sops19*) and 12 (*sops101*) candidates, genes were prioritized based on function, magnitude of amino acid change as determined by the BLOSUM62 matrix, and domain of mutation. Prioritized genes are shown here.

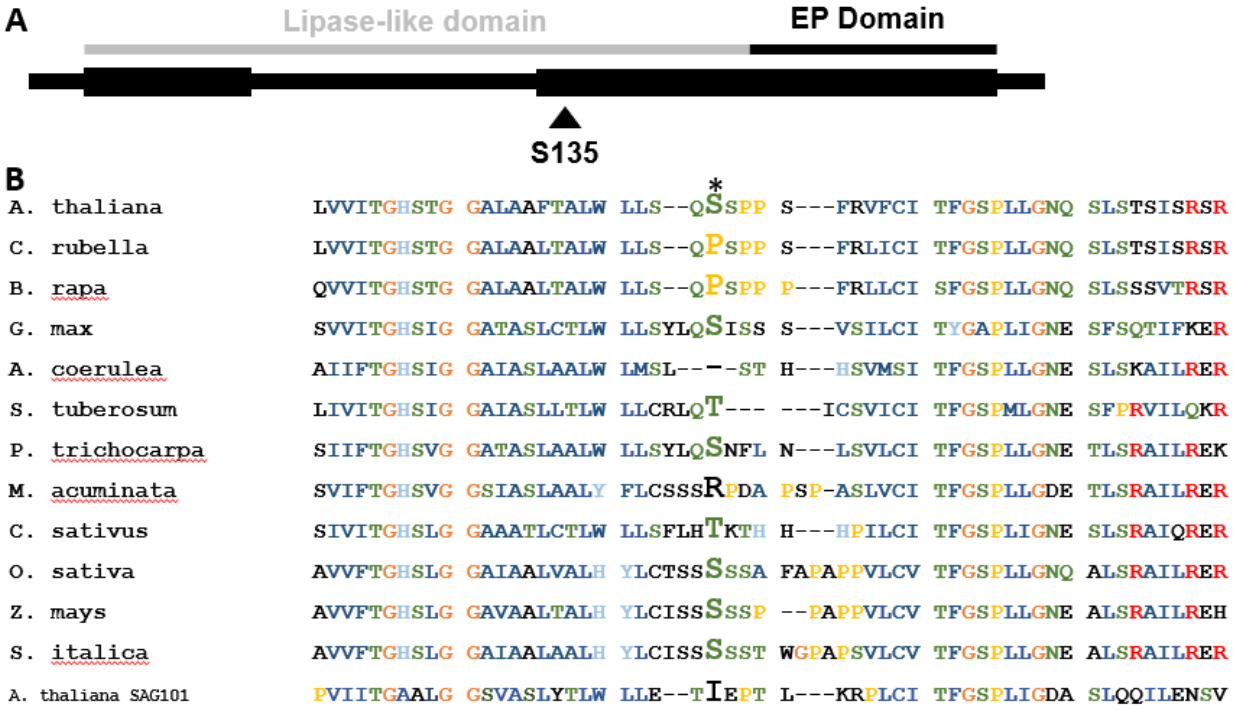

Figure 4.8: The *PAD4*^{S135F} mutation is in the lipase-like domain at a somewhat variable residue next to invariant binding site residues.
(A) The *PAD4*^{S135F} mutation is near the beginning of the second exon in the N-terminal lipase-like domain of PAD4. Site of *sops101* mutation designated by arrow.
(B) Alignment of PAD4 from 12 different species, including monocots, shows that the S135F mutation is in a region with very low variability. PAD4 amino acids 122-167 are shown, and *Arabidopsis thaliana SAG101* is shown for comparison. Locus of *PAD4*^{S135F} mutation designated by *.
(C) Overlay of PAD4 homology model onto SAG101/EDS1 heterodimer crystal structure. The region of SAG101 (green) that creates the hydrophobic pocket for EDS1 (gray) was selected and PAD4 (blue) was structurally aligned to that with Chimera's MatchMaker function. An important EDS1-binding residue, PAD4^{Phe143}, is shown in purple. This site is homologous to SAG101^{Leu171}. Residues shown in the binding site in Wagner et al., 2013 are shown in yellow (PAD4^{R141}, SAG101^{R169}) and red (PAD4^{Val113}, SAG101$^{Ile\ 141}$). The locus of the putative causal mutation of *sops101*, *PAD4*^{S135}, is shown in orange and circled (SAG101^{Ile163}).

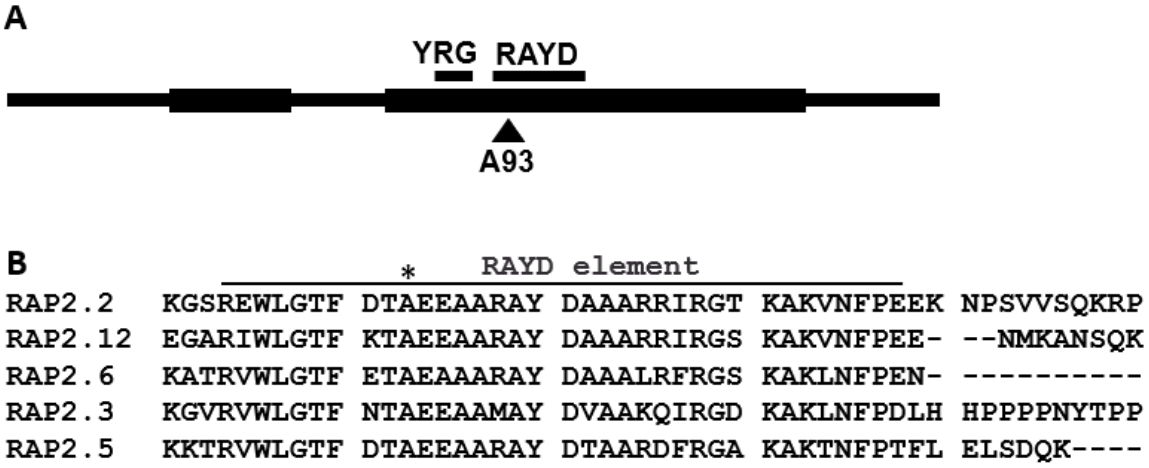

Figure 4.9: *RAP2.6*^{A93V} mutation is in invariant DNA binding RAYD element
(A) Schematic of *RAP2.6* with AP2 DNA binding domain comprised of YRG and RAYD elements. *RAP2.6*^{A93} indicated by arrow.
(B) Amino acid alignment of RAYD element of RAP2.6 and other RAP2s in *Arabidopsis thaliana*. The *RAP2.6*^{A93V} mutation (*) is at an invariant residue in the RAYD element for DNA binding. RAP2.6 amino acids 81-119 are shown.

acid stimulus, biotic stimulus, other organism, fungus, bacterium, and others were overrepresented (Table 4.3). Specifically, *PAD4*, *PR1*, *ICS1*, *PBS3*, *EDS5*, and *WRKY38* were upregulated in Col-0 24 hpt UV-C, confirming that UV-C is an effective inducer of SA-dependent responses.

3,294 genes were differentially expressed between *pbs3* 24 hpt UV-C and *pbs3* UT including *RAP2.6* and *PAD4*. Overrepresented GO terms were similar as with Col-0, but included additional categories such as "response to jasmonic acid stimulus" and several metabolism and phosphorylation related categories (Table 4.4). 2,155 of these 3,294 genes were in common with Col-0 24 hpt UV-C vs Col-0 UT (Fig. 4.10b, sections iv, v). 615 genes were differentially expressed between Col-0 24 hpt UV-C and *pbs3* 24 hpt UV-C, including *PR1* which was approximately 17x higher in Col-0 than *pbs3*. These 615 genes included differences in the expression of genes involved in the response to jasmonic acid stimulus, endogenous stimulus, and salicylic acid stimulus (Table 4.5). 503 of these 615 genes were upregulated in *pbs3* 24 hpt UV-C as compared to Col-0 24 hpt UV-C and 112 were upregulated in Col-0 as compared to *pbs3*. This implies that PBS3 functionally represses a set of genes as opposed to only upregulating SA-related genes. This pattern of gene expression in *pbs3* mutants was also identified using mini-array data (Wang et al., 2008). The 503 genes upregulated in *pbs3* were grouped into overrepresented gene ontology categories (Table 4.6). "Response to jasmonic acid stimulus" ($p = 7.34\times10^{-9}$), "response to hormone stimulus" ($p=5.35\times10^{-5}$) and "secondary metabolic process" ($p = 8.03\times10^{-7}$) were up in *pbs3* 24 hpt UV-C. JA-related genes upregulated in *pbs3* 24 hpt UV-C as compared to Col-0 24 hpt UV-C are found in Table 4.7. These data support a role of PBS3 that may be broader than regulation of SA; it may be involved in cross talk between SA and JA.

To further investigate this possibility, I identified the genes differentially expressed in both i) Col-0 UV-C vs Col-0 UT and ii) Col-0 UVC vs *pbs3* UV-C (Fig. 4.8b, sections iv and vii). This subset should capture genes induced or repressed in response to WT with UV-C but not induced or repressed (to the same degree) in *pbs3* by UV-C (Table 4.8). It specifically pulled out many WRKY transcription factors, which are associated with hormone regulation, and several ABA and JA-specific genes. *WRKY51* (At5g64810), which is significantly lower in *pbs3* as opposed to WT ($p = 1.4\times10^{-18}$), represses JA-mediated signaling (Gao et al., 2011). *Vegetative Storage Protein 1* (VSP1; At5g24780) and *Vegetative Storage Protein 2* (VSP2; At5g24770) were both significantly increased in *pbs3* as opposed to WT. *VSP1* is induced by the JA transcriptional regulator MYC2 (At1g32640) and is associated with the JA pathway (Dombrecht et al., 2007; Lu et al., 2016). Their upregulation suggests that JA repression is alleviated in *pbs3*, tipping the balance of cross talk between these two phytohormones towards JA and away from SA.

RAP2.6 is induced in *pbs3* in response to UV-C treatment. Its $\log_2$ fold change was 2.99 with a FDR of 3.9×10^{-6}. RAP2.6 is a transcription factor involved in JA/ethylene (ET) signaling, and its increased expression in *pbs3* is reflective of the overall increase in JA-related genes in *pbs3*. *PAD4* is induced by UV-C in Col-0 and *pbs3* with FDR 2.8×10^{-18} and 8×10^{-24}, respectively. Its induction is not dependent on *pbs3*.

DISCUSSION

To identify additional factors in PBS3-related defense induction, we performed a forward genetic suppressor screen in the *pPR1::GUSpbs3* mutant background and selected mutants with

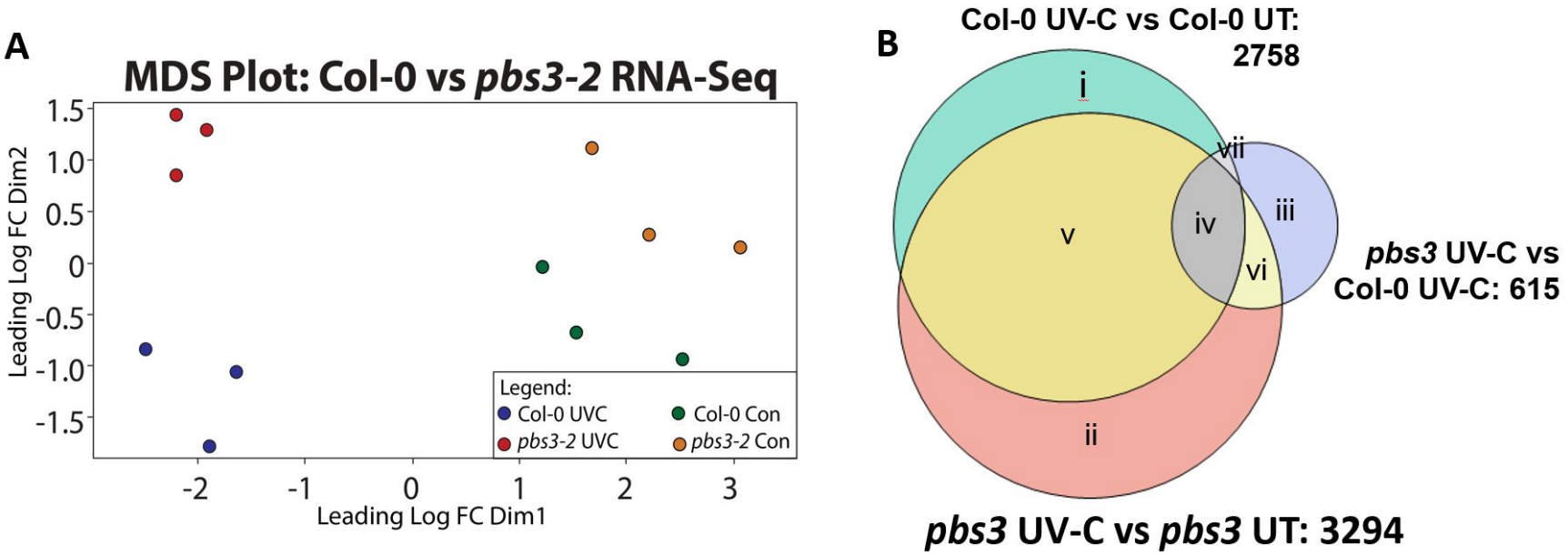

Figure 4.10: RNA-Sequencing shows genetic reprograming in response *pbs3* in response to UV-C

(A) Multidimensional scaling shows segregation based on genotype and treatment, with more pronounced differences between genotypes 24 HPT UV-C than controls.

(B) Venn diagram of comparisons between treatments and genotypes. 2758 genes were differentially expressed between Col-0 24 HPT UV-C and Col-0 UT (sections i, iv, v, vii). 615 genes were differentially expressed between Col-0 24 HPT UV-C and *pbs3* 24 HPT UV-C (sections iii, iv, vi, vii). 3294 genes were differentially expressed between *pbs3* 24 HPT UV-C and *pbs3* UT (sections ii, iv, v, vi).

Table 4.3: TAIR/TIGR GO terms for differentially expressed genes in Col-0 24 hpt UV-C vs Col-0 Con

GO Term	p-value
response to stimulus	3.14E-42
response to biotic stimulus	3.23E-22
response to other organism	7.51E-22
response to stress	2.26E-20
multi-organism process	4.18E-20
response to abiotic stimulus	5.86E-20
response to chemical stimulus	9.92E-20
response to organic substance	4.41E-19
defense response	2.48E-17
photosynthesis	5.50E-14
response to endogenous stimulus	6.16E-13
response to fungus	2.28E-12
defense response to fungus	1.62E-11
response to hormone stimulus	4.66E-10
response to chitin	1.63E-09
response to radiation	5.75E-09
response to bacterium	8.97E-09
response to light stimulus	1.61E-08
response to carbohydrate stimulus	2.21E-08
defense response to bacterium	9.44E-08
response to cold	4.72E-07
secondary metabolic process	1.17E-06
generation of precursor metabolites and energy	2.41E-06
response to wounding	4.67E-06
photosynthetic electron transport chain	5.49E-06
response to abscisic acid stimulus	1.08E-05
response to temperature stimulus	1.32E-05
aromatic compound biosynthetic process	1.86E-05
response to karrikin	2.27E-05
cellular aromatic compound metabolic process	4.60E-05
signal transduction	4.90E-05
response to salicylic acid stimulus	6.76E-05
photosynthetic electron transport in photosystem I	7.15E-05

Table 4.4: TAIR/TIGR GO terms for differentially expressed genes in *pbs3* 24 hpt UV-C vs *pbs3* Con

GO Term	p-value
response to stimulus	4.92E-51
response to stress	2.31E-28
response to other organism	1.71E-26
response to biotic stimulus	1.77E-26
response to chemical stimulus	2.51E-26
multi-organism process	7.76E-25
response to abiotic stimulus	1.34E-23
defense response	7.10E-22
response to organic substance	7.10E-22
response to endogenous stimulus	4.07E-15
response to fungus	4.98E-13
response to hormone stimulus	2.84E-12
defense response to fungus	6.63E-12
response to bacterium	7.25E-12
response to radiation	1.10E-11
response to light stimulus	2.30E-11
photosynthesis	1.74E-10
secondary metabolic process	1.13E-09
defense response to bacterium	5.02E-09
signal transduction	1.10E-08
response to wounding	4.05E-08
response to jasmonic acid stimulus	7.43E-08
response to chitin	1.10E-07
response to salicylic acid stimulus	1.31E-07
cellular aromatic compound metabolic process	6.02E-07
response to temperature stimulus	1.28E-06
response to carbohydrate stimulus	1.51E-06
aromatic compound biosynthetic process	2.68E-06
biological regulation	4.67E-06
immune system process	6.02E-06
protein phosphorylation	6.65E-06
phosphorus metabolic process	6.65E-06
phosphate metabolic process	9.09E-06
response to cold	1.02E-05
phosphorylation	1.05E-05
generation of precursor metabolites and energy	1.18E-05
immune response	1.24E-05
photosynthetic electron transport chain	1.47E-05
innate immune response	1.47E-05
response to osmotic stress	1.77E-05
regulation of cellular process	2.68E-05
response to oxidative stress	4.27E-05
defense response, incompatible interaction	4.27E-05
toxin metabolic process	4.92E-05
toxin catabolic process	4.92E-05
photosynthetic electron transport in photosystem I	7.35E-05
response to salt stress	9.85E-05

Table 4.5: TAIR/TIGR GO terms for Col-0 24 hpt UV-C vs *pbs3* 24 hpt UV-C

GO Term	p-value
response to stimulus	3.03E-22
response to stress	3.39E-20
defense response	7.57E-15
response to biotic stimulus	8.57E-13
response to chemical stimulus	8.57E-13
response to organic substance	8.88E-13
response to other organism	4.65E-12
multi-organism process	7.03E-12
response to endogenous stimulus	1.90E-11
response to fungus	1.32E-10
response to wounding	3.31E-10
response to jasmonic acid stimulus	4.88E-08
response to osmotic stress	8.63E-08
response to hormone stimulus	2.32E-07
secondary metabolic process	3.80E-07
defense response to fungus	3.82E-07
response to abiotic stimulus	3.98E-07
response to salt stress	5.71E-07
response to salicylic acid stimulus	3.93E-05
phenylpropanoid biosynthetic process	9.38E-05

Table 4.6: TAIR/TIGR GO terms for upregulated genes in *pbs3* 24 hpt UV-C vs Col-0 24 hpt UV-C

GO Term	p-value
response to stress	5.43E-18
response to stimulus	5.43E-18
response to wounding	1.7E-11
defense response	8.98E-11
response to biotic stimulus	2.85E-10
response to fungus	8.37E-10
response to organic substance	2.04E-09
response to other organism	2.89E-09
multi-organism process	3.06E-09
response to endogenous stimulus	3.66E-09
response to chemical stimulus	4.66E-09
response to jasmonic acid stimulus	7.34E-09
response to abiotic stimulus	1.15E-08
response to osmotic stress	2.49E-08
defense response to fungus	1.05E-07
response to salt stress	3.09E-07
secondary metabolic process	8.03E-07
response to hormone stimulus	5.35E-05

ATG #	Short name	JA gene upregulated in pbs3 vs Col UV-C	Log_2 FC pbs3 UV-C vs Col UV-C	Statistically DEG Col-0 UV-C vs Col Con
AT1G21910	DREB26	Integrase-type DNA-binding superfamily protein	2.30	
AT5G13220	JAZ10	jasmonate-zim-domain protein 10	1.65	
AT1G56650	MYB75/PAP1	production of anthocyanin pigment 1	1.58	-1.55
AT5G44420	PDF1.2	plant defensin 1.2	3.42	
AT3G23240	ERF1	ethylene response factor 1	1.73	
AT3G06490	MYB108	myb domain protein 108	2.38	
AT1G61120	GES	terpene synthase 04	2.14	2.15
AT2G02990	RNS1	ribonuclease 1	3.08	
AT4G35770	DIN1	Rhodanese/Cell cycle control phosphatase superfamily protein	1.71	
AT1G72260	THI2.1	thionin 2.1	5.14	-3.71
AT4G34710	ADC2	arginine decarboxylase 2	1.93	
AT1G18710	MYB47	myb domain protein 47	2.03	-2.76
AT3G16470	JAC1	Mannose-binding lectin superfamily protein	2.57	
AT5G24780	VSP1	vegetative storage protein 1	4.24	-5.64
AT5G24770	VSP2	vegetative storage protein 2	3.57	-4.66
AT2G31180	MYB14	myb domain protein 14	2.86	
AT4G23600	JR2	Tyrosine transaminase family protein	2.19	
AT2G24210	TPS10	terpene synthase 10	4.38	
AT1G19640	JMT	jasmonic acid carboxyl methyltransferase	3.57	-3.11
AT4G05100	MYB74	myb domain protein 74	2.05	

Table 4.7: Jasmonic acid associated genes with increased expression in *pbs3* 24 hpt UV-C compared to Col-0 24 hpt UV-C

The GO group “response to jasmonic acid stimulus” was overrepresented with $p = 7.34\times10^{-9}$ in *pbs3*. Those genes are listed below with Log_2 fold change. Positive fold change values between *pbs3* UV-C and Col-0 UV-C indicate higher expression in *pbs3*. Negative values in Col-0 UV-C vs Col-0 Con indicate negative expression in Col-0 UV-C. DEG = Differentially expressed genes

Table 4.8: TAIR/TIGR GO terms for differentially expressed genes in common between Col-0 24 hpt UV-C vs Col-0 Con and Col-0 24 hpt UV-C vs *pbs3* 24 hpt UV-C

GO Term	p-value
response to stress	1.49E-08
response to stimulus	1.58E-07
defense response	1.62E-06
response to other organism	1.40E-05
multi-organism process	2.57E-05
response to biotic stimulus	3.66E-05

restored GUS staining in response to SA-inducing UV-C teatment. *Sops19* and *sops101*, identified from two different pools, restore PBS3-mediated SA induction and *PR1* expression. *Sops101* is a dominant mutation, while *sops19* showed non-Mendelian segregation in the F2 and its dominance is uncertain. High-throughput sequencing using the Illumina Hi-Seq 4000 platform was used to identify candidate causal mutations for *sops19* and *sops101*. *Sops101* had 12 possible causal mutations, which was narrowed down to 4 likely mutations whereas *sops19* had 121 possible causal mutations narrowed down to 11 candidates. In each case, there is a clear candidate that is most likely, and confirmation is in progress.

The *sops101* phenotype is likely caused by the *PAD4*^{S135F} mutation

The dominance of *sops101* suggests it may act as an activation mutant to increase defense responses. Defense induction is not constitutive in *sops101*, suggesting that the mutation causes hyperactivity upon induction to overcome *pbs3*-related susceptibility. PAD4 is a well-known component of SA signaling and a strong candidate for causing the *sops101* phenotype. *PAD4* was induced equally in Col-0 and *pbs3* 24 hpt UV-C and thus is likely upstream of, or in concert with, *PBS3* in SA-signaling. Further evidence of this is reported in Wang et al., 2008 wherein extensive transcriptional profiling of multiple SA-associated mutants using microarrays showed that *PBS3* induction is partially lost in *pad4* (see Chapter II). *PBS3* and *PAD4* both show biphasic induction in response to UV-C treatment (Chapter III), mirroring the expression and protein accumulation of SA-biosynthetic ICS1. PAD4 is also likely upstream of ICS1; *pad4* mutants have compromised *ICS1* accumulation and all genes differentially expressed in the *ICS1* mutant *sid2* were also differentially expressed in *pad4* (Wang et al., 2008). In addition, *pad4* affected the expression of JA/Et genes, supporting a role in SA/JA crosstalk. Based on clustering analysis, PBS3 was placed downstream of PAD4 and upstream of ICS1 and NPR1 (Wang et al., 2008).

PAD4 has high sequence identity with and interacts *in planta* with EDS1 (Feys et al., 2001). Both proteins are lipase-like, having N-terminal α/ß hydrolase domains with canonical S-D-H catalytic triads and unique C-terminal EDS1-PAD4 (EP) domains (Wagner et al., 2013). Catalytic lipase activity does not appear to be important for the function of EDS1 or PAD4 (Wagner et al., 2013). The *sops101* mutated residue, Serine135, is in the N-terminal lipase-like domain, and may be involved in PAD4-EDS1 interaction (Fig. 4.8). Although EDS1 and PAD4 are highly similar, their functions do not entirely overlap (Feys et al., 2005; Rietz et al., 2011). EDS1 also binds to SAG101 (Feys et al., 2005). While PAD4 and EDS1 accumulate in both the cytosol and nucleus, SAG101 is localized only to the nucleus (Feys et al., 2005). *EDS1*^{L262P}, an *eds1* mutant deficient in binding PAD4, compromises basal resistance and partially compromises system acquired resistance (SAR) (Rietz et al., 2011).

I hypothesize that *PAD4*^{S135F} causes the *sops101* phenotype through altered binding of PAD4 and EDS1. Wagner et al., 2013 reported the crystal structure for the SAG101/EDS1 heterodimer and found that an EDS1 alpha helix fits into a SAG101 hydrophobic pocket. Modeling showed that PAD4 likely interacts with EDS1 in the same way and identified amino acid 143, phenylalanine, as important for this interaction (Wagner et al., 2013). The *PAD4*^{S135F} mutation in *sops101* loops behind the active site ß-sheet and could feasibly affect PAD4-EDS1 heterodimerization (Fig. 4.8c).

While PAD4 is well known to be essential for SA-dependent processes (e.g. Jirage et al., 1999; Zhou et al., 1998), it also has SA-independent functions. An *Arabidopsis eds1pad4* mutant crossed into the SA biosynthetic mutant *sid2* with a *35S::EDS1* construct and estradiol-inducible *PAD4* had partially restored bacterial resistance when treated with estradiol as compared to mock

treated (Cui et al., 2017). This suggests that PAD4 promotes resistance both in ICS1/SA dependent and independent ways, consistent with Wang et al., 2008's findings. Glazebrook et al., 2003 and Gupta et al., 2000 also identified SA-independent, JA/Et related effects of PAD4. Brodersen et al., 2006 showed a potential upstream mechanism of this crosstalk. *MAP Kinase 4* (*MPK4*; At4g01370) is induced by the microbial-associated molecular pattern flg22 and promotes JA responses while suppressing SA responses via inhibition of PAD4 (Brodersen et al., 2006; Ichimura et al., 2006; Petersen et al., 2000). *Mpk4* mutants are dwarfed, accumulate higher SA than WT, and have increased induction of *PR1*. These phenotypes partially revert back to WT in *mpk4pad4* mutants, suggesting that MPK4 uses PAD4 to mediate its effects, at least partially (Brodersen et al., 2006). PBS3 may work with PAD4 to mediate SA-JA crosstalk.

We hypothesize that $PAD4^{S135F}$ is the causal mutation of *sops101* and causes greater PAD4 activity in *sops101* than in *pPR1::GUSpbs3*. This increase in PAD4 activity may be independent of the state of *PBS3* (mutant or WT), or the restoration of some activity or interaction in *sops101* that is lost in *pbs3*. Taken together, the body of previously published work coupled with our analyses indicates a strong likelihood that $PAD4^{S135F}$ is causal of *sops101* and suggests that PBS3 may function in repressing JA activity through PAD4. This is the first activation mutant identified in *PAD4*.

The *sops19* phenotype is likely caused by the $RAP2.6^{A93V}$ mutation

Confirmation of $RAP2.6^{A93V}$ as the causal mutation of *sops19* would provide additional evidence of PBS3 involvement in SA/JA crosstalk. *RAP2.6* is an *ethylene response factor/apetala2* (ERF/AP2) transcription factor with a binding domain consisting of single YRG and RAYD elements (Okamuro et al., 1997). Amino acid 93 is in the RAYD domain, specifically in the amphipathic alpha-helix, which is important for protein conformation and function (Okamuro et al., 1997). The four most closely related genes to *RAP2.6*, namely *RAP2.2*, *RAP2.3*, *RAP2.5*, and *RAP2.12* are all invariant at that position (Fig. 4.8). While the precise targets of RAP2.6 transcriptional activity are unknown, it binds to GCC and CE1 *cis* elements which are generally found in the promoters of stress-induced genes such as the JA-responsive *PDF1.2* (Brown et al., 2003; Hao et al., 2002; Niu et al., 2002; Van der Does et al., 2013; Zhu et al., 2010). The capacity of RAP2.6 for DNA binding can be changed by interaction with other proteins (i.e., RACK1B) with its AP2 domain (Guo and Sun, 2017).

RAP2.6 has previously been shown to be involved in both SA and JA responses (Krishnaswamy et al., 2011). Additionally, it is important in the response to abscisic acid and abiotic stresses such cold, salinity and wounding (Chen et al., 2002; Fowler and Thomashow, 2002; Krishnaswamy et al., 2011; Zhu et al., 2010). Its expression increases during infection of the SA-deficient mutants *pad4*, *NahG*, and *npr1* with virulent *Pma* ES4326 while its expression decreases in JA-associated *coi1* and ethylene-associated *ein2* (Chen et al., 2002). This suggests that *RAP2.6* expression is correlated with expression of jasmonic acid related genes and suppressed by SA-associated processes. Virulent *P. syringae* induce *RAP2.6* in an effector-dependent and coronatine-dependent manner, suggesting that induced *RAP2.6* promotes pathogenicity through greater activation of the JA pathway and suppression of SA-mediated defense (Chen et al., 2002; He et al., 2004). Furthermore, overexpression of *RAP2.6* resulted in earlier flowering time (Krishnaswamy et al., 2011). Plants with a loss or altered function of *rap2.6* would then be expected to flower later, which we observe in *sops19* mutants. We propose that in WT, PBS3 inhibits RAP2.6, or inhibits an upstream inducer of *RAP2.6*, which is supported by our RNA-seq data wherein *RAP2.6* expression increases 24 hpt UV-C in *pbs3* mutants, but is not induced in WT.

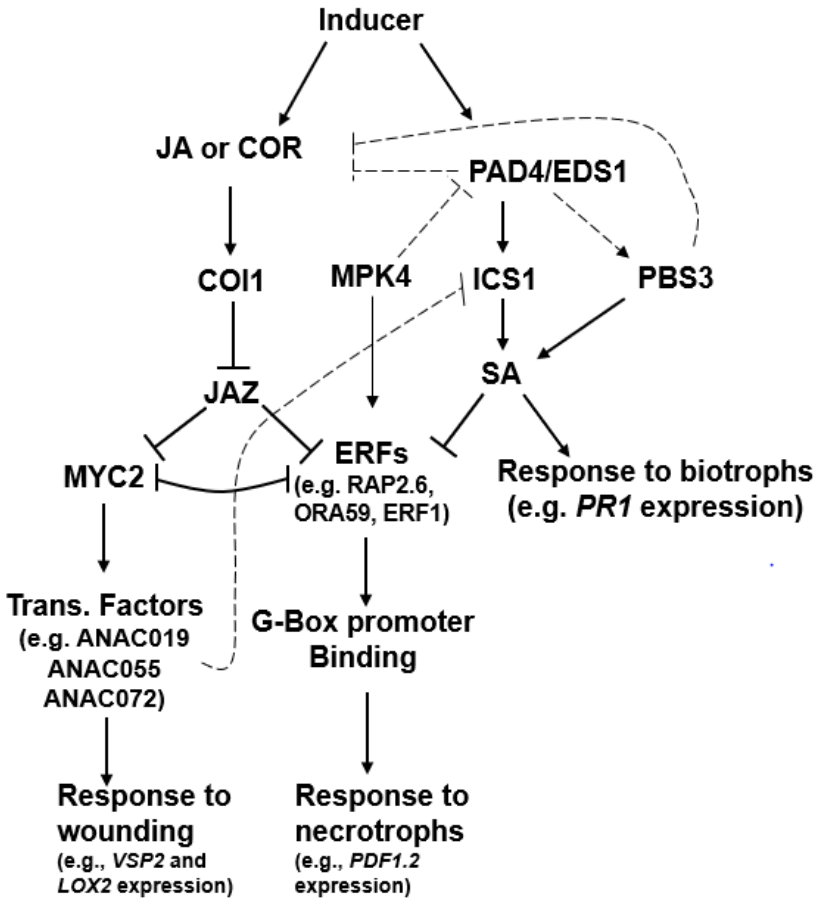

Figure 4.11: Model of PBS3-mediated cross-talk between SA and JA pathways

Jasmonic acid and the pathogen secreted JA mimic, coronatine, activates two signaling pathways; one mediated by the MYC2 transcription factor in response to wounding (e.g. by herbivorous insects) and the other associated with ethylene signaling, mediated by ERF transcription factors in response to necrotrophic pathogens (Lorenzo et al., 2004). These two pathways are mutually antagonistic (Wasternack and Hause, 2013). MYC2 activates ANAC family transcription factors, some of which promote JA genes such as *VSP1* and *VSP2* while simultaneously inhibiting SA biosynthetic *ICS1* expression (Kazan and Manners, 2013; Zheng et al., 2012). The ERF transcription factor family, to which RAP2.6 belongs, bind to G boxes to promote JA pathogen response genes such as *PDF1.2* (Brown et al., 2003; Hao et al., 2002; Niu et al., 2002; Van der Does et al., 2013; Zhu et al., 2010).

The salicylic acid response is also influenced by several factors; ICS1 is necessary for SA biosynthesis (Wildermuth et al., 2001). *Pad4* mutants have compromised *ICS1* expression and partially compromised *PBS3* expression, and thus PAD4 is placed upstream of ICS1 and partially upstream of PBS3 (Wang et al., 2008, Jagadeeswaran et al., 2007). However, while SA accumulation is dependent on PBS3, *ICS1* expression and protein accumulation is not dependent on PBS3 (Chapter III).

JA and SA pathways are antagonistic, but the mechanisms of hormone cross talk are not clear.SA inhibits ORA59 protein stability, and may inhibit other ERFs such as RAP2.6 (Van der Does et al., 2013). However, PAD4 also has SA/ICS1 independent functions, potentially inhibiting JA/ET (Glazebrook et al., 2003; Gupta et al., 2000, Brodersen et al., 2006). This additional PAD4 activity could act through PBS3. MPK4 is a coactivator of some components of the JA/ET ERF pathway and suppresses PAD4 inhibition of JA signaling and PAD4 activation of SA. Our analyses suggest that PBS3 plays a higher level regulatory role of SA/JA crosstalk as genes on both sides of the JA signaling pathway have enhanced expression in UV-C treated *pbs3* mutants.

Partial induction or inhibition indicated by thinner, dashed lines.

Cross talk between SA and JA

In the presence of active jasmonic acid, JA-Ile, the SCF^{COI1} interacts with JAZ repressor proteins and marks them for degradation (Chini et al., 2007; Thines et al., 2007; Xie et al., 1998; Yan et al., 2007). JAZ proteins repress transcription factors such as MYC2, EIN3, and EIL1, which activate JA-associated genes (Chini et al., 2007; Zhu et al., 2011). Two mutually antagonistic JA pathways can be activated (Lorenzo et al., 2004); the first is MYC2-dependent and is co-regulated with ABA while the second is ERF-dependent and is co-regulated by ET (Fig. 4.11) (Verhage et al., 2011; Wasternack and Hause, 2013). A common output marker of MYC2-dependent responses is *VSP2* and a common output marker of ERF-dependent responses is *PDF1.2* (Caarls et al., 2015). *VSP2* had much higher expression in *pbs3* UV-C than in Col-0 UV-C, with $\log_2$ FC = 3.569 and FDR = 7.41×10^{-22}. *PDF1.2* does not change expression between Col-0 UV-C vs Col-0 control, but is induced in *pbs3* UV-C vs *pbs3* control. These results indicate that in *pbs3*, both sides of JA signaling increase in expression.

SA inhibition of JA responses takes place downstream of JA synthesis and JAZ degradation (Caarls et al., 2015; Leon-Reyes et al., 2010; Van der Does et al., 2013). MeJA activates genes with a GCC box in their promoters, and SA is sufficient to block this gene synthesis (Van der Does et al., 2013). Accumulation of transcripts of the AP2/ERF transcription factor *ORA59* (same family as *RAP2.6*), was not inhibited by SA, but protein accumulation was (Van der Does et al., 2013). Therefore, it is likely that SA inhibits expression of JA-related genes by destabilizing AP2/ERF transcription factor(s), thereby stopping the expression of target GCC box containing JA genes. It is possible that, like ORA59, RAP2.6 protein accumulation is inhibited by SA. If this were mediated by PBS3, then the lifting of PBS3 inhibition of RAP2.6 in *pbs3* would lead to increasing JA gene expression and less SA. If so, then it may be that the $RAP2.6^{A93V}$ mutation in *sops19* stops RAP2.6 transcriptional activity, causing suppression of JA related genes.

The other branch of JA signaling, mediated by MYC2, also has dependency on SA. MYC2 protein levels were inhibited by egg extract from *Pieris brassicae*, but this inhibition was abolished in the SA biosynthetic mutant *sid2* (Schmiesing et al., 2016). ANAC transcription factors ANAC019, ANAC055, and ANAC072 act downstream of MYC2 and suppress expression of SA-biosynthetic *ICS1* while enhancing expression of SA conjugating *SAGT1* and *BSMT1* (Kazan and Manners, 2013; Zheng et al., 2012). *ANAC032* is induced by *Pto* with higher expression at 6 hpi than 24 hpi (Allu et al., 2016). *MYC2*, *PDF1.2A*, *THI2.1*, *VSP1*, and *VSP2* were all upregulated in the mutant *anac032-1* and had decreased expression in *35S::ANAC032* (Allu et al., 2016). In fact, ANAC032 binds to the promoters of *MYC2*, *PDF1.2A*, and the SA-repressing *NIMIN1* (Allu et al., 2016). The rapid induction of *ANAC032* and its role in suppressing *MYC2* and other JA-related genes suggests that it responds early to pathogens to suppress JA signaling and promote SA signaling.

NPR1, the master regulator of SA-responsive transcriptional change, inhibits expression of both ERF-pathway (*PDF1.2*) and MYC pathway (*VSP2, LOX2*) genes (Spoel et al., 2003). Interestingly, it does so from the cytosol, not the nucleus, suggesting that the cross talk between SA and JA is not confined to nuclear transcriptional activity (Spoel et al., 2003).

CONCLUSIONS

Herein, I present the results of a suppressor screen in the *pPR1::GUSpbs3* mutant background. I identified 163 mutants with some level of restored *PR1* expression in response to UV-C and six of those also showed restored SA accumulation and pathogen resistance. High throughput sequencing was used to identify loci with mutations specific to individual *sops* line. The likely causal mutation for *sops101* is $PAD4^{S135F}$ and for *sops19* is $RAP2.6^{A93V}$. PAD4 is a known protein that promotes and protects SA-induced pathogen defense. The mutation likely increases or alters its activity, allowing the plant to overcome *pbs3* susceptibility. This is the first PAD4 activation mutant identified, and I hypothesize that it restores SA in *pbs3* (partially) through inhibition of the JA pathway. RAP2.6 is a transcription factor involved in the ERF branch of JA signaling and is a strong candidate for *sops19*. The $RAP2.6^{A93V}$ mutation is in the highly conserved DNA binding domain and may stop RAP2.6 activation of SA-antagonizing JA responses. *RAP2.6* is induced in *pbs3* in response to UV-C treatment, but not in WT, suggesting PBS3-mediated repression of the JA pathway. Given these data, we hypothesize that PBS3-mediated defense is not exclusively dependent upon SA, but is also partially the result of inhibition of the JA pathway in induced WT plants. These results suggest that PBS3 is a higher order regulator of SA/JA antagonism, and contributes to our understanding of salicylic acid accumulation and regulation in pathogen-challenged plants.

ACKNOWLEDGEMENTS

Román Ramos screened EMS mutagenized M2s and performed early characterization of *sops* mutants. Haneih Barkhodari assisted with screening M2s, as did the undergraduate students of PMB101L (spring 2016, 2017) (University of California, Berkeley), directed by Dr. M.C. Wildermuth. This work used the Vincent J. Coates Genomics Sequencing Laboratory at UC Berkeley, supported by NIH S10 OD018174 Instrumentation Grant.

FUTURE EXPERIMENTS

It will be very important to transform *pRAP2.6::*$RAP2.6^{A93V}$ and *pPAD4::*$PAD4^{S135F}$ constructs into the *pPR1::GUSpbs3* background. Constructs for this have been made and will be transformed shortly. I expect this will recapitulate the *sops19* and *sops101* phenotypes, respectively. If *sops19* is the result of multiple mutations including $RAP2.6^{A93V}$, I do expect to see partial restoration of the *sops19* phenotype. I would then analyze additional mutants and prioritize which are most likely to have additive effects with $RAP2.6^{A93V}$, transforming the most likely ones into *pPR1::GUSpbs3*$RAP2.6^{A93V}$. If true, this work will yield new insights into the highest order of SA-JA crosstalk regulation.

REFERENCES

Abreu, M.E., Munne-Bosch, S., 2009. Salicylic acid deficiency in NahG transgenic lines and sid2 mutants increases seed yield in the annual plant Arabidopsis thaliana. J. Exp. Bot. 60, 1261–1271. doi:10.1093/jxb/ern363

Afgan, E., Baker, D., van den Beek, M., Blankenberg, D., Bouvier, D., Čech, M., Chilton, J., Clements, D., Coraor, N., Eberhard, C., Grüning, B., Guerler, A., Hillman-Jackson, J., Von Kuster, G., Rasche, E., Soranzo, N., Turaga, N., Taylor, J., Nekrutenko, A., Goecks, J., 2016. The Galaxy platform for accessible, reproducible and collaborative biomedical analyses: 2016 update. Nucleic Acids Res. 44, W3–W10. doi:10.1093/nar/gkw343

Allen, M.D., Yamasaki, K., Ohme-Takagi, M., Tateno, M., Suzuki, M., 1998. A novel mode of DNA recognition by a beta-sheet revealed by the solution structure of the GCC-box binding domain in complex with DNA. EMBO J. 17, 5484–96. doi:10.1093/emboj/17.18.5484

Allu, A.D., Brotman, Y., Xue, G.-P., Balazadeh, S., 2016. Transcription factor ANAC032 modulates JA/SA signalling in response to Pseudomonas syringae infection. EMBO Rep. 17, 1578–1589. doi:10.15252/embr.201642197

Altschul, S.F., Madden, T.L., Schäffer, A.A., Zhang, J., Zhang, Z., Miller, W., Lipman, D.J., 1997. Gapped BLAST and PSI-BLAST: a new generation of protein database search programs. Nucleic Acids Res. 25, 3389–402.

Anders, S., Pyl, P.T., Huber, W., 2015. HTSeq--a Python framework to work with high-throughput sequencing data. Bioinformatics 31, 166–169. doi:10.1093/bioinformatics/btu638

Aoki, Y., Okamura, Y., Tadaka, S., Kinoshita, K., Obayashi, T., 2016. ATTED-II in 2016: A Plant Coexpression Database Towards Lineage-Specific Coexpression. Plant Cell Physiol. 57, e5–e5. doi:10.1093/pcp/pcv165

Austin, R.S., Vidaurre, D., Stamatiou, G., Breit, R., Provart, N.J., Bonetta, D., Zhang, J., Fung, P., Gong, Y., Wang, P.W., McCourt, P., Guttman, D.S., 2011. Next-generation mapping of Arabidopsis genes. Plant J. 67, 715–25. doi:10.1111/j.1365-313X.2011.04619.x

Axtell, M.J., Staskawicz, B.J., 2003. Initiation of RPS2-specified disease resistance in Arabidopsis is coupled to the AvrRpt2-directed elimination of RIN4. Cell 112, 369–77.

Brodersen, P., Petersen, M., Bjørn Nielsen, H., Zhu, S., Newman, M.-A., Shokat, K.M., Rietz, S., Parker, J., Mundy, J., 2006. Arabidopsis MAP kinase 4 regulates salicylic acid- and jasmonic acid/ethylene-dependent responses via EDS1 and PAD4. Plant J. 47, 532–546. doi:10.1111/j.1365-313X.2006.02806.x

Brown, R.L., Kazan, K., McGrath, K.C., Maclean, D.J., Manners, J.M., 2003. A role for the GCC-box in jasmonate-mediated activation of the PDF1.2 gene of Arabidopsis. Plant Physiol. 132, 1020–32. doi:10.1104/pp.102.017814

Caarls, L., Pieterse, C.M.J., Van Wees, S.C.M., 2015. How salicylic acid takes transcriptional control over jasmonic acid signaling. Front. Plant Sci. 6, 170. doi:10.3389/fpls.2015.00170

Chen, W., Provart, N.J., Glazebrook, J., Katagiri, F., Chang, H.-S., Eulgem, T., Mauch, F., Luan, S., Zou, G., Whitham, S.A., Budworth, P.R., Tao, Y., Xie, Z., Chen, X., Lam, S., Kreps, J.A., Harper, J.F., Si-Ammour, A., Mauch-Mani, B., Heinlein, M., Kobayashi, K., Hohn, T., Dangl, J.L., Wang, X., Zhu, T., 2002. Expression profile matrix of Arabidopsis transcription factor genes suggests their putative functions in response to environmental stresses. Plant Cell 14, 559–74. doi:10.1105/TPC.010410

Chini, A., Fonseca, S., Fernández, G., Adie, B., Chico, J.M., Lorenzo, O., García-Casado, G.,

López-Vidriero, I., Lozano, F.M., Ponce, M.R., Micol, J.L., Solano, R., 2007. The JAZ family of repressors is the missing link in jasmonate signalling. Nature 448, 666–671. doi:10.1038/nature06006
Cui, H., Gobbato, E., Kracher, B., Qiu, J., Bautor, J., Parker, J.E., 2017. A core function of EDS1 with PAD4 is to protect the salicylic acid defense sector in Arabidopsis immunity. New Phytol. 213, 1802–1817. doi:10.1111/nph.14302
Dempsey, D.A., Vlot, a C., Wildermuth, M.C., Klessig, D.F., 2011. Salicylic Acid biosynthesis and metabolism. Arabidopsis Book 9, e0156. doi:10.1199/tab.0156
Dombrecht, B., Xue, G.P., Sprague, S.J., Kirkegaard, J.A., Ross, J.J., Reid, J.B., Fitt, G.P., Sewelam, N., Schenk, P.M., Manners, J.M., Kazan, K., 2007. MYC2 Differentially Modulates Diverse Jasmonate-Dependent Functions in Arabidopsis. PLANT CELL ONLINE 19, 2225–2245. doi:10.1105/tpc.106.048017
Feys, B.J., Moisan, L.J., Newman, M.A., Parker, J.E., 2001. Direct interaction between the Arabidopsis disease resistance signaling proteins, EDS1 and PAD4. EMBO J. 20, 5400–5411. doi:10.1093/emboj/20.19.5400
Feys, B.J., Wiermer, M., Bhat, R.A., Moisan, L.J., Medina-Escobar, N., Neu, C., Cabral, A., Parker, J.E., 2005. Arabidopsis SENESCENCE-ASSOCIATED GENE101 Stabilizes and Signals within an ENHANCED DISEASE SUSCEPTIBILITY1 Complex in Plant Innate Immunity. PLANT CELL ONLINE 17, 2601–2613. doi:10.1105/tpc.105.033910
Fowler, S., Thomashow, M.F., 2002. Arabidopsis transcriptome profiling indicates that multiple regulatory pathways are activated during cold acclimation in addition to the CBF cold response pathway. Plant Cell 14, 1675–90. doi:10.1105/TPC.003483
Gao, Q.-M., Venugopal, S., Navarre, D., Kachroo, A., 2011. Low Oleic Acid-Derived Repression of Jasmonic Acid-Inducible Defense Responses Requires the WRKY50 and WRKY51 Proteins. Plant Physiol. 155.
Glazebrook, J., Chen, W., Estes, B., Chang, H.-S., Nawrath, C., Metraux, J.-P., Zhu, T., Katagiri, F., 2003. Topology of the network integrating salicylate and jasmonate signal transduction derived from global expression phenotyping. Plant J. 34, 217–228. doi:10.1046/j.1365-313X.2003.01717.x
Guo, R., Sun, W., 2017. Sumoylation stabilizes RACK1B and enhance its interaction with RAP2.6 in the abscisic acid response. Sci. Rep. 7, 44090. doi:10.1038/srep44090
Gupta, V., Willits, M.G., Glazebrook, J., 2000. *Arabidopsis thaliana EDS4* Contributes to Salicylic Acid (SA)-Dependent Expression of Defense Responses: Evidence for Inhibition of Jasmonic Acid Signaling by SA. Mol. Plant-Microbe Interact. 13, 503–511. doi:10.1094/MPMI.2000.13.5.503
Hao, D., Yamasaki, K., Sarai, A., Ohme-Takagi, M., 2002. Determinants in the sequence specific binding of two plant transcription factors, CBF1 and NtERF2, to the DRE and GCC motifs. Biochemistry 41, 4202–8.
He, P., Chintamanani, S., Chen, Z., Zhu, L., Kunkel, B.N., Alfano, J.R., Tang, X., Zhou, J.-M., 2004. Activation of a COI1-dependent pathway in Arabidopsis by Pseudomonas syringae type III effectors and coronatine. Plant J. 37, 589–602.
Ichimura, K., Casais, C., Peck, S.C., Shinozaki, K., Shirasu, K., 2006. MEKK1 is required for MPK4 activation and regulates tissue-specific and temperature-dependent cell death in Arabidopsis. J. Biol. Chem. 281, 36969–76. doi:10.1074/jbc.M605319200
Jagadeeswaran, G., Raina, S., Acharya, B.R., Maqbool, S.B., Mosher, S.L., Appel, H.M., Schultz, J.C., Klessig, D.F., Raina, R., 2007. Arabidopsis GH3-LIKE DEFENSE GENE 1 is

required for accumulation of salicylic acid, activation of defense responses and resistance to Pseudomonas syringae. Plant J. 51, 234–46. doi:10.1111/j.1365-313X.2007.03130.x
Jefferson, R.A., 1987. Assaying chimeric genes in plants: The GUS gene fusion system. Plant Mol. Biol. Report. 5, 387–405. doi:10.1007/BF02667740
Jirage, D., Tootle, T.L., Reuber, T.L., Frost, L.N., Feys, B.J., Parker, J.E., Ausubel, F.M., Glazebrook, J., 1999. Arabidopsis thaliana PAD4 encodes a lipase-like gene that is important for salicylic acid signaling. Proc. Natl. Acad. Sci. U. S. A. 96, 13583–8.
Katari, M.S., Nowicki, S.D., Aceituno, F.F., Nero, D., Kelfer, J., Thompson, L.P., Cabello, J.M., Davidson, R.S., Goldberg, A.P., Shasha, D.E., Coruzzi, G.M., Gutiérrez, R.A., 2010. VirtualPlant: A Software Platform to Support Systems Biology Research. Plant Physiol. 152.
Kazan, K., Manners, J.M., 2013. MYC2: The Master in Action. Mol. Plant 6, 686–703. doi:10.1093/MP/SSS128
Kim, D., Langmead, B., Salzberg, S.L., 2015. HISAT: a fast spliced aligner with low memory requirements. Nat. Methods 12, 357–360.
Kim, M.G., da Cunha, L., McFall, A.J., Belkhadir, Y., DebRoy, S., Dangl, J.L., Mackey, D., 2005. Two Pseudomonas syringae type III effectors inhibit RIN4-regulated basal defense in Arabidopsis. Cell 121, 749–59. doi:10.1016/j.cell.2005.03.025
Krishnaswamy, S., Verma, S., Rahman, M.H., Kav, N.N. V., 2011. Functional characterization of four APETALA2-family genes (RAP2.6, RAP2.6L, DREB19 and DREB26) in Arabidopsis. Plant Mol. Biol. 75, 107–127. doi:10.1007/s11103-010-9711-7
Lee, M.W., Jelenska, J., Greenberg, J.T., 2008. Arabidopsis proteins important for modulating defense responses to Pseudomonas syringae that secrete HopW1-1. Plant J. 54, 452–65. doi:10.1111/j.1365-313X.2008.03439.x
Lee, M.W., Lu, H., Jung, H.W., Greenberg, J.T., 2007. A key role for the Arabidopsis WIN3 protein in disease resistance triggered by Pseudomonas syringae that secrete AvrRpt2. Mol. Plant. Microbe. Interact. 20, 1192–200. doi:10.1094/MPMI-20-10-1192
Leon-Reyes, A., Van der Does, D., De Lange, E.S., Delker, C., Wasternack, C., Van Wees, S.C.M., Ritsema, T., Pieterse, C.M.J., 2010. Salicylate-mediated suppression of jasmonate-responsive gene expression in Arabidopsis is targeted downstream of the jasmonate biosynthesis pathway. Planta 232, 1423–32. doi:10.1007/s00425-010-1265-z
Lorenzo, O., Chico, J.M., Sánchez-Serrano, J.J., Solano, R., 2004. JASMONATE-INSENSITIVE1 encodes a MYC transcription factor essential to discriminate between different jasmonate-regulated defense responses in Arabidopsis. Plant Cell 16, 1938–50. doi:10.1105/tpc.022319
Lu, M., Zhang, Y., Tang, S., Pan, J., Yu, Y., Han, J., Li, Y., Du, X., Nan, Z., Sun, Q., 2016. AtCNGC2 is involved in jasmonic acid-induced calcium mobilization. J. Exp. Bot. 67, 809–819. doi:10.1093/jxb/erv500
Mackelprang, R., Okrent, R.A., Wildermuth, M.C., 2017. Preference of Arabidopsis thaliana GH3.5 acyl amido synthetase for growth versus defense hormone acyl substrates is dictated by concentration of amino acid substrate aspartate. Phytochemistry 143, 19–28. doi:10.1016/j.phytochem.2017.07.001
Mackey, D., Belkhadir, Y., Alonso, J.M., Ecker, J.R., Dangl, J.L., 2003. Arabidopsis RIN4 is a target of the type III virulence effector AvrRpt2 and modulates RPS2-mediated resistance. Cell 112, 379–89.
Marchler-Bauer, A., Bo, Y., Han, L., He, J., Lanczycki, C.J., Lu, S., Chitsaz, F., Derbyshire,

M.K., Geer, R.C., Gonzales, N.R., Gwadz, M., Hurwitz, D.I., Lu, F., Marchler, G.H., Song, J.S., Thanki, N., Wang, Z., Yamashita, R.A., Zhang, D., Zheng, C., Geer, L.Y., Bryant, S.H., 2017. CDD/SPARCLE: functional classification of proteins via subfamily domain architectures. Nucleic Acids Res. 45, D200–D203. doi:10.1093/nar/gkw1129

Molinier, J., Oakeley, E.J., Niederhauser, O., Kovalchuk, I., Hohn, B., 2005. Dynamic response of plant genome to ultraviolet radiation and other genotoxic stresses. Mutat. Res. Mol. Mech. Mutagen. 571, 235–247. doi:10.1016/j.mrfmmm.2004.09.016

Nawrath, C., Heck, S., Parinthawong, N., Métraux, J.-P., 2002. EDS5, an essential component of salicylic acid-dependent signaling for disease resistance in Arabidopsis, is a member of the MATE transporter family. Plant Cell 14, 275–86.

Niu, X., Helentjaris, T., Bate, N.J., 2002. Maize ABI4 binds coupling element1 in abscisic acid and sugar response genes. Plant Cell 14, 2565–75. doi:10.1105/TPC.003400

Nobuta, K., Okrent, R. a, Stoutemyer, M., Rodibaugh, N., Kempema, L., Wildermuth, M.C., Innes, R.W., 2007. The GH3 acyl adenylase family member PBS3 regulates salicylic acid-dependent defense responses in Arabidopsis. Plant Physiol. 144, 1144–56. doi:10.1104/pp.107.097691

Okamuro, J.K., Caster, B., Villarroel, R., Van Montagu, M., Jofuku, K.D., 1997. The AP2 domain of APETALA2 defines a large new family of DNA binding proteins in Arabidopsis. Proc. Natl. Acad. Sci. U. S. A. 94, 7076–81.

Okrent, R.A., 2010. Biochemical and Functional Characterization of the GH3 Amino Acid-Conjugase PBS3 of Arabidopsis thaliana. Dissertation.

Okrent, R. a, Brooks, M.D., Wildermuth, M.C., 2009. Arabidopsis GH3.12 (PBS3) conjugates amino acids to 4-substituted benzoates and is inhibited by salicylate. J. Biol. Chem. 284, 9742–54. doi:10.1074/jbc.M806662200

Petersen, M., Brodersen, P., Naested, H., Andreasson, E., Lindhart, U., Johansen, B., Nielsen, H.B., Lacy, M., Austin, M.J., Parker, J.E., Sharma, S.B., Klessig, D.F., Martienssen, R., Mattsson, O., Jensen, A.B., Mundy, J., 2000. Arabidopsis map kinase 4 negatively regulates systemic acquired resistance. Cell 103, 1111–20. doi:10.1016/S0092-8674(00)00213-0

Pettersen, E.F., Goddard, T.D., Huang, C.C., Couch, G.S., Greenblatt, D.M., Meng, E.C., Ferrin, T.E., 2004. UCSF Chimera--a visualization system for exploratory research and analysis. J. Comput. Chem. 25, 1605–12. doi:10.1002/jcc.20084

Riechmann, J.L., Meyerowitz, E.M., 1998. The AP2/EREBP Family of Plant Transcription Factors. Biol. Chem. 379, 633–646.

Rietz, S., Stamm, A., Malonek, S., Wagner, S., Becker, D., Medina-Escobar, N., Corina Vlot, A., Feys, B.J., Niefind, K., Parker, J.E., 2011. Different roles of Enhanced Disease Susceptibility1 (EDS1) bound to and dissociated from Phytoalexin Deficient4 (PAD4) in Arabidopsis immunity. New Phytol. 191, 107–119. doi:10.1111/j.1469-8137.2011.03675.x

Schmiesing, A., Emonet, A., Gouhier-Darimont, C., Reymond, P., 2016. Arabidopsis MYC Transcription Factors Are the Target of Hormonal Salicylic Acid/Jasmonic Acid Cross Talk in Response to Pieris brassicae Egg Extract. Plant Physiol. 170, 2432–43. doi:10.1104/pp.16.00031

Spoel, S.H., Koornneef, A., Claessens, S.M.C., Korzelius, J.P., Van Pelt, J.A., Mueller, M.J., Buchala, A.J., Métraux, J.-P., Brown, R., Kazan, K., Van Loon, L.C., Dong, X., Pieterse, C.M.J., 2003. NPR1 modulates cross-talk between salicylate- and jasmonate-dependent defense pathways through a novel function in the cytosol. Plant Cell 15, 760–70.

Staswick, P.E., Tiryaki, I., 2004. The Oxylipin Signal Jasmonic Acid Is Activated by an Enzyme

That Conjugates It to Isoleucine in Arabidopsis. Plant Cell 16, 2117–2127. doi:10.1105/tpc.104.023549.1

Staswick, P.E., Tiryaki, I., Rowe, M.L., 2002. Jasmonate Response Locus JAR1 and Several Related Arabidopsis Genes Encode Enzymes of the Firefly Luciferase Superfamily That Show Activity on Jasmonic , Salicylic , and Indole-3-Acetic Acids in an Assay for Adenylation. Plant Cell 14, 1405–1415. doi:10.1105/tpc.000885.defect

Strawn, M. a, Marr, S.K., Inoue, K., Inada, N., Zubieta, C., Wildermuth, M.C., 2007. Arabidopsis isochorismate synthase functional in pathogen-induced salicylate biosynthesis exhibits properties consistent with a role in diverse stress responses. J. Biol. Chem. 282, 5919–33. doi:10.1074/jbc.M605193200

Thines, B., Katsir, L., Melotto, M., Niu, Y., Mandaokar, A., Liu, G., Nomura, K., He, S.Y., Howe, G.A., Browse, J., 2007. JAZ repressor proteins are targets of the SCFCOI1 complex during jasmonate signalling. Nature 448, 661–665. doi:10.1038/nature05960

Van der Does, D., Leon-Reyes, A., Koornneef, A., Van Verk, M.C., Rodenburg, N., Pauwels, L., Goossens, A., Körbes, A.P., Memelink, J., Ritsema, T., Van Wees, S.C.M., Pieterse, C.M.J., 2013. Salicylic acid suppresses jasmonic acid signaling downstream of SCFCOI1-JAZ by targeting GCC promoter motifs via transcription factor ORA59. Plant Cell 25, 744–61. doi:10.1105/tpc.112.108548

Verhage, A., Vlaardingerbroek, I., Raaymakers, C., Van Dam, N.M., Dicke, M., Van Wees, S.C.M., Pieterse, C.M.J., 2011. Rewiring of the jasmonate signaling pathway in Arabidopsis during insect herbivory. Front. Plant Sci. 2, 47. doi:10.3389/fpls.2011.00047

Wagner, S., Stuttmann, J., Rietz, S., Guerois, R., Brunstein, E., Bautor, J., Niefind, K., Parker, J.E., 2013. Structural Basis for Signaling by Exclusive EDS1 Heteromeric Complexes with SAG101 or PAD4 in Plant Innate Immunity. Cell Host Microbe 14, 619–630. doi:10.1016/j.chom.2013.11.006

Wang, G.-F., Seabolt, S., Hamdoun, S., Ng, G., Park, J., Lu, H., 2011. Multiple roles of WIN3 in regulating disease resistance, cell death, and flowering time in Arabidopsis. Plant Physiol. 156, 1508–19. doi:10.1104/pp.111.176776

Wang, L., Mitra, R.M., Hasselmann, K.D., Sato, M., Lenarz-Wyatt, L., Cohen, J.D., Katagiri, F., Glazebrook, J., 2008. The genetic network controlling the Arabidopsis transcriptional response to Pseudomonas syringae pv. maculicola: roles of major regulators and the phytotoxin coronatine. Mol. Plant-Microbe Interact. 21, 1408–20. doi:10.1094/MPMI-21-11-1408

Wasternack, C., Hause, B., 2013. Jasmonates: biosynthesis, perception, signal transduction and action in plant stress response, growth and development. An update to the 2007 review in Annals of Botany. Ann. Bot. 111, 1021–1058. doi:10.1093/aob/mct067

Weinmann, P., Gossen, M., Hillen, W., Bujard, H., Gatz, C., 1994. A chimeric transactivator allows tetracycline-responsive gene expression in whole plants. Plant J. 5, 559–569. doi:10.1046/j.1365-313X.1994.05040559.x

Westfall, C.S., Sherp, A.M., Zubieta, C., Alvarez, S., Schraft, E., Marcellin, R., Ramirez, L., Jez, J.M., 2016. Arabidopsis thaliana GH3.5 acyl acid amido synthetase mediates metabolic crosstalk in auxin and salicylic acid homeostasis. Proc. Natl. Acad. Sci. U. S. A. 113, 13917–13922. doi:10.1073/pnas.1612635113

Westfall, C.S., Zubieta, C., Herrmann, J., Kapp, U., Nanao, M.H., Jez, J.M., 2012. Structural basis for prereceptor modulation of plant hormones by GH3 proteins. Science 336, 1708–11. doi:10.1126/science.1221863

Wildermuth, M.C., Dewdney, J., Wu, G., Ausubel, F.M., 2001. Isochorismate synthase is required to synthesize salicylic acid for plant defence. Nature 414, 562–5. doi:10.1038/35107108

Xie, D.X., Feys, B.F., James, S., Nieto-Rostro, M., Turner, J.G., 1998. COI1: an Arabidopsis gene required for jasmonate-regulated defense and fertility. Science 280, 1091–4.

Yalpani, N., Enyedi, A., León, J., Raskin, I., 1994. Ultraviolet light and ozone stimulate accumulation of salicylic acid, pathogenesis-related proteins and virus resistance in tobacco. Planta 193, 372–376. doi:10.1007/BF00201815

Yan, Y., Stolz, S., Chételat, A., Reymond, P., Pagni, M., Dubugnon, L., Farmer, E.E., 2007. A downstream mediator in the growth repression limb of the jasmonate pathway. Plant Cell 19, 2470–83. doi:10.1105/tpc.107.050708

Zheng, X.-Y., Spivey, N.W., Zeng, W., Liu, P.-P., Fu, Z.Q., Klessig, D.F., He, S.Y., Dong, X., 2012. Coronatine promotes Pseudomonas syringae virulence in plants by activating a signaling cascade that inhibits salicylic acid accumulation. Cell Host Microbe 11, 587–96. doi:10.1016/j.chom.2012.04.014

Zhou, N., Tootle, T.L., Tsui, F., Klessig, D.F., Glazebrook, J., Neu, C., Cabral, A., Parker, J.E., 1998. PAD4 Functions Upstream from Salicylic Acid to Control Defense Responses in Arabidopsis. PLANT CELL ONLINE 10, 1021–1030. doi:10.1105/tpc.10.6.1021

Zhu, Q., Zhang, J., Gao, X., Tong, J., Xiao, L., Li, W., Zhang, H., 2010. The Arabidopsis AP2/ERF transcription factor RAP2.6 participates in ABA, salt and osmotic stress responses. Gene 457, 1–12. doi:10.1016/j.gene.2010.02.011

Zhu, Z., An, F., Feng, Y., Li, P., Xue, L., A, M., Jiang, Z., Kim, J.-M., To, T.K., Li, W., Zhang, X., Yu, Q., Dong, Z., Chen, W.-Q., Seki, M., Zhou, J.-M., Guo, H., 2011. Derepression of ethylene-stabilized transcription factors (EIN3/EIL1) mediates jasmonate and ethylene signaling synergy in Arabidopsis. Proc. Natl. Acad. Sci. U. S. A. 108, 12539–44. doi:10.1073/pnas.1103959108

CHAPTER V: Conclusions

SUMMARY

Herein, I investigated the role of PBS3 in salicylic acid (SA)-mediated pathogen resistance in *Arabidopsis thaliana*. While PBS3 was initially identified in a screen for susceptibility to *Pseudomonas syringae* pv. *tomato* (*Pto*) DC3000 AvrPphB (Warren et al., 1999), multiple labs later converged on its critical function for SA accumulation and associated defense induction (Jagadeeswaran et al., 2007; Lee et al., 2007; Nobuta et al., 2007). These papers demonstrated that *pbs3* mutants are more susceptible than Col-0 (WT) to a variety of bacterial pathogens, have decreased accumulation of total SA (free SA + SA glucosides), and have decreased expression of the SA-inducible gene *pathogenesis related 1* (*PR1*). Based on the ability of exogenous application of SA to rescue *pbs3* mutants after infection with *Pseudomonas syringae* pv. *tomato* (*Pto*) DC3000, PBS3 was placed upstream of SA synthesis (Jagadeeswaran et al., 2007). In *pad4* mutants, *PBS3* expression decreases and in *pad4eds1* double mutants, *PBS3* is not induced, suggesting that *PBS3* is fully dependent on PAD4/EDS1 (Cui et al., 2017; Jagadeeswaran et al., 2007; Wang et al., 2008). While PBS3 is necessary for UV-C and pathogen-induced SA accumulation and is associated with the priming and amplification phases or response, it is not necessary for expression of the SA biosynthetic *ICS1* gene or protein (Chapter III). Therefore, several research strategies were used to identify the role of PBS3 in robust induced plant defense.

Previously, PBS3 enzymatic activity was characterized (Okrent et al., 2009), but this did not yield an obvious mechanism for impacting SA metabolism. Metabolic profiling identified only three reproducibly varied peaks between Col-0 and *pbs3*, two of which were SA metabolites (Chapter III; Okrent, 2010). One was an SA glucoside which contributes to total SA. Total SA had already been identified as decreased in *pbs3* (Jagadeeswaran et al., 2007; Lee et al., 2008; Nobuta et al., 2007). The other, SA-Asp, was significantly (30-fold) increased in *pbs3* mutants as compared to WT. As such, we hypothesized that PBS3 inhibits conversion of SA to inactive forms such as SA-Asp, allowing active forms to accumulate.

In Chapter II, I describe detailed kinetic analyses of an SA-Asp synthetase, GH3.5 (Mackelprang et al., 2017). GH3.5 is active on SA, but also on indole-3-acetic acid (IAA) (Mackelprang et al., 2017; Staswick et al., 2002; Westfall et al., 2016). I hypothesized that a product of PBS3 enzyme activity inhibited GH3.5 activity in Col-0, stopping conjugation of SA, and that in *pbs3*, absent this inhibition, SA accumulation was compromised in favor of SA-Asp. In *in vitro* assays, the PBS3 product 4-HBA-Glu did not inhibit GH3.5 activity (Chapter II). GH3.5 did have differing activity with IAA and SA. While IAA was generally the preferred substrate with lower K_ms and higher V_{max} than with SA, the affinity of GH3.5 for SA increased (lower K_m) as the concentration of Asp decreased. The concentration of Asp decreases in pathogen-affected cells, which would favor GH3.5 activity on SA as opposed to IAA (Chapter II; Návarová et al., 2012). It therefore seems that the activity of GH3.5 is specific to the cellular conditions. This could serve as a regulatory mechanism to limit the extent of SA accumulation, as the concentration of SA has drastic effects on cellular outcomes. Amino acid effect on acyl substrate binding has not previously been reported for the GH3s, and this is an important insight into their function and potentially their reaction mechanism.

While I did not observe an inhibitory effect of PBS3 products on GH3.5 production of SA-Asp, the possibility remained that PBS3 inhibited SA-Asp accumulation in a different way *in planta*. I therefore created a *pbs3gh3.5* double mutant line to see if a plant deficient in SA-Asp production had restored SA accumulation (Chapter III). *Pbs3gh3.5* did not have restored pathogen resistance, but also did not lose all accumulation of SA-Asp. I therefore identified other members of the GH3 family that were likely SA-Asp synthetases. Selecting the most promising among those, I created a *pbs3gh3.1gh3.3gh3.4gh3.5gh3.6* sextuple mutant called *gh6x*. When infiltrated with *Pto* DC3000 AvrRpt2, *gh6x* SA-Asp levels returned to WT levels. However, this did not restore the accumulation of SA (Chapter III), suggesting PBS3's function is broader than inhibition of SA-Asp. Indeed, the function of PBS3 may extend further than SA, as exogenous application of SA did not restore WT bacterial growth in *pbs3*.

I therefore used a forward genetic suppressor screen to identify additional factors involved in *pbs3*-susceptibility (Chapter IV). I created a *pPR1::GUSpbs3* line, which is deficient in *PR1* expression and therefore negative for GUS activity. After EMS mutagenesis, I hoped to identify mutant *suppressors of pbs3 susceptibility* (*sops*), which would restore *GUS* expression in the *pbs3* background. Through screening approximately 5200 M2s, 163 mutants with restored GUS staining in response to SA-inducing UV-C treatment were identified. Interestingly, not all had the robust *PR1* induction and SA accumulation associated with defense, indicating that i) this assay is sensitive to low levels of *PR1* expression and ii) *PR1* may be activated to low levels via SA-independent means. Due to this, I employed a secondary screen to identify GUS positive plant lines with restored total SA in response to UV-C. Six of the 35 lines assayed did have restored SA, representing two M2 parent pools. Two plant lines, *sops19* and *sops101*, one from each of the two M2 parent pools, were carried forward for further characterization.

Sops19 and *sops101* both demonstrated restored SA accumulation and *PR1* expression in response to UV-C treatment. In response to virulent *Pseudomonas syringae* pv. *maculicola* (*Pma*) ES4326, *sops101* showed restored resistance, and *sops19* showed even greater resistance than WT. Furthermore, *sops19* and *sops101* restored wild type flowering time; reproductive growth occurs early in *pbs3* mutant lines. These data suggest that *sops19* and *sops101* contain mutations that restore all reported wildtype phenotypes in the *pbs3* background (Chapter IV).

I used Illumina Hi-Seq 4000 high throughput sequencing to identify candidate causal mutations in *sops19* and *sops101*, yielding a shortlist of likely candidates. $RAP2.6^{A93V}$ and $PAD4^{S135F}$ were identified as the most likely causal mutations in *sops19* and *sops101*, respectively (Chapter IV). Both enzymes have previously been identified as important in pathogen resistance, but not specifically connected to PBS3. RAP2.6 especially, but also PAD4, has involvement with the jasmonic acid (JA) pathway, which is responsible for defense against necrotrophic pathogens and wounding. PAD4 is likely upstream of PBS3 in SA signaling (Chapter IV; Jagadeeswaran et al., 2007; Wang et al., 2008). The S135F mutation occurs near its putative interaction site with EDS1 and likely alters binding between PAD4 and EDS1 (Chapter IV). It is possible that in wild type, a product of PBS3, or the PBS3 protein itself, affects PAD4/EDS1 binding and that such binding is restored in *sops101*. $RAP2.6^{A93}$ is an invariant position in the DNA-binding domain of this AP2/ERF-like transcription factor. As such, this mutation is likely to alter RAP2.6 transcriptional activity. *RAP2.6* is induced by both SA and JA (Krishnaswamy et al., 2011). Its expression was induced in *pbs3* plants after exposure to UV-C, consistent with other work that showed *RAP2.6* expression increased in SA-deficient *pad4*, *NahG*, and *npr1* when infected with *Pma* ES4326 (Chen et al., 2002). RAP2.6 binds to GCC and CE1 *cis* elements, likely activating JA-associated genes at the expense of SA-associated genes

(Brown et al., 2003; Hao et al., 2002; Niu et al., 2002; Van der Does et al., 2013; Zhu et al., 2010). A mutation in the *RAP2.6* DNA-binding domain would explain a decrease of JA related and increase in SA-related gene expression.

I hypothesize that PBS3 mediates SA/JA crosstalk, acting as a higher order regulator of defense induction. In support of this idea, RNA-seq data (Chapter IV) and microarray data (Wang et al., 2008) show that the majority of differentially expressed genes in *pbs3* after UV-C treatment have increased expression compared to WT. Comparison of differentially expressed genes between Col-0 and *pbs3* 24 hpt UV-C showed that *pbs3* had 503 genes with higher expression and only 112 genes with lower expression than Col-0. While SA controls responses to biotrophic pathogens, JA controls responses to necrotrophs. Consistent with a role for PBS3 in JA antagonism, the necrotrophic fungal pathogen *Botrytis cinerea* allows more disease symptoms in *Arabidopsis thaliana pbs3* mutants as opposed to WT (Wang et al., 2011). In fact, *pbs3* mutants had similar phenotypes to mutants in the JA-pathway (*jar1* and *ein2*), suggesting that PBS3 does not simply promote SA signaling, but moderates the SA/JA crosstalk during complex interactions between organisms (Wang et al., 2011).

Future Directions

Many questions remain unanswered as to the mechanism by which PBS3 promotes SA accumulation. Great strides will be made through identification and confirmation of *sops19* and *sops101* causal mutations. At this writing, the constructs have been made for *Agrobacterium*-mediated transformation of $PAD4^{S135F}$ and $RAP2.6^{A93V}$ into the clean *pPR1::GUSpbs3* background. These may need to be crossed into *pad4* and *rap2.6* mutant backgrounds, respectively. Additionally, mutants will be put into the WT background. This will allow us to distinguish if the mutations are additive with PBS3, or if they restore a specific aspect of PBS3 function in the *pbs3* background. If transformation of mutant lines into *pPR1::GUSpbs3* recapitulates the *sops* phenotypes, many additional experiments would be warranted to further understand this node of PBS3 defense resistance.

After identification of the causal mutations of *sops19* and *sops101*, several critical questions for understanding plant immunity could be addressed. Importantly, it will be valuable to understand if the *sops19* and *sops101* causal mutations restore SA through restoration of some activity or product, or whether they function independently to overcome the SA deficit of *pbs3*. If the phenotypes are able to specifically overcome the defense deficits incurred by *pbs3*, it will be fascinating to learn how. The build-up of a substrate of PBS3 or the lack of PBS3 product could alter the activity of an enzyme (such as PAD4 binding to EDS1 or RAP2.6 transcriptional activity). Alternatively, PBS3 may have as yet unknown protein-protein interactions that alter its own enzymatic activity or the enzymatic activity of a partner. Regardless of mechanism, an important question emerges from this work: What role does PBS3 play in modulating cross talk between the SA and JA pathways?

Several individual components of SA and JA crosstalk have been identified, but a clear picture of the most important factors for different spatio-temporal conditions has not emerged. While ANAC transcription factors and enzymes such as MPK4 seem to be important (Allu et al., 2016; Brodersen et al., 2006; Petersen et al., 2000; Zheng et al., 2012), they do not seem to be major regulatory nodes. It may be that PBS3, perhaps in conjugation with PAD4, occupies such a node. Indeed, evidence suggests that PBS3 may serve as such a node for the modulation of hormone crosstalk.

GH3 family members have now been described as being essential for activation of JA, mediators of SA/IAA crosstalk (Chapter II), important for IAA homeostasis, and necessary for

accumulation of SA in plant defense and now for SA/JA crosstalk. The evolutionary history of a gene family with such diverse but consistently critical roles would be interesting to study in more detail. Okrent and Wildermuth, 2011 identified PBS3 syntelogs in other species such as poplar, grape, columbine, maize and rice, suggesting a common ancestral chromosome region before the split of monocots and dicots. These enzymes represent an expeditious way to modulate hormone concentration and associated responses. Analysis of the function of these syntelogs may yield interesting insight into the evolution of hormone crosstalk not only between SA and JA, but other plant hormones too that may be conjugated by GH3s in other plant lineages.

Ultimately, the work herein coupled with further research may open possibilities for improvement in crop disease resistance. The salicylic acid pathway is conserved throughout plants, and as the evolutionary arms race between plants and their pathogens continues, understanding the underlying plant defense regulators may assist in breeding and/or engineering more durable resistance to plant pathogens. PBS3 may be a key player in this process that functions as a high-level node between the SA and JA responses.

REFERENCES

Allu, A.D., Brotman, Y., Xue, G.-P., Balazadeh, S., 2016. Transcription factor ANAC032 modulates JA/SA signalling in response to Pseudomonas syringae infection. EMBO Rep. 17, 1578–1589. doi:10.15252/embr.201642197

Brodersen, P., Petersen, M., Bjørn Nielsen, H., Zhu, S., Newman, M.-A., Shokat, K.M., Rietz, S., Parker, J., Mundy, J., 2006. Arabidopsis MAP kinase 4 regulates salicylic acid- and jasmonic acid/ethylene-dependent responses via EDS1 and PAD4. Plant J. 47, 532–546. doi:10.1111/j.1365-313X.2006.02806.x

Brown, R.L., Kazan, K., McGrath, K.C., Maclean, D.J., Manners, J.M., 2003. A role for the GCC-box in jasmonate-mediated activation of the PDF1.2 gene of Arabidopsis. Plant Physiol. 132, 1020–32. doi:10.1104/pp.102.017814

Chen, W., Provart, N.J., Glazebrook, J., Katagiri, F., Chang, H.-S., Eulgem, T., Mauch, F., Luan, S., Zou, G., Whitham, S.A., Budworth, P.R., Tao, Y., Xie, Z., Chen, X., Lam, S., Kreps, J.A., Harper, J.F., Si-Ammour, A., Mauch-Mani, B., Heinlein, M., Kobayashi, K., Hohn, T., Dangl, J.L., Wang, X., Zhu, T., 2002. Expression profile matrix of Arabidopsis transcription factor genes suggests their putative functions in response to environmental stresses. Plant Cell 14, 559–74.

Cui, H., Gobbato, E., Kracher, B., Qiu, J., Bautor, J., Parker, J.E., 2017. A core function of EDS1 with PAD4 is to protect the salicylic acid defense sector in Arabidopsis immunity. New Phytol. 213, 1802–1817. doi:10.1111/nph.14302

Hao, D., Yamasaki, K., Sarai, A., Ohme-Takagi, M., 2002. Determinants in the sequence specific binding of two plant transcription factors, CBF1 and NtERF2, to the DRE and GCC motifs. Biochemistry 41, 4202–8.

Jagadeeswaran, G., Raina, S., Acharya, B.R., Maqbool, S.B., Mosher, S.L., Appel, H.M., Schultz, J.C., Klessig, D.F., Raina, R., 2007. Arabidopsis GH3-LIKE DEFENSE GENE 1 is required for accumulation of salicylic acid, activation of defense responses and resistance to Pseudomonas syringae. Plant J. 51, 234–46. doi:10.1111/j.1365-313X.2007.03130.x

Krishnaswamy, S., Verma, S., Rahman, M.H., Kav, N.N. V., 2011. Functional characterization of four APETALA2-family genes (RAP2.6, RAP2.6L, DREB19 and DREB26) in Arabidopsis. Plant Mol. Biol. 75, 107–127. doi:10.1007/s11103-010-9711-7

Lee, M.W., Jelenska, J., Greenberg, J.T., 2008. Arabidopsis proteins important for modulating defense responses to Pseudomonas syringae that secrete HopW1-1. Plant J. 54, 452–65. doi:10.1111/j.1365-313X.2008.03439.x

Lee, M.W., Lu, H., Jung, H.W., Greenberg, J.T., 2007. A key role for the Arabidopsis WIN3 protein in disease resistance triggered by Pseudomonas syringae that secrete AvrRpt2. Mol. Plant. Microbe. Interact. 20, 1192–200. doi:10.1094/MPMI-20-10-1192

Mackelprang, R., Okrent, R.A., Wildermuth, M.C., 2017. Preference of Arabidopsis thaliana GH3.5 acyl amido synthetase for growth versus defense hormone acyl substrates is dictated by concentration of amino acid substrate aspartate. Phytochemistry 143, 19–28.

doi:10.1016/j.phytochem.2017.07.001

Návarová, H., Bernsdorff, F., Döring, A.-C., Zeier, J., 2012. Pipecolic acid, an endogenous mediator of defense amplification and priming, is a critical regulator of inducible plant immunity. Plant Cell 24, 5123–41. doi:10.1105/tpc.112.103564

Niu, X., Helentjaris, T., Bate, N.J., 2002. Maize ABI4 binds coupling element1 in abscisic acid and sugar response genes. Plant Cell 14, 2565–75. doi:10.1105/TPC.003400

Nobuta, K., Okrent, R. a, Stoutemyer, M., Rodibaugh, N., Kempema, L., Wildermuth, M.C., Innes, R.W., 2007. The GH3 acyl adenylase family member PBS3 regulates salicylic acid-dependent defense responses in Arabidopsis. Plant Physiol. 144, 1144–56. doi:10.1104/pp.107.097691

Okrent, R.A., 2010. Biochemical and Functional Characterization of the GH3 Amino Acid-Conjugase PBS3 of Arabidopsis thaliana. Dissertation.

Okrent, R. a, Brooks, M.D., Wildermuth, M.C., 2009. Arabidopsis GH3.12 (PBS3) conjugates amino acids to 4-substituted benzoates and is inhibited by salicylate. J. Biol. Chem. 284, 9742–54. doi:10.1074/jbc.M806662200

Okrent, R. a, Wildermuth, M.C., 2011. Evolutionary history of the GH3 family of acyl adenylases in rosids. Plant Mol. Biol. 76, 489–505. doi:10.1007/s11103-011-9776-y

Petersen, M., Brodersen, P., Naested, H., Andreasson, E., Lindhart, U., Johansen, B., Nielsen, H.B., Lacy, M., Austin, M.J., Parker, J.E., Sharma, S.B., Klessig, D.F., Martienssen, R., Mattsson, O., Jensen, A.B., Mundy, J., 2000. Arabidopsis map kinase 4 negatively regulates systemic acquired resistance. Cell 103, 1111–20. doi:10.1016/S0092-8674(00)00213-0

Staswick, P.E., Tiryaki, I., Rowe, M.L., 2002. Jasmonate Response Locus JAR1 and Several Related Arabidopsis Genes Encode Enzymes of the Firefly Luciferase Superfamily That Show Activity on Jasmonic , Salicylic , and Indole-3-Acetic Acids in an Assay for Adenylation. Plant Cell 14, 1405–1415. doi:10.1105/tpc.000885.defect

Van der Does, D., Leon-Reyes, A., Koornneef, A., Van Verk, M.C., Rodenburg, N., Pauwels, L., Goossens, A., Körbes, A.P., Memelink, J., Ritsema, T., Van Wees, S.C.M., Pieterse, C.M.J., 2013. Salicylic acid suppresses jasmonic acid signaling downstream of SCFCOI1-JAZ by targeting GCC promoter motifs via transcription factor ORA59. Plant Cell 25, 744–61. doi:10.1105/tpc.112.108548

Wang, G.-F., Seabolt, S., Hamdoun, S., Ng, G., Park, J., Lu, H., 2011. Multiple roles of WIN3 in regulating disease resistance, cell death, and flowering time in Arabidopsis. Plant Physiol. 156, 1508–19. doi:10.1104/pp.111.176776

Wang, L., Mitra, R.M., Hasselmann, K.D., Sato, M., Lenarz-Wyatt, L., Cohen, J.D., Katagiri, F., Glazebrook, J., 2008. The genetic network controlling the Arabidopsis transcriptional response to Pseudomonas syringae pv. maculicola: roles of major regulators and the phytotoxin coronatine. Mol. Plant-Microbe Interact. 21, 1408–20. doi:10.1094/MPMI-21-11-1408

Warren, R.F., Merritt, P.M., Holub, E., Innes, R.W., 1999. Identification of three putative signal

transduction genes involved in R gene-specified disease resistance in Arabidopsis. Genetics 152, 401–12.

Westfall, C.S., Sherp, A.M., Zubieta, C., Alvarez, S., Schraft, E., Marcellin, R., Ramirez, L., Jez, J.M., 2016. Arabidopsis thaliana GH3.5 acyl acid amido synthetase mediates metabolic crosstalk in auxin and salicylic acid homeostasis. Proc. Natl. Acad. Sci. U. S. A. 113, 13917–13922. doi:10.1073/pnas.1612635113

Zheng, X.-Y., Spivey, N.W., Zeng, W., Liu, P.-P., Fu, Z.Q., Klessig, D.F., He, S.Y., Dong, X., 2012. Coronatine promotes Pseudomonas syringae virulence in plants by activating a signaling cascade that inhibits salicylic acid accumulation. Cell Host Microbe 11, 587–96. doi:10.1016/j.chom.2012.04.014

Zhu, Q., Zhang, J., Gao, X., Tong, J., Xiao, L., Li, W., Zhang, H., 2010. The Arabidopsis AP2/ERF transcription factor RAP2.6 participates in ABA, salt and osmotic stress responses. Gene 457, 1–12. doi:10.1016/j.gene.2010.02.011